

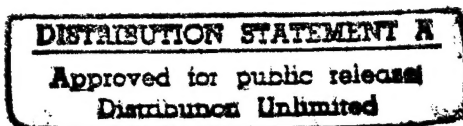
ADD 443229

NASA Contractor Report 178246

Test Results for Composite Specimens and Elements Containing Joints and Cutouts

P. T. Sumida, R. C. Madan, and A. V. Hawley

Douglas Aircraft Company
McDonnell Douglas Corporation
Long Beach, CA 90846



Contract NAS1-17701

August 1988

19960611 145

FOR EARLY DOMESTIC DISSEMINATION

Because of its possible early commercial potential, this data, which has been developed under a U.S. Government program, is being disseminated within the United States in advance of general publication. This data may be duplicated and used by the recipient with the express limitation that it not be published. Release of this data to other domestic parties by the recipient shall be made subject to these limitations. Foreign release may be made only with prior NASA approval and appropriate export licenses. This legend shall be marked on any reproduction of this data in whole or in part. Date for general release will be three (3) years from date of publication on the document.

PLASTICS
ARDEC PICTINNY ARSENAL, N.J. 07806

UNCLASSIFIED

~~USG AND COM~~

NASA

National Aeronautics and
Space Administration

Langley Research Center
Hampton, Virginia 23665

DEPARTMENT OF DEFENCE
PLASTICS TECHNICAL EVALUATION CENTER
ARDEC PICTINNY ARSENAL, N.J. 07806

PLASTEC 054122

NASA Contractor Report 178246

Test Results for Composite Specimens and Elements Containing Joints and Cutouts

P. T. Sumida, R. C. Madan, and A. V. Hawley

**Douglas Aircraft Company
McDonnell Douglas Corporation
Long Beach, CA 90846**

**Contract NAS1-17701
August 1988**

FOR EARLY DOMESTIC DISSEMINATION

Because of its possible early commercial potential, this data, which has been developed under a U.S. Government program, is being disseminated within the United States in advance of general publication. This data may be duplicated and used by the recipient with the express limitation that it not be published. Release of this data to other domestic parties by the recipient shall be made subject to these limitations. Foreign release may be made only with prior NASA approval and appropriate export licenses. This legend shall be marked on any reproduction of this data in whole or in part. Date for general release will be three (3) years from date indicated on the document.



National Aeronautics and
Space Administration

Langley Research Center
Hampton, Virginia 23665

ABSTRACT

This report covers the test efforts associated with the McDonnell Douglas program (NAS1-17701) to develop the technology for joints and cutouts in a composite fuselage that meets all design requirements of a large transport aircraft for the 1990s. An advanced trijet derivative of the DC-10 was selected as the baseline aircraft. Design and analysis of a 30-foot-long composite fuselage barrel provided a realistic basis for the test effort. The primary composite material was Hexcel F584 resin on 12K IM6 fiber, in tape and broadgoods form. Fiberglass broadgoods were used in E-glass and S-glass fiber form in the cutout region of some panels. Additionally, injection-molded chopped graphite fiber/PEEK was used for longeron-to-frame shear clips. The test effort included four groups of test specimens, beginning with coupon specimens of monolayer and cross-ply laminates, progressing through increasingly larger and more complex specimens, and ending with two 4- by 5-foot curved fuselage side panels. One of the side panels incorporated a transverse skin splice, while the second included two cabin window cutouts.

FOREWORD

This report was prepared by McDonnell Douglas Corporation, Douglas Aircraft Company, under contract NAS1-17701, Development of Composites Technology for Joints and Cutouts in Fuselage Structure of Large Transport Aircraft. Test specimens and elements representative of joints and areas containing cutouts in the fuselage of a commercial transport were designed, fabricated, and tested. This report provides details on geometry of the specimens and elements, their fabrication, test procedures used, and test results obtained.

The program was sponsored by the National Aeronautics and Space Administration, Langley Research Center (NASA-LRC), Hampton, Virginia. Dr. John C. Davis, Jr., was the NASA technical program manager for this project.

The identification of commercial products in this report does not constitute official endorsement of such products, either expressed or implied, by the National Aeronautics and Space Administration.

Dr. Ram C. Madan and A. V. Hawley revised this report, which is presented here in final form. Principal contributors to the report were:

Project Manager
P. T. Sumida

Materials Laboratories
R. W. Allen

Structural Analysis
J. B. Black, Jr.
F. F. Behzadpour

Manufacturing Research and Development
V. P. Bailey

Design
B. R. Fox

CONTENTS

Section	Page
1 INTRODUCTION	1
2 TEST PROGRAM	3
2.1 Design Concepts	3
2.1.1 Composite Fuselage Barrel	3
2.1.2 Longeron Concepts	4
2.1.3 Skin Splices	4
2.1.4 Passenger Door Cutout	4
2.1.5 Cabin Window Cutout	6
2.2 Material Selection	6
2.3 Development Specimens	6
2.3.1 Group A	7
2.3.2 Group B	11
2.3.3 Group C	13
2.3.4 Group D	17
3 TEST ARTICLE MANUFACTURING	19
3.1 Process Technology	19
3.1.1 Lay-Up Procedures	19
3.1.2 Autoclave Curing	19
3.1.3 Adhesive Bonding	20
3.1.4 Machining and Hole Drilling	22
3.1.5 Quality Inspection Methods	22
3.2 Group A Test Specimens	24
3.3 Group B Test Specimens	24
3.3.1 Stiffened Cutout Shear Panels	24
3.4 Group C Test Specimens	25
3.4.1 Skin Splice Specimens	26
3.4.2 Longeron Runout Specimen	26
3.4.3 Transverse Skin/Longeron Specimen	27
3.5 Group D Fuselage Side Panels	27
3.5.1 Transverse Splice Panel	27
3.5.2 Composite Window Belt Panel	30
4 TEST SETUP AND PROCEDURE	33
4.1 Group A	33
4.2 Group B	42
4.3 Group C	44
4.4 Group D	48

CONTENTS
(Continued)

Section	Page
5 TEST RESULTS	51
5.1 Group A	51
5.2 Group B	70
5.3 Group C	78
5.4 Group D	86
6 CONCLUDING REMARKS	97
REFERENCES	99
FORM DOT F 1700.7	101

ILLUSTRATIONS

Figure		Page
1-1	Baseline Fuselage Barrel	1
2-1	Joint and Cutout Locations	3
2-2	Structural Details	3
2-3	Composite Shell Design	4
2-4	Passenger Door Cutouts	5
2-5	Cabin Window Structural Concept	6
2-6	Group A Tension Specimens	8
2-7	Group A Compression Specimens	9
2-8	Group A Shear and Shear Joint Specimens	10
2-9	Group A Biaxial Stress Specimen	11
2-10	Group B Unstiffened Cutout Tension Panels	11
2-11	Group B Stiffened Cutout Shear Panels	12
2-12	Group B Shear-Tee Pull-Off Specimens	13
2-13	Group C Longitudinal Skin Splice Specimens	14
2-14	Details of Longitudinal Splice Joints	14
2-15	Group C Transverse Skin Splice Specimens	15
2-16	Group C Longeron Runout Specimen	16
2-17	Group C Transverse Skin/Longeron Splice Panel	16
2-18	Transverse Splice Shear Interaction Panel	17
2-19	Passenger Window Belt Shear Interaction Panel	18
3-1	No-Bleed Bagging Method	20
3-2	Autoclave Cure Cycle for F584/IM6 Laminate	21
3-3	Defect Size Limitations	23
3-4	Distortion of Glass/Graphite Cutout Panels	25
3-5	Sealant Diagram for Splice Specimens	26
3-6	Graphite-Epoxy Tape Lay-Up of Skin Assembly for Transverse Splice Panel	27
3-7	Transfer of Debulked Longeron Preforms to Metal Mandrels	28
3-8	Aluminum Tool for Transverse Splice Panel Frames	29
3-9	Lay-Up Sequence for Longerons	30
3-10	Installation of Composite Window Belt Panel Assembly into Test Fixture	31
4-1	Test Setup for DLT Specimens	33
4-2	Test Circuit for Lightning Simulation	34
4-3	Measured Waveforms for Simulated Lightning Strike Components	35
4-4	X-Ray of -505 CAI Specimen Showing Damage to Nickel-Coated Fibers	37
4-5	After Strike Damage on Wire-Woven Panel (UNC-505-2)	38
4-6	X-Ray of -507 CAI Specimen Showing Damage to Aluminum Wires	39
4-7	After Strike Damage on Nickel-Coated Panel (UNC-507-3)	40
4-8	After Strike Damage on Unprotected Panel (UNC-509-3)	41
4-9	Test Setup for Biaxial Specimens (BAS)	42
4-10	Typical Test Setup for Group B Tension Panel Test	43
4-11	Typical Strain Gage Locations for Shear Cutout Panel (-501)	43
4-12	Photoelastic Measurements of a Group B Cutout Panel	44

ILLUSTRATIONS

(Continued)

Figure		Page
4-13	Schematic of Test Fixture for Transverse Splice Panels	45
4-14	Longitudinal Skin Splice Strain Gage Locations	46
4-15	Longeron Runout Strain Gage Locations	46
4-16	Transverse Splice Panel Strain Gage Locations	47
4-17	Shear/Compression Interaction Test Fixture	48
4-18	Transverse Splice Panel Strain Gage Locations	49
4-19	Transverse Splice Panel Strain Gage Locations Additional Detail	49
4-20	Strain Gage Locations, Window Belt Panel	50
5-1	Method for Calculating Monolayer Shear Properties	52
5-2	Unnotched Tension and Compression Specimen Test Results	53
5-3	Failures of the Dogboned UNT Specimens	53
5-4	Unloaded-Hole Tension Specimen Test Results	54
5-5	Narrow DLT Specimen (Loaded Hole) Test Results	56
5-6	Bearing and Shear-Out Failures of Wide DLT Specimens ($W/D = 6$)	57
5-7	DLT Specimen Test Results (Bearing and Shear-Out Failures)	58
5-8	Unloaded-Hole Compression Specimen Test Results	60
5-9	Typical Failure of ULC Specimen with 3/16-Inch Fastener (Lay-Up No. 4)	61
5-10	Double-Lap Compression Specimen Test Results	62
5-11	Typical Failure of Narrow DLC Specimen (Lay-Up No. 2)	63
5-12	Unloaded-Hole Tension Specimen Results (Lay-Up No. 2, Countersunk)	63
5-13	ULC Specimen Test Results (Lay-Up No. 2, Countersunk)	64
5-14	Typical Failure of Countersunk ULC Specimen (Tested Without Fastener)	65
5-15	Typical Failure of Countersunk ULC Specimen (Tested With Fastener)	65
5-16	DLT Specimen Test Results (Lay-Up No. 2, Countersunk Fastener)	66
5-17	DLC Specimen Test Results (Lay-Up No. 2, Countersunk Fastener)	67
5-18	SLT Specimen Test Results	68
5-19	BAS Specimen Test Results	69
5-20	CAI Specimen Test Results	70
5-21	Failure Locations for Group B Tension Cutout Panels	71
5-22	Photoelastic Fringe Pattern for -501 Tension Cutout Panel	72
5-23	Typical Strain Gage Data for Tension Cutout Panel (-501)	73
5-24	Typical Photoelastic Data for Tension Cutout Panel (-501)	73
5-25	Failure Loads for Group B Shear Cutout Panels	74
5-26	Failure Locations for -501 Shear Cutout Panel	75
5-27	Strain Gage Data at Top Corner of Shear Panel Cutout (-501)	75
5-28	Failure Locations for -503 Shear Cutout Panel	76
5-29	Posttest Photograph of Shear Cutout Panel (-505)	77
5-30	Apparent Failure Sequence for Shear-Tee Pull-Off Specimens	79
5-31	Failure Loads for Group C Skin Splice Specimens	80
5-32	Failure Mode of Tailored Longitudinal Splice Specimens	81
5-33	Failed Baseline Transverse Skin Splice Specimen	81
5-34	Failure Mode for Tailored Transverse Skin Splice Specimens	82

ILLUSTRATIONS (Continued)

Figure		Page
5-35	Failure of Longeron Runout Specimen	83
5-36	Transverse Skin/Longeron Splice Typical Strain Gage Data (Tension)	84
5-37	Failure Mode of Longeron Splices (Tension Specimen)	85
5-38	Longeron/Skin Splice Panel (Compression Specimen) Under Load	85
5-39	Failure of Longeron/Skin Splice Panel (Compression Specimen)	86
5-40	Failure of Longeron/Skin Splice Panel (Compression Specimen)	87
5-41	Failure of Longeron/Skin Splice Panel (Compression Specimen)	87
5-42	Load Schedules for the Group D Panels	89
5-43	Group D Transverse Skin Splice Panel — Partially Failed	90
5-44	Areas of Delamination of Transverse Skin Splice Panel (from NDI)	90
5-45	Postbuckling Response of Transverse Skin Splice Panel (Shear)	91
5-46	Group D Window Belt Panel Showing Failure Locations	92
5-47	Group D Window Belt Panel — Area of Initial Failure	93
5-48	Group D Window Belt Panel — Failure of Skin, Longerons, and Frame	93
5-49	Group D Window Belt Panel — Failure of Skin, Longerons, and Frame	94
5-50	Group D Window Belt Panel — Areas of Skin Damage Detected by NDI	94
5-51	Selected Strain Gage Readings for Window Belt Panel	95

TABLES

Table		Page
2-1	Lightning Protection Materials	7
2-2	Graphite Laminate Descriptions	7
3-1	Limitations on Clumped Scattered Defects	23
4-1	Lightning Discharge Test Values	36
4-2	Lightning Damage	36
5-1	Monolayer Properties	51
5-2	Tension Cutout Test Results	71
5-3	Shear-Tee Pull-Off Test Results	78

SECTION 1 INTRODUCTION

NASA programs have provided aircraft manufacturers, the FAA, and the airlines with the experience and confidence needed for extensive use of composites in secondary and medium-primary structures. While these applications have produced worthwhile weight savings, the use of composite materials in wing and fuselage primary structures offers a far greater opportunity for saving weight since these structures comprise approximately 75 percent of the total structural weight of a large transport aircraft.

In 1984, under the Advanced Composite Structures Technology (ACST) program, NASA awarded this contract to Douglas Aircraft Company to expand the technology base for greater understanding of joints and cutouts in composite structures of large transport aircraft. The baseline aircraft for this program was an advanced trijet derivative of the DC-10, which provided the necessary design criteria, structural loads, and a representative structural arrangement for doors, windows, and manufacturing joints. The component selected for design-development was the fuselage barrel immediately forward of the wing (Figure 1-1). This section is 364 inches long with a constant 118.5-inch radius and two 42- by 76-inch passenger doors, a 104- by 68-inch cargo door, 26 windows, 17 full frames, 19 floor beams, and 103 longerons.

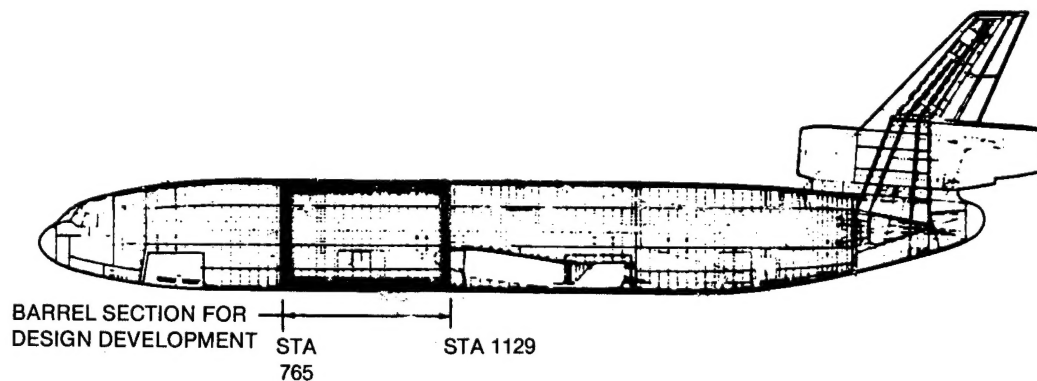


Figure 1-1. Baseline Fuselage Barrel

This report is limited to the description of test results of composite specimens and components containing joints and cutouts only. In concert with engineering activities, the manufacturing effort included establishing manufacturing criteria, developing tooling, and fabricating hardware. This manufacturing effort supported the test program and broadened the technology base for the fabrication and assembly of composite primary structure. The test program included four groups of test specimens, beginning with coupon specimens, progressing through increasingly larger and more complex specimens, and ending with two 4- by 5-foot curved fuselage panels.

SECTION 2 TEST PROGRAM

The program development plan encompassed a multifaceted engineering, manufacturing, and testing effort to develop the technology for fuselage joints and cutouts.

2.1 DESIGN CONCEPTS

The criteria selected contain the requirements of the applicable Federal Aviation Regulations Part 25 (FAR 25) with appropriate modifications consistent with the scope of this program. The criteria data are based on preliminary specifications for an advanced trijet derivative of the DC-10. All critical flight and ground conditions are included.

2.1.1 Composite Fuselage Barrel

The composite fuselage barrel has fewer longitudinal skin splices than the baseline, a reduction from 10 in the baseline to 4 in the composite design. Details of skin joints, cabin windows, doors, and structural features are shown in Figures 2-1, 2-2, and 2-3.

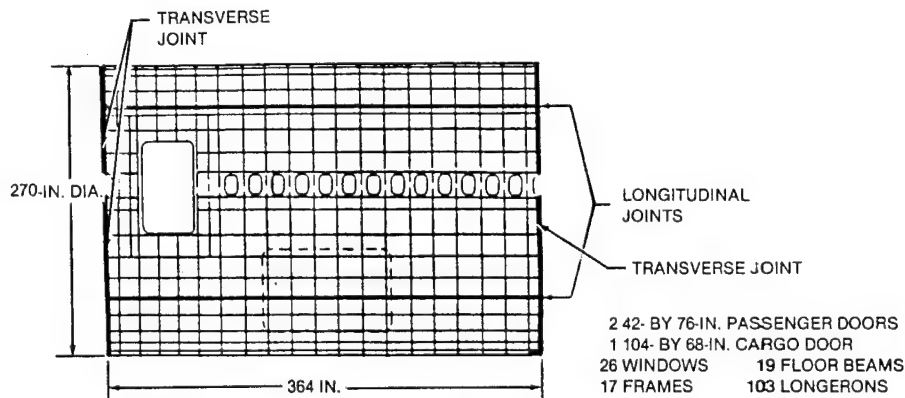


Figure 2-1. Joint and Cutout Locations

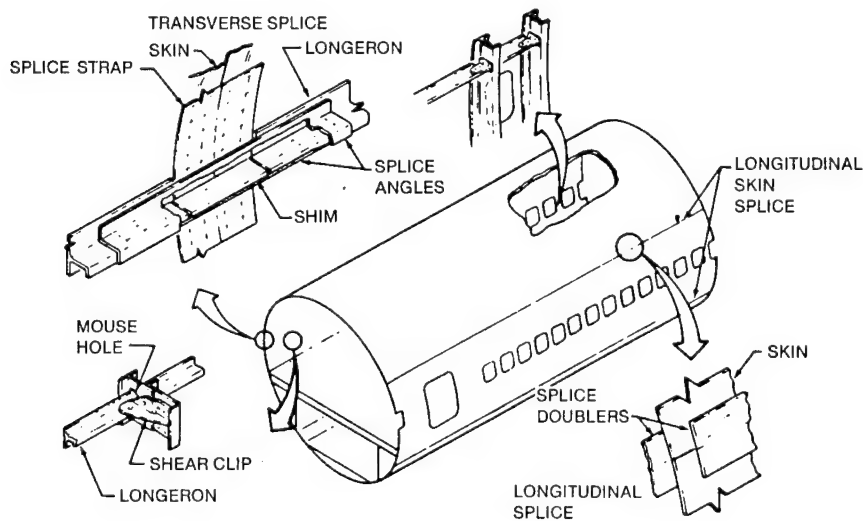


Figure 2-2. Structural Details

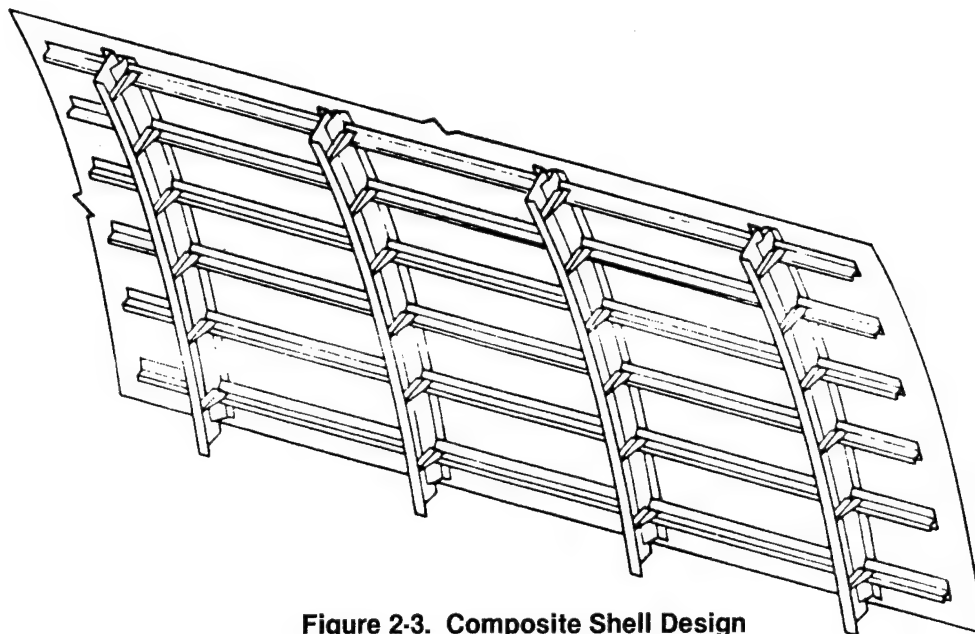


Figure 2-3. Composite Shell Design

The fuselage shell is composed of four discretely stiffened skin panel assemblies, which are mechanically joined with fasteners and splice members to form a complete barrel section. Longerons and shear-tees are secondarily bonded to the skin with FM-300 adhesive. Intersections between the longerons and frames are provided for by “mouse holes” in the shear-tees at each longeron location to allow the longeron to pass through. Stability of the shell is enhanced by a shear clip between the frame and longeron at each intersection. The floor beams, struts, frames, and shear-tees are joined by mechanical fasteners. The barrel section is joined to the nose and aft fuselage sections by mechanically fastened skin and longeron joints.

2.1.2 Longeron Concepts

Longerons are used throughout the fuselage to carry fuselage bending loads, to stabilize the skins from shear and compression buckling, and to provide additional residual strength for damaged skin panels. The same shape and height are generally used for all longerons.

Desirable features for the longeron configuration include a high bending rigidity (EI), flange and standing leg dimensions that permit installation of splice bolts, a cross-plyed pattern for adequate joint strength, and a convenient method for frame-to-longeron attachment at over 5,000 intersections. Attaching to the shear webs is preferable to attaching to the cap flanges. The skin flange must also be designed to sustain peel forces from pressure pillowing action. The results of the previous study (Reference 1) confirmed that the J-section longeron is the preferred configuration.

2.1.3 Skin Splices

The fuselage skin is spliced in the longitudinal direction at four locations, resulting in about 6,000 running inches of mechanically joined skin splice structure on the entire fuselage. The fuselage shell has five transverse splices to allow the manufacture of barrel sections with a practical size for assembly and handling. The five splices produce a total of 3,700 running inches of skin splice plus 103 longeron splices at each of the five locations.

2.1.4 Passenger Door Cutout

Two basic concepts were initially formulated and evaluated. These concepts, shown in Figure 2-4, were

(A) discrete stiffeners and (B) honeycomb. The discrete stiffener concept was nearly equivalent to the honeycomb in terms of structural efficiency and ease of manufacture, and was selected primarily on the basis of its freedom from moisture entrapment, which can cause structural damage, and its ease of inspection.

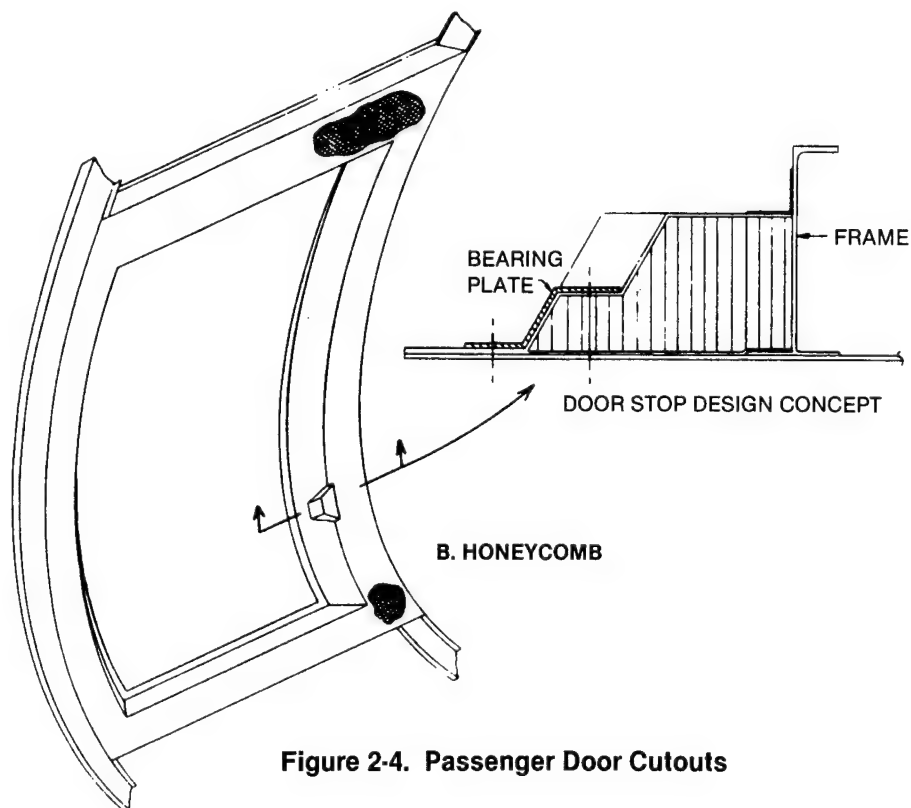
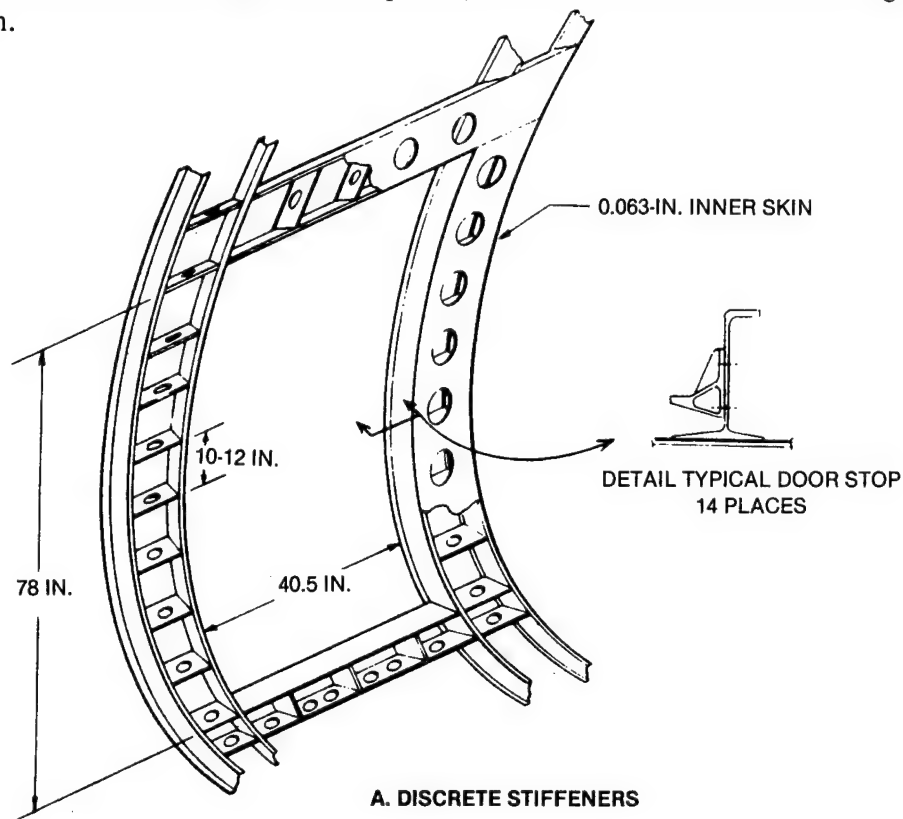


Figure 2-4. Passenger Door Cutouts

2.1.5 Cabin Window Cutout

The cabin window cutout concept is essentially the baseline airplane arrangement. The aluminum skin and doublers are replaced by carbon-epoxy skin and doublers (Figure 2-5).

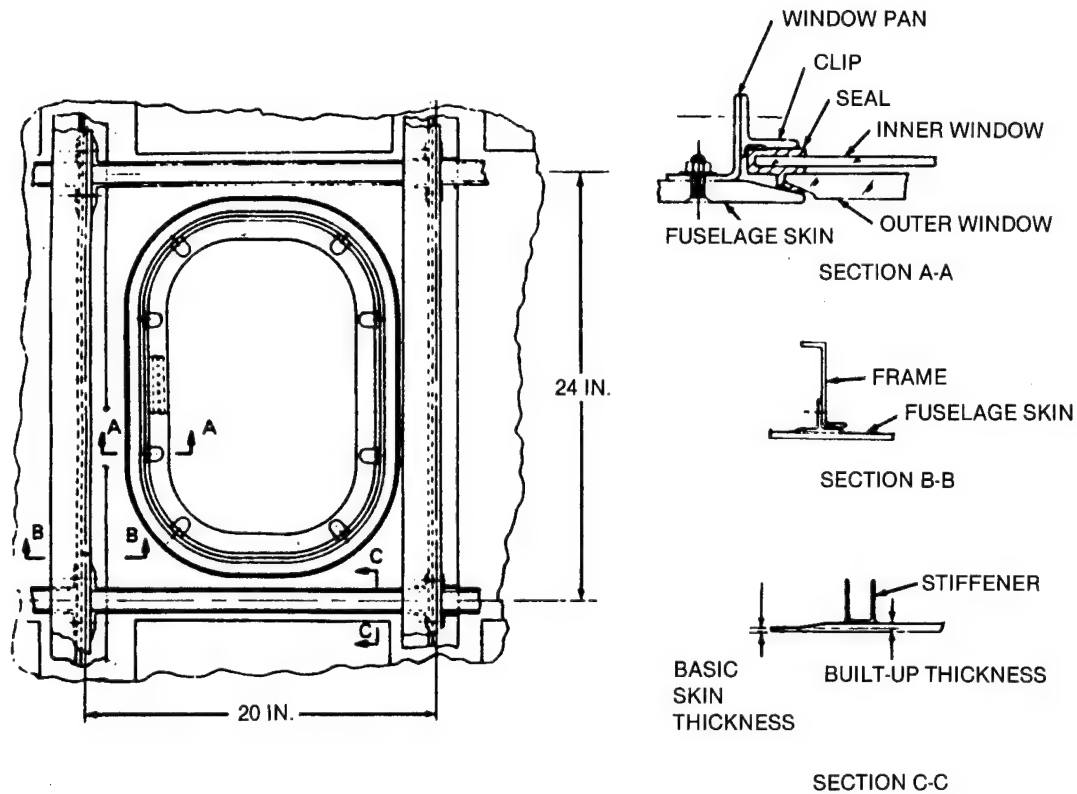


Figure 2-5. Cabin Window Structural Concept

2.2 MATERIAL SELECTION

The basic material system selected for this program was Hexcel F584 resin on 12K IM6 graphite fiber. The fiber areal weights for the tape and cloth were 0.267 lb/yd² and 0.682 lb/yd², respectively. The cloth is a five-harness satin weave. The F584 resin system has shown good processing characteristics as well as acceptable mechanical, environmental, and toughness properties. The tape was used primarily for skin panels, doublers, splice members, and longerons. The cloth was used primarily for shear-tees and frame sections.

Some E-glass 120-weave cloth and S2-glass unidirectional tape material were incorporated for softening the corner regions around some of the specimen cutouts. Frame/longeron shear clips were injection-molded with chopped graphite fiber-PEEK resin material. Some Group A tension and compression-after-impact specimens incorporated the lightning protection materials listed in Table 2-1.

2.3 DEVELOPMENT SPECIMENS

The development specimens were divided into four different groups: A, B, C, and D. The purpose of the Group A specimens was to yield monolayer data for the chosen material systems, as well as laminate data for four typical lay-up patterns utilized in the design of fuselage barrel (Table 2-2). The Group B specimens were intended to provide basic data for correlation/calibration of the analysis methods for

Table 2-1
Lightning Protection Materials

SPECIMEN	WIRE-WOVEN	NICKEL-COATED
PROTECTION SYSTEM	8-MIL-DIA ALUMINUM WIRE, 1/8-IN. CENTERS, WARP AND FILL	NICKEL-COATED GRAPHITE FIBER
WEAVE	FIVE-HARNESS SATIN, GRAPHITE FIBER	PLAIN WEAVE, GRAPHITE FIBER
WEIGHT, CURED	0.206 LB/FT ²	0.168 LB/FT ²
RESIN	F584 EPOXY RESIN	F584 EPOXY RESIN
SUPPLIER	CIBA-GEIGY	AMERICAN CYANAMID

Table 2-2
Graphite Laminate Descriptions

NUMBER	DESCRIPTION	LAY-UP PATTERN
1	BASIC SKIN (ALL TAPE) t = 0.0684 IN.	(0,90,45,0, - 45,90) _s
2	REINFORCED SKIN (ALL TAPE) t = 0.0912 IN.	(0,90,45, - 45,0,45, - 45,90) _s
3	REINFORCED LONGERON (CLOTH AND TAPE) t = 0.1476 IN.	(0/90,0,0, ± 45,0,0,0/90) _s
4	BASIC LONGERON (ALL CLOTH) t = 0.102 IN.	(0/90, ± 45,0/90) _s

cutouts and frame shear-tees attached to fuselage skins. The Group C specimens were intended to serve as a design selection/screening tool. The areas of investigation for this group included longitudinal and transverse skin splices, and longeron runout or termination at a typical frame adjacent to a door jamb. In addition, a transverse skin/longeron splice was included. The Group D specimens included a transverse skin splice and a cabin window panel.

2.3.1 Group A

The Group A specimens included unnotched and open hole tension, unnotched and open hole compression, single- and double-lap shear, compression-after-impact, and biaxial stress configurations (Figures 2-6 through 2-9). Specifically, the data included basic monolayer properties, laminate allowables and stiffness, load-deflection and strength properties for joints, and damage tolerance properties including resistance to impact damage and lightning strike.

NAME	ID	QTY	
MONOLAYER TENSION (MLT) GRAPHITE 0/TAPE IM6 GRAPHITE 90/TAPE IM6 GRAPHITE 0/90/CLOTH IM6 E GLASS, NO BLEED E GLASS, BLEED S2 TAPE, NO BLEED S2 TAPE, BLEED GLASS CLOTH, NO BLEED GLASS CLOTH, BLEED	-501 -503 -505 -507 -509 -511 -513 -515 -517	3 3 3 3 3 3 3 3 3	
UNNOTCHED TENSION (UNT) GRAPHITE LAY-UP NO. 1 GRAPHITE LAY-UP NO. 2 GRAPHITE LAY-UP NO. 3 GRAPHITE LAY-UP NO. 4	-501 -503 -505 -511	3 3 3 3	
GRAPHITE LAY-UP NO. 1 NICKEL-COATED LIGHTNING PROTECTION GRAPHITE LAY-UP NO. 1 ALUMINUM WIRE-WOVEN LIGHTNING PROTECTION	-507 -509	3 3	
GRAPHITE LAY-UP NO. 1 GRAPHITE LAY-UP NO. 2 GRAPHITE LAY-UP NO. 3 GRAPHITE LAY-UP NO. 4	-513 -515 -517 -519	3 3 3 3	
UNLOADED HOLE TENSION (ULT) GRAPHITE LAY-UP NO. 4 GRAPHITE LAY-UP NO. 2 GRAPHITE LAY-UP NO. 3 GRAPHITE LAY-UP NO. 2 COUNTERSUNK GRAPHITE	-501 -503 -505 -507 -509	3 3 3 3 3	

Figure 2-6. Group A Tension Specimens

NAME	ID	QTY	
MONOLAYER COMPRESSION (MLC) GRAPHITE 0/TAPE IM6 GRAPHITE 90/TAPE IM6 GRAPHITE 0/90/CLOTH IM6 E GLASS, NO BLEED S2 TAPE, BLEED GLASS CLOTH, BLEED UNNOTCHED COMPRESSION (UNC) GRAPHITE LAY-UP NO. 1 GRAPHITE LAY-UP NO. 2 GRAPHITE LAY-UP NO. 3 GRAPHITE LAY-UP NO. 4	-501 -503 -505 -507 -509 -511 -501 -503 -505 -507	3 3 3 3 3 3 3 3 3 3	
UNLOADED HOLE COMPRESSION (ULC) LAY-UP NO. LOOSE-FIT 5/32-IN. BOLT 4 LOOSE-FIT 5/32-IN. BOLT 2 LOOSE-FIT 5/32-IN. BOLT 3 NET-FIT 3/16-IN. BOLT 4 NET-FIT 3/16-IN. BOLT 2 NET-FIT 3/16-IN. BOLT 3 COUNTERSUNK NO FASTENER 2 COUNTERSUNK NET-FIT 3/16-IN. BOLT 2	-513 -515 -517 -519 -521 -523 -525 -527	3 3 3 3 3 3 3 3	
COMPRESSION AFTER IMPACT (CAI) IMPACT AT 4 FT-LB 0.50-IN.-DIA HOLE SUBJECTED TO LIGHTNING — ALUMINUM WIRE-WOVEN PROTECTION SUBJECTED TO LIGHTNING — NICKEL-COATED PROTECTION SUBJECTED TO LIGHTNING — UNPROTECTED	-501 -503 -505 -507 -509	3 3 3 3 3	

Figure 2-7. Group A Compression Specimens

NAME	ID	QTY	
SHEAR SPECIMEN, 45 DEG OFF-AXIS (MLS) MONOLAYER SHEAR (MLS) GRAPHITE TAPE IM6 GRAPHITE CLOTH IM6 E GLASS, NO BLEED E GLASS, BLEED S2 TAPE, BLEED	- 501 - 503 - 505 - 507 - 509	3 3 3 3 3	
SINGLE-LAP TENSION (SLT) W/D = 3 COUNTERSUNK W/D = 10 COUNTERSUNK W/D = 3 PROTRUDING HEAD W/D = 3 COUNTERSUNK W/D = 10 COUNTERSUNK	- 501 - 503 - 505 - 507 - 509	3 3 3 3 3	
DOUBLE-LAP TENSION (DLT) LAY-UP NO. W/D = 3 W/D = 3 W/D = 3 COUNTERSUNK W/D = 6 W/D = 6 W/D = 6 COUNTERSUNK	4 2 3 - 525 4 2 3 - 527	3 3 3 3 3 3 3 3	
DOUBLE-LAP COMPRESSION (DLC) LAY-UP NO. W/D = 3 W/D = 3 W/D = 3 W/D = 6 W/D = 6 W/D = 6 SPLICE MEMBER COUNTERSUNK W/D = 3 SPLICE MEMBER COUNTERSUNK W/D = 6	4 2 3 4 2 3 2 2 - 531	3 3 3 3 3 3 3 3 3	

Figure 2-8. Group A Shear and Shear Joint Specimens

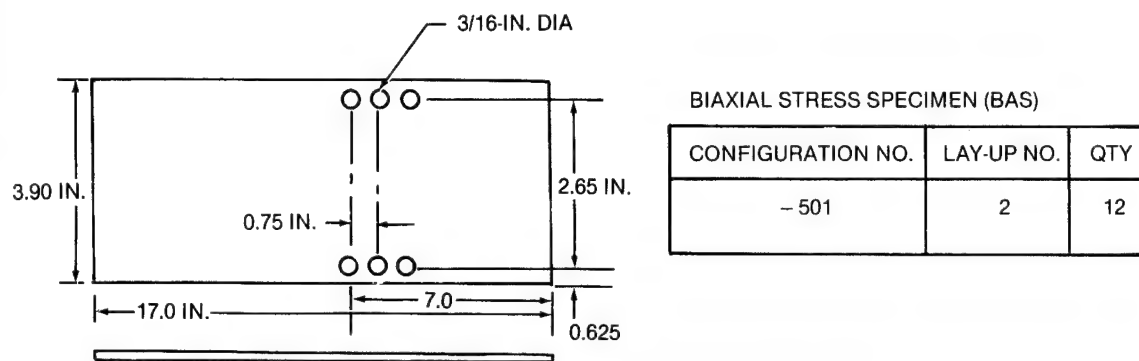
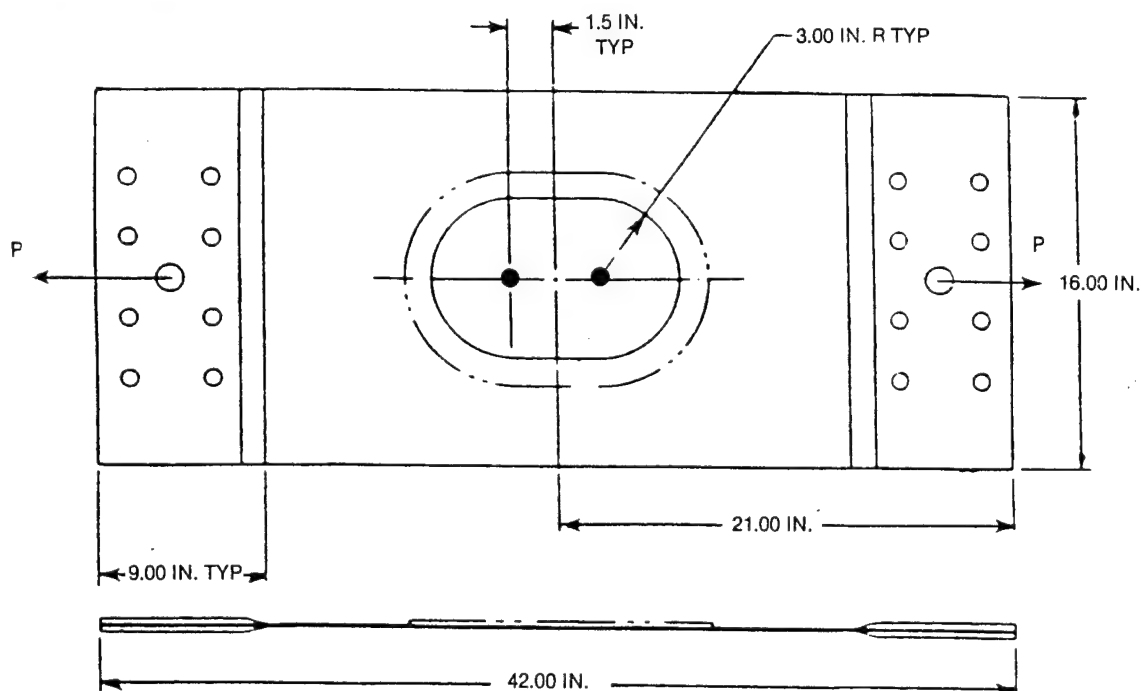


Figure 2-9. Group A Biaxial Stress Specimen

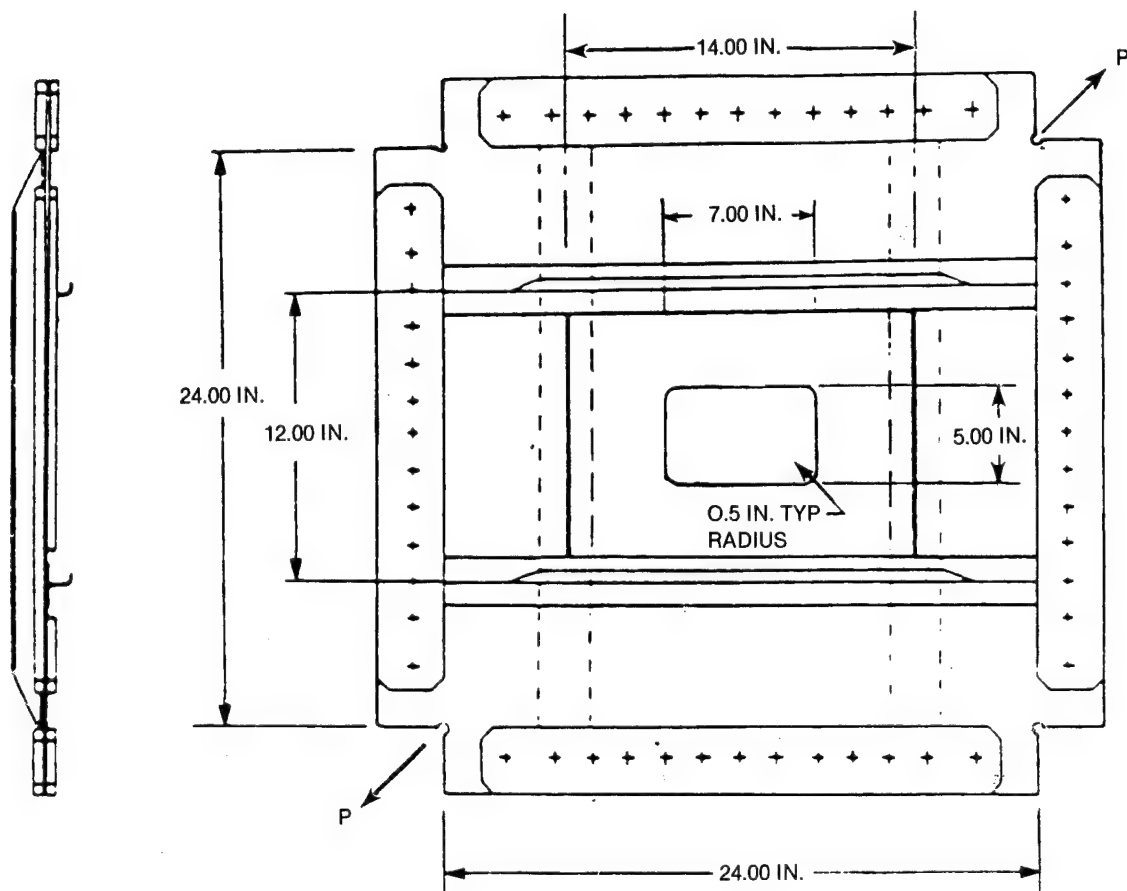
2.3.2 Group B

The test specimens in tension and shear and the shear-tee pull-off configurations are shown in Figures 2-10 through 2-12. The cutout specimens were used to evaluate the effects of stress concentrations due to large cutouts. The shear-tee pull-off specimens provided data to evaluate the behavior of six shear-tee/skin configurations.



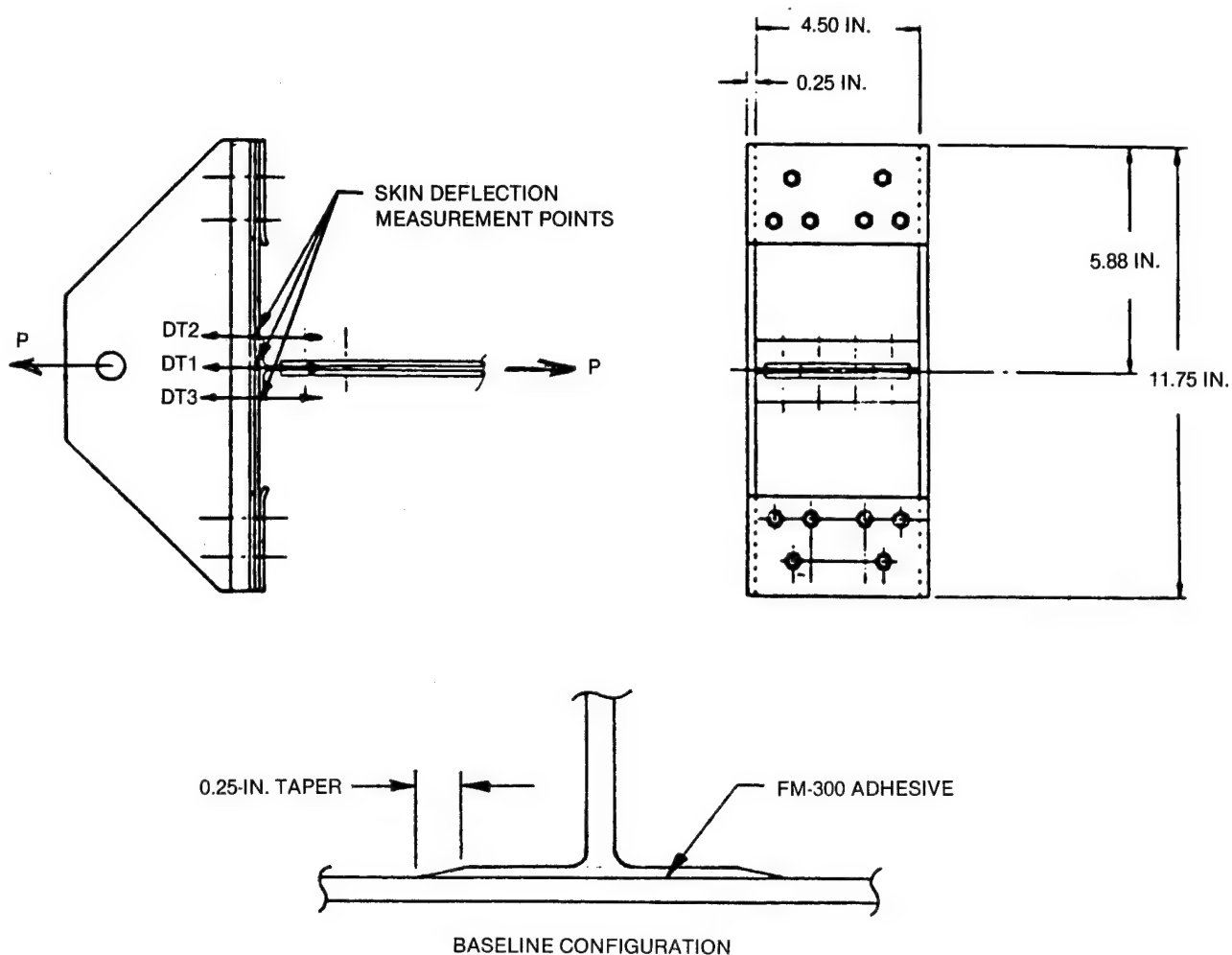
CONFIGURATION	DESCRIPTION (B-B)	QTY
-501	BASLINE (NO REINFORCEMENT)	1
-503	SOFTENED WITH E GLASS IN 0/90 DIRECTION	1
-505	BUILDUP AROUND CUTOUT WITH G/E	1
-507	FULLY SOFTENED WITH E GLASS	1
-509	SOFTENED WITH S2 GLASS IN 0/90 DIRECTION	1
A-A LAY-UP IS LAY-UP NO. 2 (PAD-UP SKIN) (0/90/45/ - 45/0/45/ - 45/90)		

Figure 2-10. Group B Unstiffened Cutout Tension Panels



CONFIGURATION	DESCRIPTION (B-B)	QTY
-501	BASELINE (NO REINFORCEMENT)	1
-503	S2 GLASS, ± 45 -DEG PLIES	1
-505	GRAPHITE BUILDUP	1
A-A LAY-UP IS LAY-UP NO. 2 (PAD-UP SKIN) (0/90/45/ - 45/0/45/ - 45/90/90/ - 45/45/0/ - 45/45/90/0)		

Figure 2-11. Group B Stiffened Cutout Shear Panels



ID		QTY
- 501	ADDITIONAL 0/90 PLY ACROSS FLANGES	3
- 503	BASELINE	3
- 505	TAPERED FLANGES	3
- 507	"SOFT" TEE (REDUCED FLANGE THICKNESS)	3
- 509	AF-163 ADHESIVE	3
- 511	FOUR 90-DEG PLYS EMBEDDED IN SKIN	3

Figure 2-12. Group B Shear-Tee Pull-Off Specimens

2.3.3 Group C

The Group C specimens included longitudinal and transverse skin splices, longeron runout at a fuselage frame, and a transverse skin/longeron splice (Figures 2-13 through 2-17). These specimens provided data on selected design concepts representative of actual fuselage structure. Representative portions of joints and splices generated durability and static strength data.

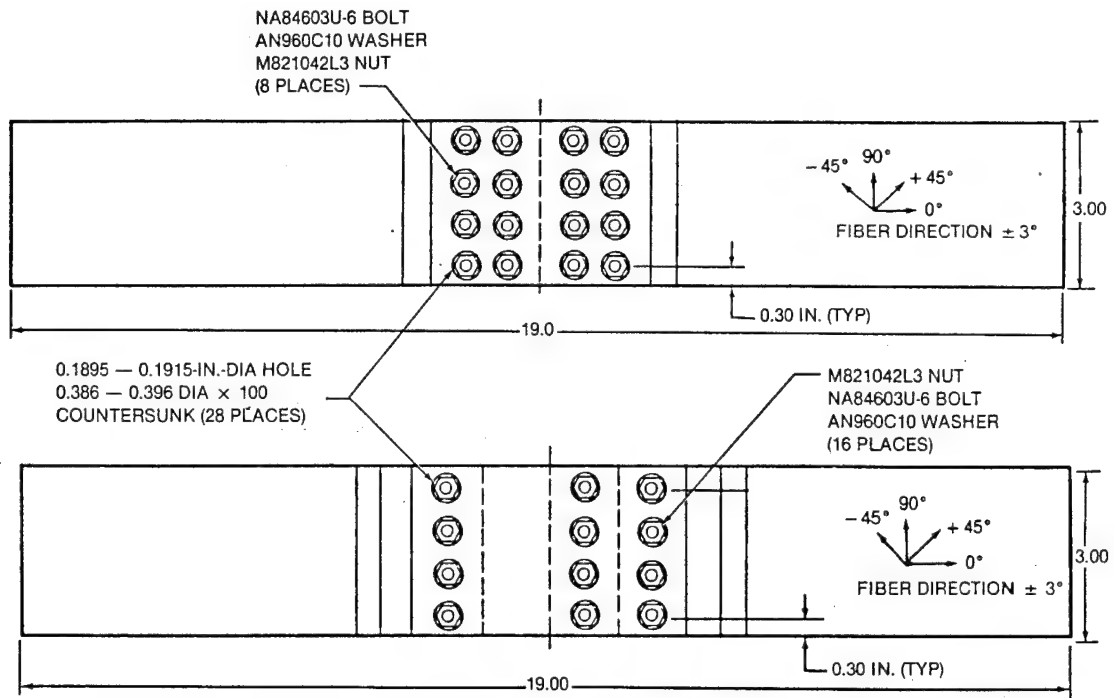


Figure 2-13. Group C Longitudinal Skin Splice Specimens (see Figure 2-14)

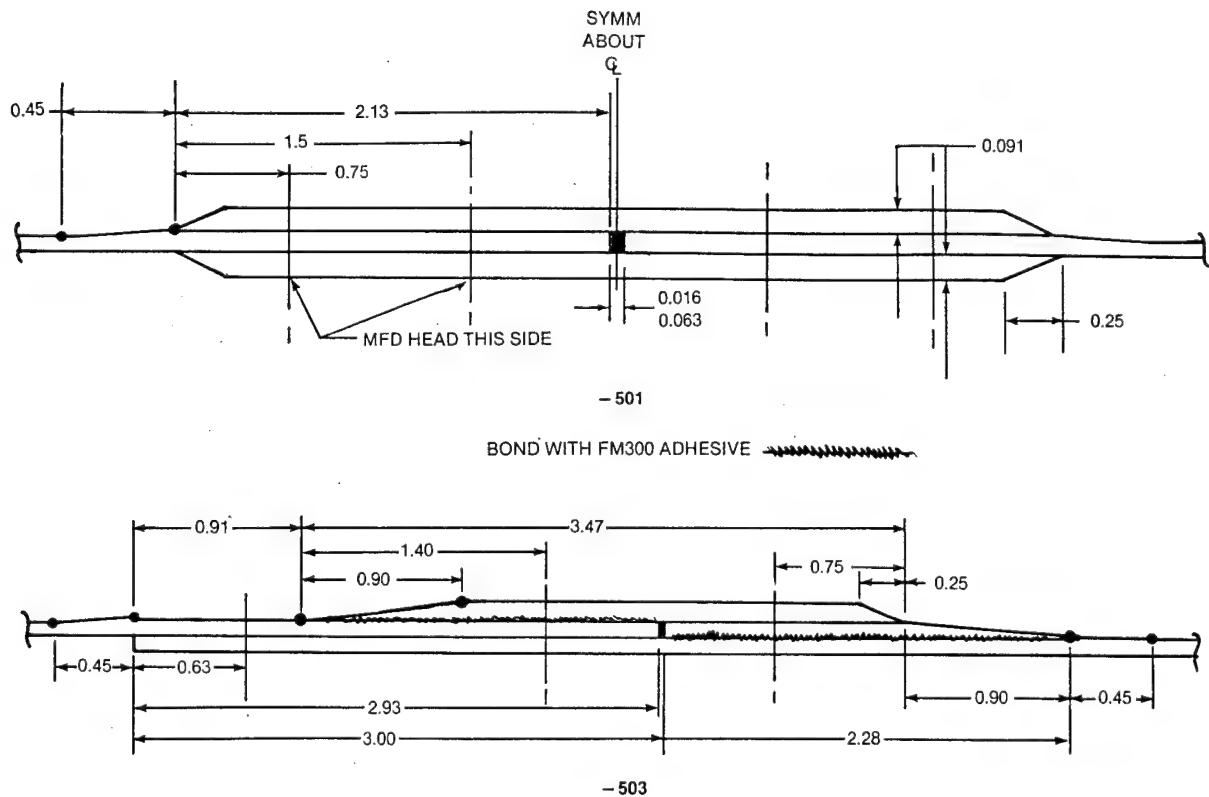


Figure 2-14. Details of Longitudinal Splice Joints

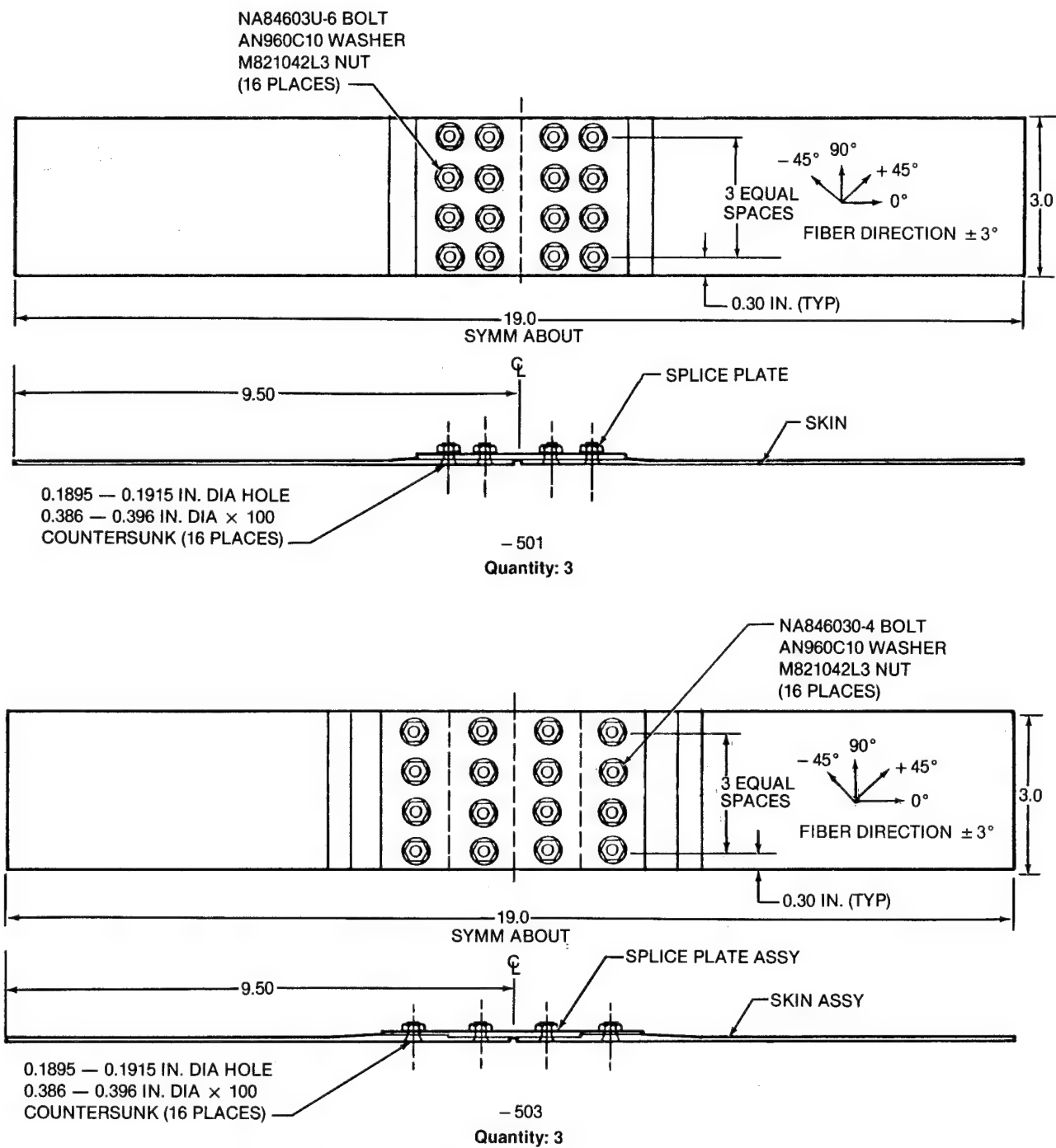


Figure 2-15. Group C Transverse Skin Splice Specimens

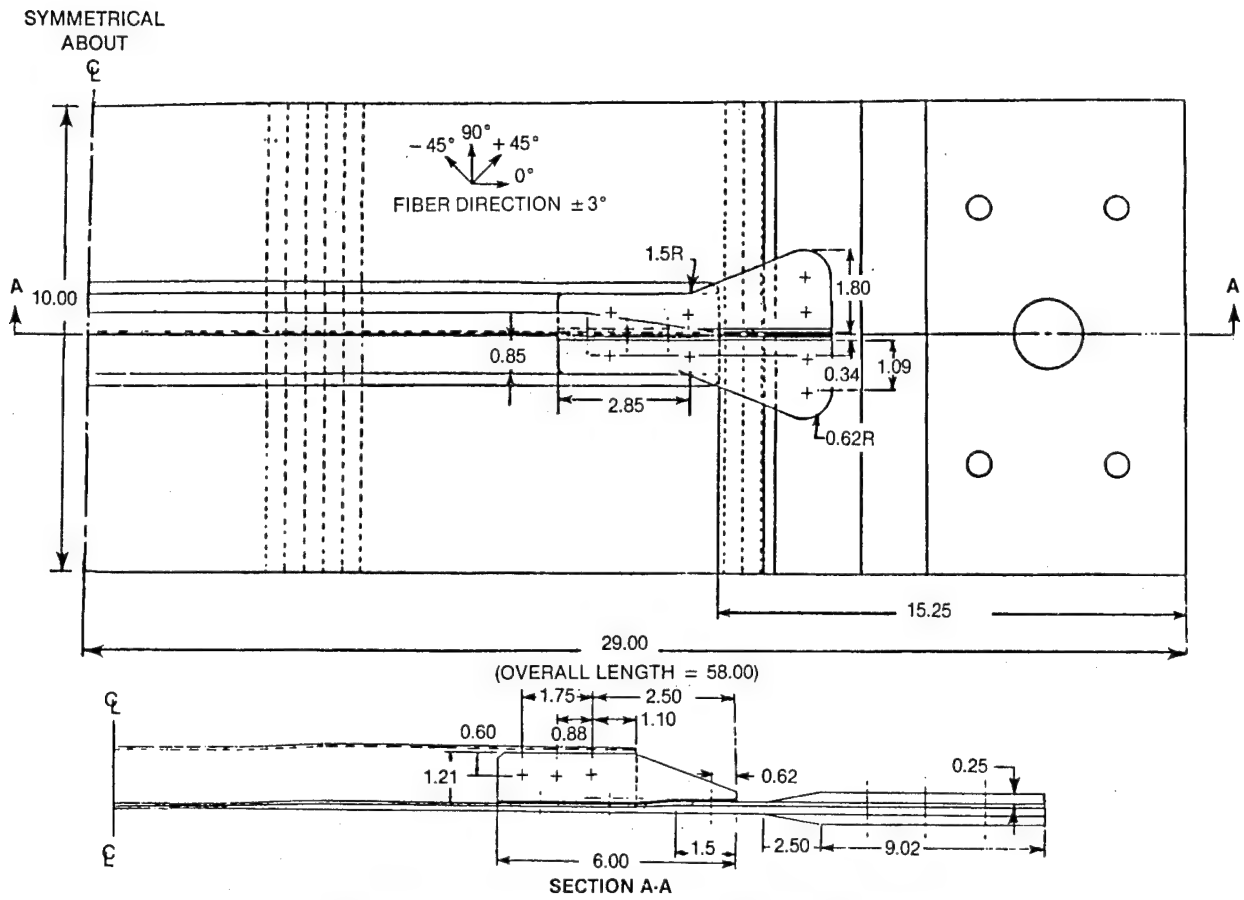


Figure 2-16. Group C Longeron Runout Specimen

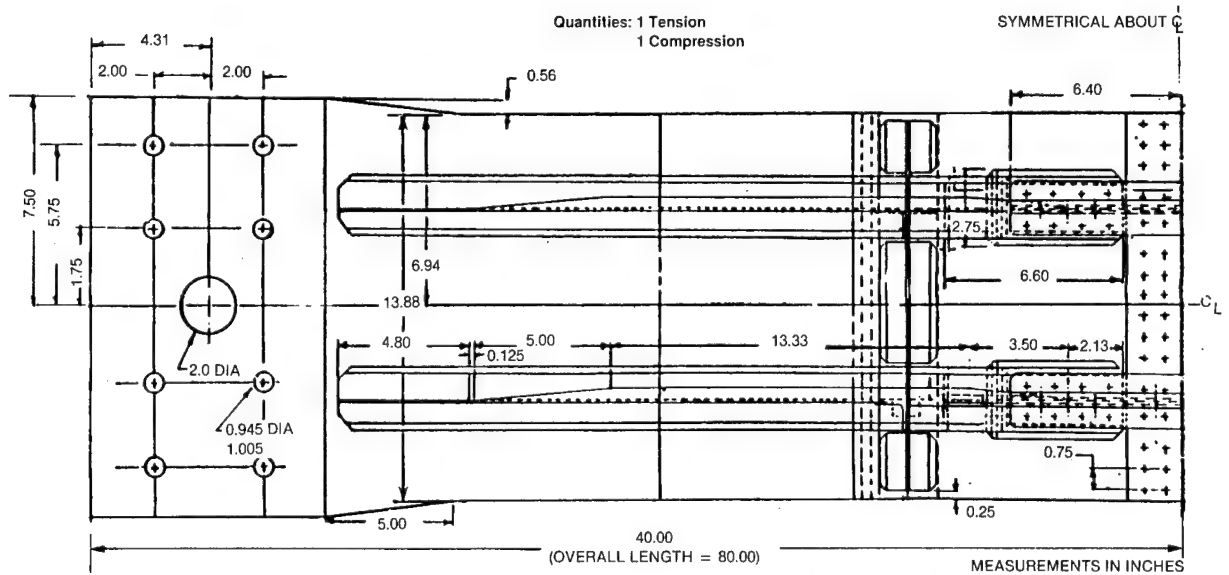


Figure 2-17. Group C Transverse Skin/Longeron Splice Panel

2.3.4 Group D

The two curved fuselage panels in this group included a panel with a transverse skin splice and another panel with two cabin window cutouts. Each panel was approximately 4 feet wide by 5 feet high with a radius of curvature of 135 inches (Figures 2-18 and 2-19). These specimens provided data on curved fuselage panels that were representative of actual fuselage structure. Each panel provided a complete set of strain-gage data, deflection measurements, and corresponding loads.

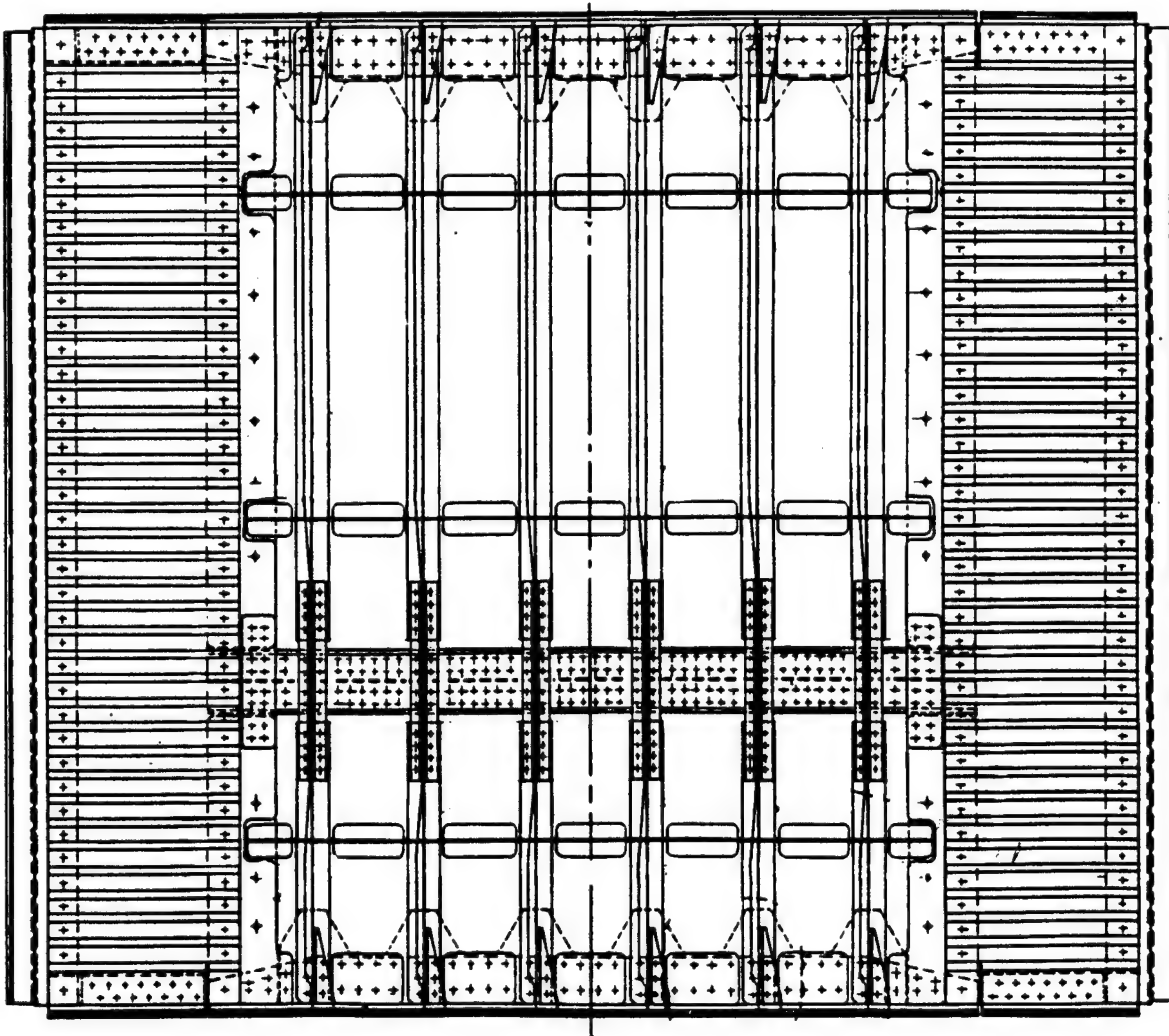


Figure 2-18. Transverse Splice Shear Interaction Panel

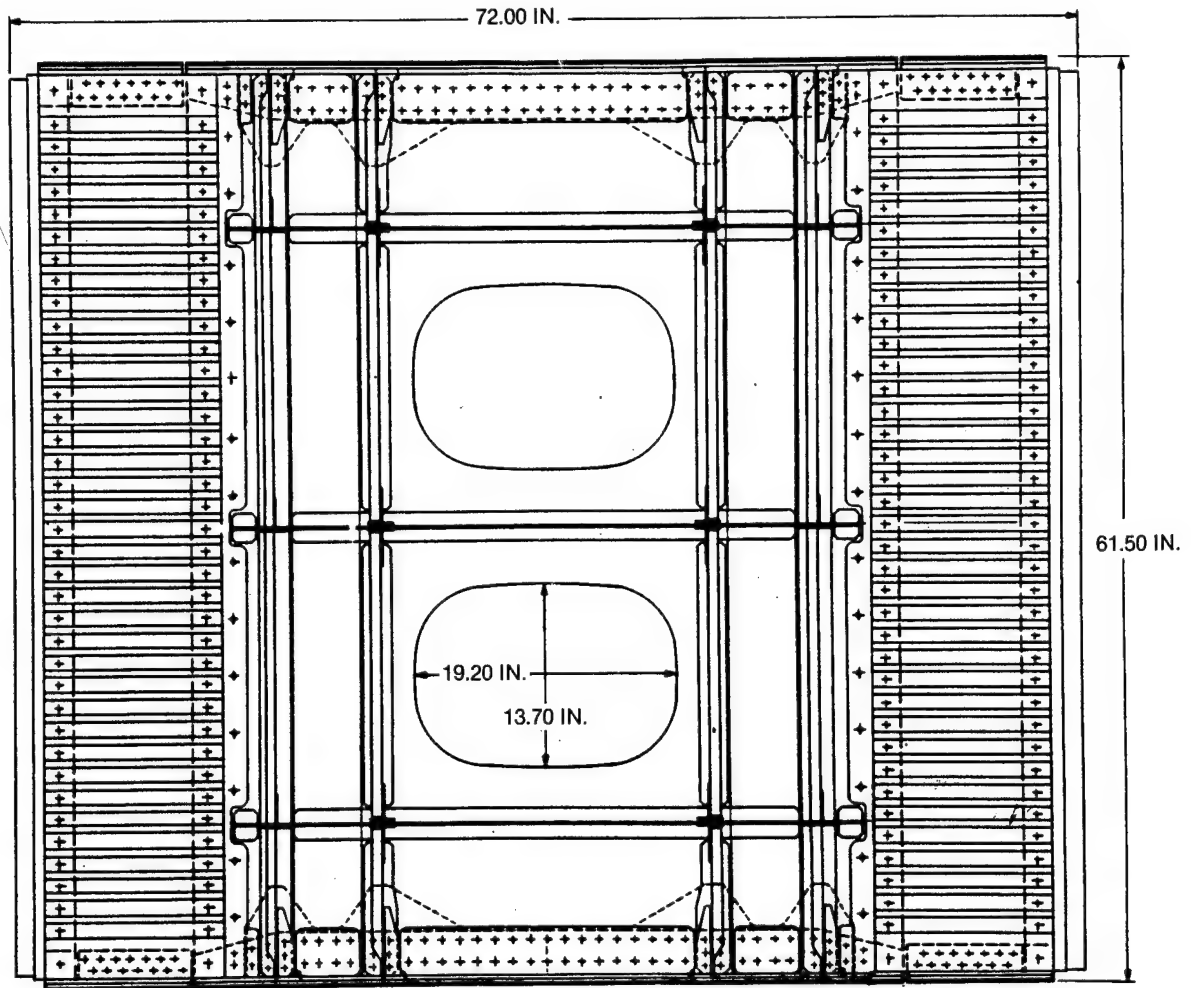


Figure 2-19. Passenger Window Belt Shear Interaction Panel

SECTION 3 TEST ARTICLE MANUFACTURING

3.1 PROCESS TECHNOLOGY

3.1.1 Lay-Up Procedures

The composite details fabricated during this program were laid up by hand using ply alignment templates or measured edge guides (where needed) for proper placement of drop-offs and buildups. After placement of each ply, release paper was removed, and flexible polyethylene squeegees or teflon bars were used to compact and smooth out the added ply. After every 12 plies, the panel was subjected to 15-psi vacuum pressure for 15 minutes at room temperature. When Group C splice specimens were fabricated, an extra densification period was provided during the cure cycle because the panels were over 0.60 inch thick and contained 108 plies in some areas.

More complex items with cross sections such as tees and zeos were densified at 100 psi for 15 minutes every four plies when problems with conformability developed. The tack properties of the F584 resin systems were found to diminish noticeably at temperatures below 67°F. In addition, as material out-time at ambient temperature exceeded 48 hours, tack diminished markedly. A hot-air gun was used occasionally to improve tack and conformability in problem areas. For lay-ups expected to exceed 2 working days, the procedure was to place the roll of material in the freezer each night in order to maintain the tackiness of the prepreg. Frozen material was allowed to warm up to ambient temperature before removal from the sealed polyethylene bag in order to prevent moisture from condensing on the material.

3.1.2 Autoclave Curing

In order to evaluate the planned process cure cycle, a 24-ply, 24- by 24-inch test panel was fabricated and cured using the following cure cycle:

- a. Apply 100-psi pressure at start of part heat-up.
- b. Heat to 350°F at a rate of 2° to 5°F per minute.
- c. Hold at 350°F and 100 psi for 120 minutes.
- d. Cool to 150°F, maintaining 100-psi pressure.
- e. Dump pressure.

The bagging technique and materials used are shown in Figure 3-1. The laminate was bagged to prevent resin loss during low-viscosity periods of the cure cycle. In the no-bleed bagging process, the panel is placed between two layers of separator release film. Resin can only exit the panel via single yarns, which inhibit resin transfer but allow the escape of volatiles. On larger panels, fine perforations were made in the separator film, allowing volatiles to be drawn from central areas of the part into the breather cloth above the separator film. The holes were sufficiently fine to prevent resin loss from the part.

The computerized process control program utilized for these and other F584/IM6 panel cures calls for a part heat-up rate of 5°F per minute with a tolerance of $\pm 3^\circ\text{F}$. For most panels, this heat-up rate continues until the cure temperature, 350°F, is reached. For a panel such as the splice panel, which has extensive ply buildups and a high ply count, a densification phase at 160°F is required to prevent porosity. This densification, seen in Figure 3-2, lasts 30 minutes, at which point part heat-up is resumed. The autoclave, at a slightly higher temperature than the part, can be seen driving the part temperature up in a controlled fashion. With the straight-up pressure program, the pressure is held constant at 100 psi from the beginning of part heat-up until the part has cured and cooled down to 150°F. This straight-up cure is

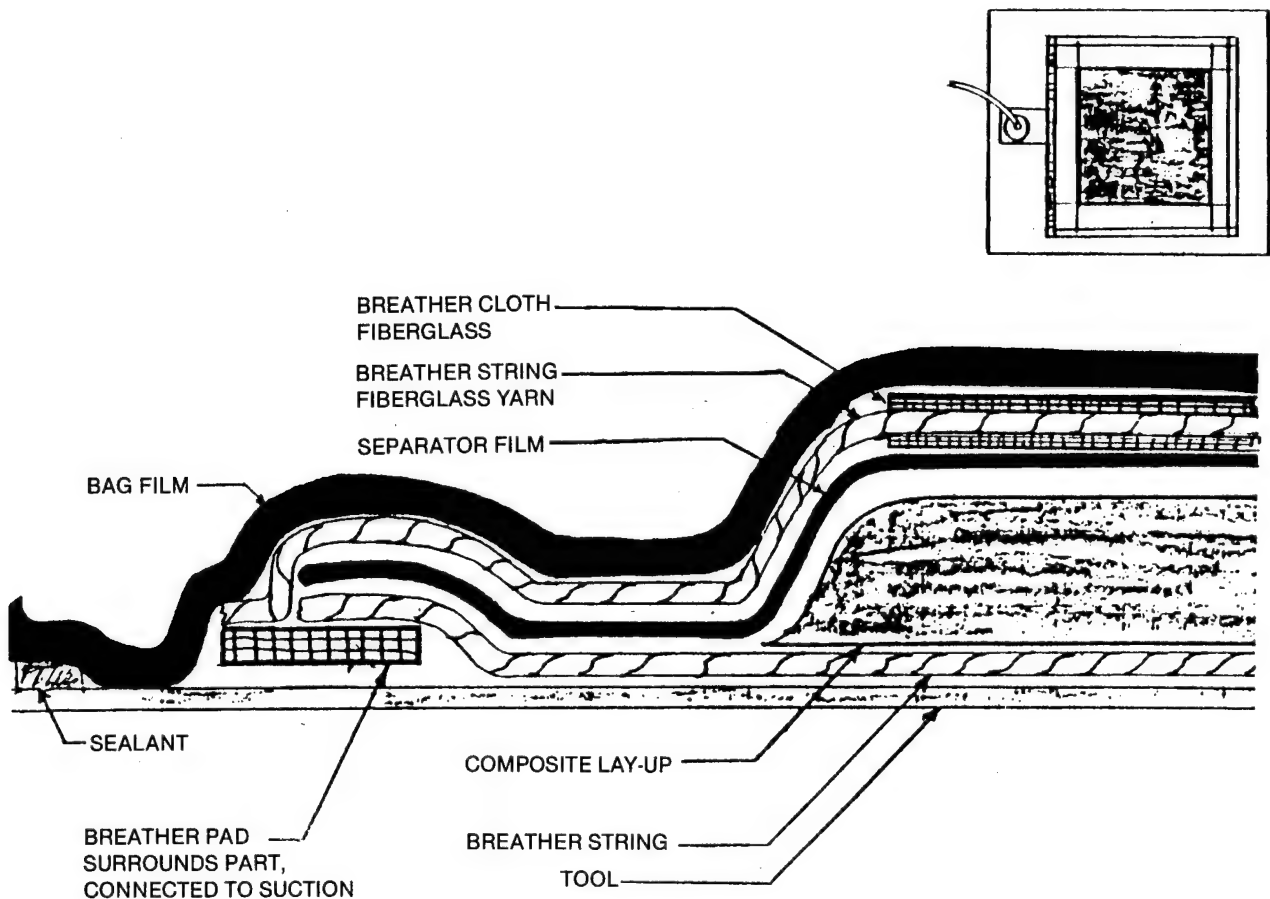


Figure 3-1. No-Bleed Bagging Method

made possible by the low-flow nature of the F584 resin system. There are several advantages to this procedure. By achieving full cure pressure prior to actual part curing, the integrity of the bag can be tested and corrected without damage to the panel. Also, elevated pressure early in the cure densifies the lay-up and provides more opportunity for trapped air and volatiles to escape. Finally, it is not necessary for an operator to wait for a certain viscosity window before high pressure is introduced, as is done with lower viscosity resin systems.

3.1.3 Adhesive Bonding

Adhesive bonding methods are crucial to the successful fabrication of the more complex composite fuselage panels. The attachment of longeron, shear-tee, and various splice specimen components was accomplished using FM 300, a modified epoxy film adhesive system, which cures at 350°F and 50-psi pressure for 60 minutes. It is a high-flow adhesive, exhibiting 350- to 450-percent flow, making it especially suited to secondary bonding. A knitted tricot carrier is incorporated into the adhesive film for good bondline thickness control. The precured nominal film weight is 0.081 lb/ft². The thickness is 0.013 inch before cure and approximately 0.007 inch after cure. Service temperature for this adhesive is -67°F to 300°F. The minimum shear strength at 75°F is 4,400 psi. The adhesive has shown excellent resistance to aircraft de-icing fluids, hydraulic fluids and oils, and salt spray. Pressure is applied for clamping purposes and to eliminate volatile entrapment as the adhesive cures.

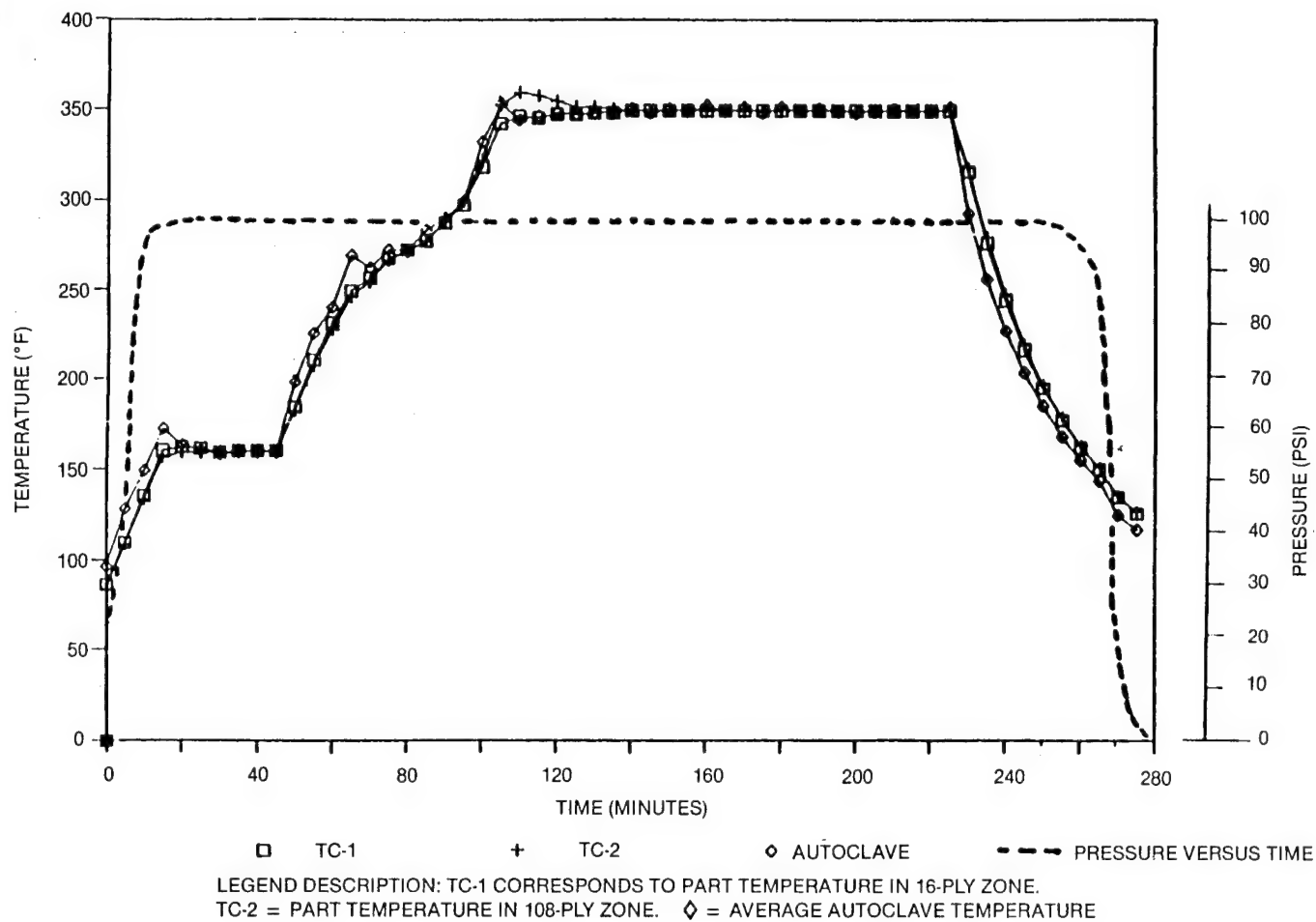


Figure 3-2. Autoclave Cure Cycle for F584/IM6 Laminate

Faying surfaces of the details to be bonded must first be cleaned with solvent to eliminate oils and greasy contamination. Next, grit-blasting of the laminate surfaces is conducted in order to abrade the glossy epoxy surface so that intimate chemical bonding can take place between the adhesive and epoxy skin. Aluminum oxide No. 280 grit is sprayed with 40-psi gun pressure in a sweeping motion without damaging fibers.

The completeness of surface roughening is determined by wetting the faying surface with deionized water, holding it in the horizontal position, and then checking to see that an unbroken film of water is maintained for 60 seconds. Following water-break inspection, the wetted surface is thoroughly dried with a hot-air gun or hot-air oven.

Following surface preparation, the adhesive film is sandwiched between the faying surfaces. The assembled parts are secured during cure to prevent dislocation. The assembly is vacuum-bagged and cured for 60 minutes at 350°F and 50 psi. Flashbreaker film is applied where needed to minimize flash attachment in critical areas.

3.1.4 Machining and Hole Drilling

The nonhomogenous, layered nature of graphite composites and the hardness of the carbon reinforcement create a need for special cutting and drilling procedures. The tools most commonly used for cutting through graphite-epoxy with maximum efficiency and minimum wear are made of carbide steel or have sintered diamond cutting surfaces. Specimens in this program were cut using a rotating diamond-impregnated cutting disk. The cutting is actually accomplished by a grinding action.

A diamond-impregnated router bit was used in conjunction with a template to create large cutouts in composite test panels. Holes in the 3/16-inch-diameter range, for example, were best drilled at approximately 1,200 to 1,600 rpm. Holes in the splice specimens were created by first opening up the holes to within 1/64 inch of the required diameter, and then final-sizing the holes with a carbide steel reamer. Carbide twist drills were substituted for spade drills on occasion. Cobalt steel bits were also used for the first stage of drilling in noncritical holes. Composite phenolic backup boards were firmly clamped to the rear side of panels to prevent rear surface ply damage upon drill breakthrough. Countersinks were accomplished using countersinking tools with a single carbide steel blade insert. Countersinking spindle speeds were between 800 and 1,000 rpm. A Freon coolant was used during drilling operations.

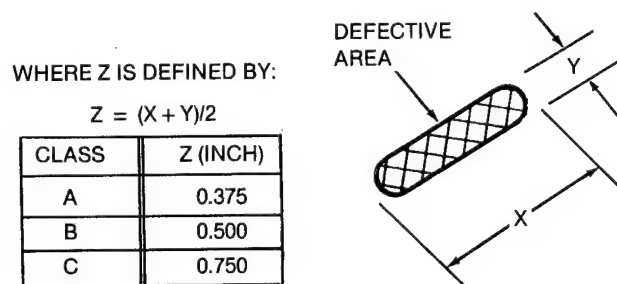
For details joined by mechanical fasteners, pilot holes were drilled to serve as cleco points for clamping. Specifics on drilling and assembly sequences for each assembly step are discussed in the appropriate sections.

3.1.5 Quality Inspection Methods

Nondestructive inspection of the fuselage test panels was conducted using several techniques, after which defects were evaluated and accepted or rejected on a case-by-case basis. Cured panels were visually inspected for edge delaminations, dry spots, and wrinkles. Bonded details were inspected for discontinuities in fillets and for fillets that were frothy or discolored. The thickness of each specimen was measured, and from this an average ply thickness was calculated and compared to the expected value. The cured, per-ply thickness range for the F584/IM6 tape was 0.0055 to 0.0059 inch. For cloth, the range was 0.0165 to 0.0175 inch per ply. Unacceptably low or high resin contents, as well as missing plies, could easily be detected this way. In some cases, ply count and orientation of a cured laminate were checked by removing a portion of material from a trim area, burning off the matrix, and then carefully checking the ply orientation and count of individual plies as they were removed.

Process requirements for the F584/IM6 tape material used in this program allowed a void content of no more than 2 percent and a resin content of 34 ± 2 percent for the tape and 39 ± 2 percent for the cloth. The average tape void content was under 1.0 percent. The average cloth void content was about 1.8 percent. Resin content was routinely determined by a percentage comparison between the weight of the cured laminate and the weight of fibers collected following nitric acid digestion of the matrix.

Skin panels were inspected for internal defects using ultrasonic through-transmission C-scan. To pass accept/reject criteria, the maximum flaw dimension ($x + y$) could not exceed 0.75 (Figure 3-3 Class C). Isolated groups below the above size were still unacceptable if they were less than 0.750 inch apart. Density limitations of minute defects under 0.10 inch are indicated in Table 3-1.



NOTE: Y IS THE MAXIMUM PROJECTED WIDTH MEASURED ACROSS THE DEFECT (DELAM, VOID, OR UNBOND) IN THE NARROW DIRECTION AS SHOWN IN THE SKETCH; X IS THE PROJECTED DEFECT LENGTH MEASURED PERPENDICULAR TO Y.

Figure 3-3. Defect Size Limitations

**Table 3-1
Limitations on Clumped Scattered Defects**

CLASS	PART L/W * RATIO EQUAL TO OR GREATER THAN 10/1	PART L/W * RATIO LESS THAN 10/1
	MAXIMUM DEFECT AREA FOR EACH 10 IN. ²	MAXIMUM DEFECT AREA FOR EACH 24 IN. ²
A	10% OR 1.0 IN. ²	10% OR 2.4 IN. ²
B	15% OR 1.5 IN. ²	15% OR 3.6 IN. ²
C	25% OR 2.5 IN. ²	25% OR 6.0 IN. ²

* "L" DENOTES INSPECTION AREA LENGTH, AND "W" DENOTES INSPECTION AREA WIDTH

Bonded details were inspected with a Fokker Bondtester Model 70 or a Bondascope 2100 Bondtester by NDT Instruments, Inc. Both employ the resonance impedance principle. The Bondascope 2100 is especially useful for detecting delamination depth. In some cases, the Bondascope was used following the test of large panels to map out internal failure zones.

3.2 GROUP A TEST SPECIMENS

Group A fabrication effort comprised 231 test specimens as described in Section 2.3.1.

Certain panels required lightning strike conditioning before compression testing. Two basic skin panels were laid up, one with a nickel-coated protection sheet and the other with a wire-woven protection sheet. The lightning protection sheet replaced the outer 0- and 90-degree plies in the protected panels. Whereas the unprotected pattern was 12-ply, the protected panels were 11-ply — 10 plies of tape plus 1 ply of protection cloth.

The exact protection materials used are described in Table 2-1. The two panels were painted as they would be in production using an impact-resistant paint system. The composite surface was first prepared for glazing by solvent cleaning, abrading, and water-break testing. An epoxy fill or glazing compound was then applied. Next, the topcoat was applied using a polyurethane primer, followed by a polyurethane topcoat for nondecorative surfaces. The total coating thickness, including fill coat, primer, and finish coat, was between 4 and 5 mils. A 1.0-inch strip on each end was left uncoated to allow contact between the lightning strike ground plate and the composite surface.

3.3. GROUP B TEST SPECIMENS

The Group B specimens include five unstiffened cutout panels, three stiffened shear panel specimens, and 18 shear-tee/skin pull-off specimens, as described in Paragraph 2.3.2. Aluminum doublers were cold-bonded to both sides of each end using a room-temperature-curing epoxy adhesive in conjunction with a nylon scrim cloth for bondline thickness control. Following this, the test fixture hole pattern was machined in the panel ends.

The first glass/graphite hybrid cutout panels were fabricated using the Style 120, Type E fiberglass. The fabrication approach was to lay up glass prepreg disks into cutouts made in the carbon tape layers. Upon removal from the autoclave, the -503 and -507 unstiffened panels exhibited excessive bowing and warping, as depicted in Figure 3-4. The resin content of the E-glass cloth was found to be too high to achieve the proper mechanical strength properties and to arrive at the desired cured ply thickness. In order for the glass softening material to be effective in this application, it was critical that the cured thickness per ply be close to that of the adjoining carbon tape layers. S2 glass was subsequently chosen as the preferred softening material.

Fabrication details for the more complex stiffened cutout shear panels are given below.

3.3.1. Stiffened Cutout Shear Panels

The stiffened cutout panels consisted of 24- by 24-inch panels with two longerons bonded to each side, a rectangular cutout in the center, and steel doublers bonded to all four edges. The lay-up of the three stiffened cutout panels required a buildup around the perimeter.

The panels were identical except for the cutout. The -501 contained an unreinforced cutout, the -503 contained a cutout with S2-glass tape spliced into the cutout region, and the -505 had a 64-ply graphite doubler around the cutout. Prepreg trim templates fabricated from 1/8-inch-thick clear plexiglass sheet were used for creating cutouts and disks in prepreg for the -503 and -505 panels.

Tooling consisted of trim and drill templates for the cured skins as well as aluminum lay-up mandrels for both flat and ramped-base longerons. The ramped longerons were made to match the surface of the panels containing the buildup discussed above.

3.4.1. Skin Splice Specimens

Two transverse and two longitudinal skin splice specimens were designed. Three replicates of each configuration were fabricated. The graphite details of the -503 specimens in both cases had to be secondarily bonded to the basic skin with FM300 adhesive. About 30 percent less time was required to fabricate the simpler -501 versions because the extra lay-up and secondary bonding procedures were eliminated.

Splice specimen holes had to be machined in two stages to ensure a clean circular hole that would allow a close-to-net fit with the titanium fasteners. A polysulfide elastomeric sealant, identical to that used for pressure containment of joints in commercial aircraft, was applied to one of the three replicates of each splice configuration in order to determine the effect of sealant on overall splice strength. This sealant is applied not only to prevent air and moisture passage, but also, in the case of composites, to prevent harmful galvanic-type interactions between the fasteners and the composite. Figure 3-5 illustrates the location of sealant for the transverse splice specimen and is representative of how all four splice specimens were sealed. Sealant was applied to all faying surfaces, all fasteners, and in each hole. Upon assembly, the fasteners were torqued sequentially to ensure proper extrusion and thickness control of the sealant. A fillet seal was then applied as shown.

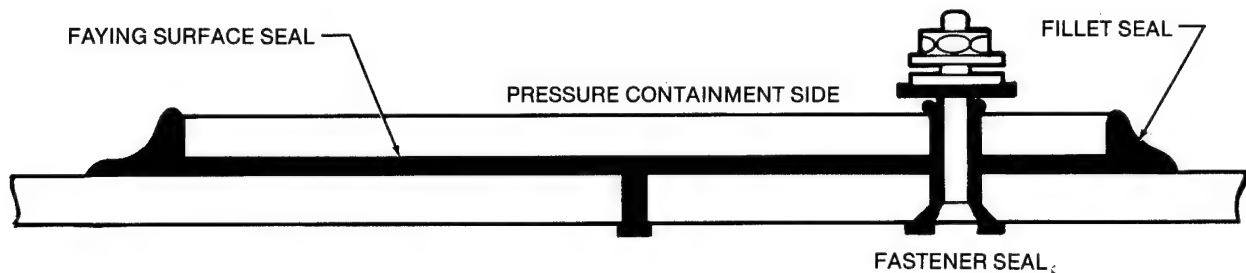


Figure 3-5. Sealant Diagram for Splice Specimens

3.4.2. Longerons Runout Specimen

The graphite-epoxy skin panel for this test specimen included integral ply buildups within the laminate at both ends. The skin's ply buildup affected the faying surface of the skin and longeron. The longeron base flange (faying surface) was fabricated to match the inner surface of the skin for subsequent bonding. A four-piece matched aluminum mandrel was designed for the fabrication of the longeron for this test. This mandrel was used to fabricate a longeron whose base surface matched the joggled faying surface of the skin panel mentioned above. The two graphite-epoxy doublers and four graphite-epoxy clips were laid up, cured, and trimmed. Ultrasonic C-scan and resin void test results were acceptable for all parts.

The trimmed longeron was bonded to the skin using FM300 adhesive. A Fokker bondline tester was used to inspect the bonded details, and the bond was found to be acceptable. The presence of a continuous extruded bead of adhesive from beneath the longeron flange indicated good pressure during cure. Next, the graphite-epoxy and aluminum doublers were simultaneously bonded to the panel ends using a room-temperature-curing epoxy adhesive system. An additional doubler strip made from graphite-epoxy cloth was then cold-bonded near each end of the longeron to allow proper positioning of the shear clips. Holes were machined in the skin and longeron ends, and the shear clips were then attached and test fixture holes machined in the ends of the panel.

3.4.3. Transverse Skin/Longeron Specimen

Two replicates of the transverse skin/longeron splice specimen were fabricated. Each of the panel assemblies consisted of two identical 40-inch skin panel halves, which were spliced together to complete an 80-inch panel. Each skin varied in thickness from a 12-ply (0.068 inch) basic skin to a 108-ply (0.620 inch) end section.

Additionally, two skin splice plates, eight longeron splice members, four shear-tees, and four each of a right and left J-section longeron were fabricated. Longerons and shear-tees were bonded to the skin panels using a high-temperature (350°F cure) adhesive. Final assembly of the right and left panel halves was accomplished by joining the two subassemblies with a mechanically fastened skin splice plate and splicing the longerons with Z and L members. A polysulfide sealant was used between the faying surfaces and in the fastener holes that penetrate the exterior skin.

Rohacell core was sandwiched between the longeron splice details, and mechanical fasteners were installed. All fasteners through the skin panel in this region were countersunk on the outer mold line skin surface. Shear clips at the intersection of the longerons and shear-tees were also mechanically fastened. The close-tolerance holes required for installing the panel into the test fixture were drilled through the assembled halves at both ends. This was done on a numerically controlled jig bore bed to ensure center-to-center alignment of these holes.

3.5 GROUP D FUSELAGE SIDE PANELS

3.5.1 Transverse Splice Panel

The graphite-epoxy skin details were fabricated simultaneously and trimmed after cure at the skin-splice line to make the two respective skin details. The prepreg tape laminate was laid up on the 135-inch radius aluminum laminating surface (Figure 3-6). The lay-up was 50 by 62 inches to allow for process control test coupons before final trim. Plies were vacuum-debulk every two layers to ensure good compaction between successive laminate layers. The cured skin panel was trimmed to 48 by 60 inches and then cut along the splice line.



Figure 3-6. Graphite-Epoxy Tape Lay-Up of Skin Assembly for Transverse Splice Panel

The basic longeron laminate was six plies of cloth and four plies of tape. A "basic plate" of three-ply cloth and four-ply tape was added as the longeron approached its last 6 inches before becoming discontinuous at the splice plate. The longeron faying surface against the skin had to joggle to match a 0.022-inch buildup at the splice region and under the shear-tee.

To increase finished part rate of this complex lay-up, an aluminum matched metal tool and a graphite roving/epoxy cast mandrel (two pieces) were utilized for laying up the longeron details. The mandrel was used only to debulk plies while the metal tool was in the autoclave or being cleaned. Debulk laminates were then transferred onto the metal tooling for bagging and curing (Figure 3-7).

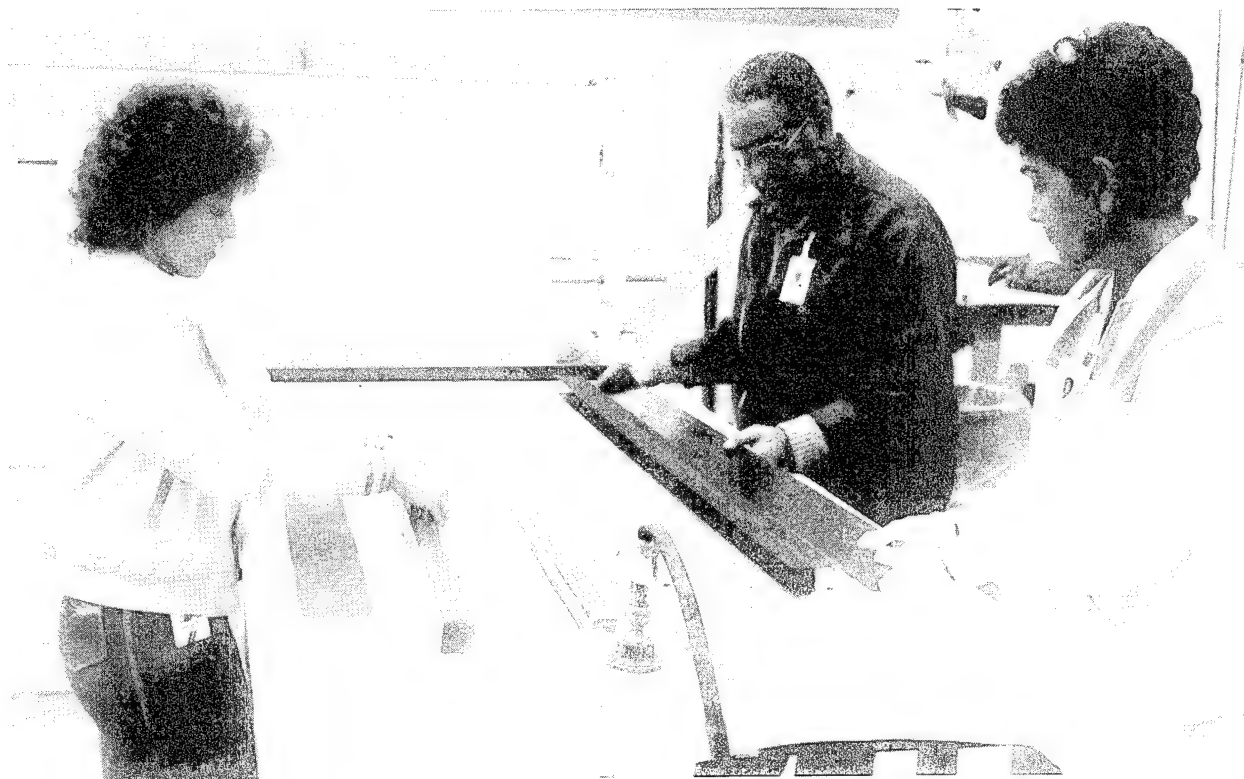


Figure 3-7. Transfer of Debulk Longeron Preforms to Metal Mandrels

The graphite-epoxy frame detail was laminated on a numerical control machined aluminum tool surface shown in Figure 3-8. The laminate had a finely woven, nylon peel-ply against both surfaces to provide a surface free of resin-rich/resin-starved areas.

The shear-tee for this panel was debulked as two curved Ls on wooden mandrels covered with a Teflon release film. The debulked L halves were joined to form the final T shape of this detail part. While these joined halves were still uncured, they were transferred to the cured skin panel. When all three shear-tee forms were in place with their support tooling, the entire skin and shear-tee mandrel arrangement was vacuum-bagged and cured.

Before final installation of the fasteners through the skin splice, a polysulfide sealant, similar to that used for conventional fuselage pressure and fuel containment, was applied to the mating surfaces between the skin splice and skin panel sections. The titanium countersunk-head fasteners were then torqued in an alternating pattern across the splice center to avoid unequal clamp-up.

An engineering disposition was made regarding the condition of the bonded subassembly. It was determined that a pattern of 3/16-inch-diameter fasteners through the base flanges of the longeron and shear-tee details and the skin panel would provide the structural integrity required for a valid panel assembly test. The fasteners through the center shear-tee and through the base flange closest to the window cutouts of the other two shear-tees were countersunk on the outside of the fuselage skin. The fasteners through the discontinuous longeron base flanges were also countersunk on the outside surface of the fuselage skin. It was determined that countersinking the fasteners through the longerons in this region would provide an opportunity for testing a window cutout panel with extensive rework.

The aluminum doublers around the panel periphery were bonded in place using EA9321. Pilot holes through the aluminum details and through the faying surface of the skin were drilled where fasteners would later be installed. The adhesive assembly was bagged and vacuum was applied to ensure good contact pressure while the epoxy adhesive cured.

The frame members were attached to the shear-tee details using mechanical fasteners. The butterfly clips and shear clips were installed at shear-tee/frame/longeron intersections. Roll-formed tee sections and details were attached to the ends of the composite panel. The machined fittings, which attached the longeron ends to the curved tee, were mechanically fastened through the skin panel and tee section. A decision was made to reuse the corrugations and hat section subassembly since these were not visibly damaged or deformed during the previous test.

The composite panel was positioned in the fixture with the bottom edge free. The upper tee section was bolted to the upper test fixture plate. The lower tee section was then permanently attached to the end of the composite panel. The fittings were attached to the longeron ends and the tee was bolted to the lower test fixture plate. This sequence avoided any preload in the panel due to tolerance differences in the assembled panel and the test fixture attach points. The right- and left-half corrugations were attached to the composite panel edges through the doubler that extended down the 60-inch length. The panel is shown installed in the test fixture in Figure 3-10.

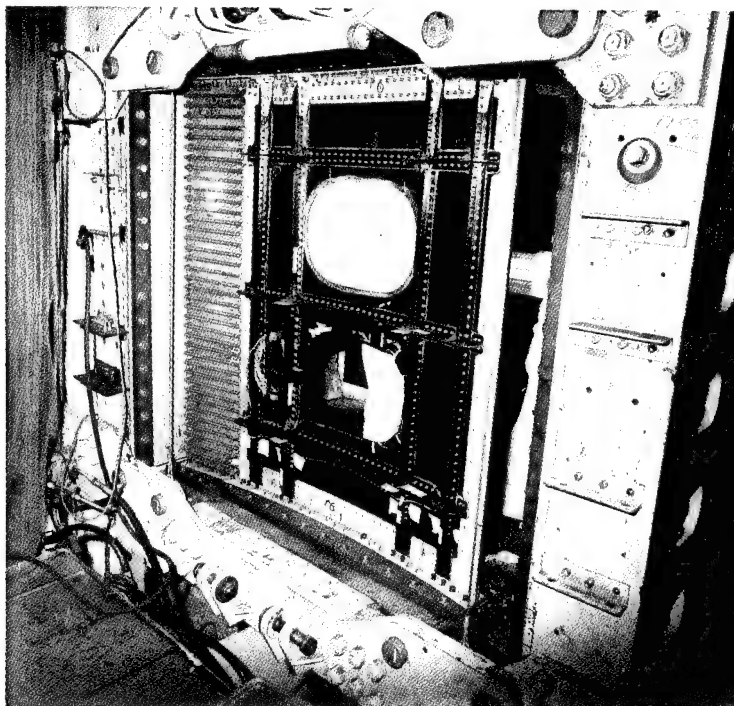


Figure 3-10. Installation of Composite Window Belt Panel Assembly into Test Fixture

SECTION 4

TEST SETUP AND PROCEDURE

4.1 GROUP A

Many of the Group A tests were straightforward tension tests on small, 3- to 12-inch-long specimens and required no special fixtures or unusual procedures. The specimens were tested in a 100,000-pound-capacity MTS servohydraulic test machine. Hydraulic grips were used to apply test loads to the specimen ends where applicable. Load rates for these tests were generally very close to 0.05 inch per minute for both tension and compression specimens (except for the biaxial specimens, for which a special loading procedure was used).

Strain gages (required for the monolayer and unnotched laminate specimens) were single-channel, axial-foil, resistance-type gages. These were applied with a layer of room-temperature-curing epoxy adhesive after the specimen surface was lightly sanded. For specimens requiring strain gage or deflection readings, data were collected at predetermined load increments based on the expected failure load. Generally, increments were chosen so that between 12 and 20 data points would be collected before failure.

For the single-lap tension (SLT) and double-lap tension (DLT) tests, it was critical to record the relative displacement of the specimen edges in relation to the bolt centerlines. These fastener flexibility data are required to determine relative load sharing between rows of fasteners in a multirow bolted joint. Special fixtures (developed under an independent Douglas program) were used to make these measurements (Figure 4-1).

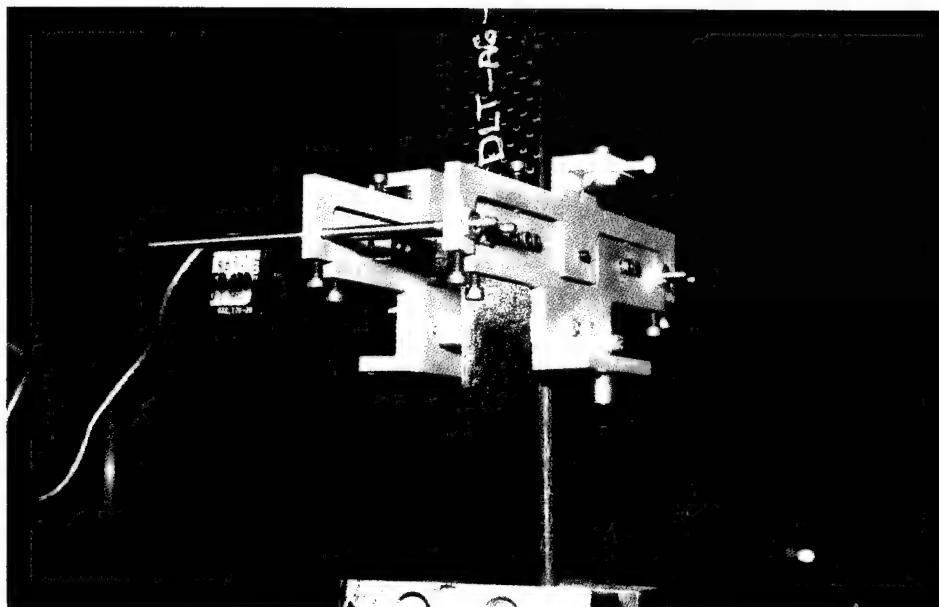


Figure 4-1. Test Setup for DLT Specimens

The CAI compression panels were tested in a fixture similar to that used in the NASA standard test, ST-1. This fixture, however, was designed to be used with 0.25-inch-thick specimens and therefore provided inadequate lateral support for the 0.068-inch-thick CAI specimens. Antibuckling plates were fabricated from 0.25-inch-thick aluminum plates, each reinforced with two angle-iron sections. These plates were placed on either side of the test specimen and lightly clamped in place using C-clamps.

The impact damage test was conducted per the ST-1 NASA standard test specification except that the impact energy was reduced to 4 foot-pounds because of the reduced thickness of the CAI specimens. A 10-pound impactor with a 0.5-inch-diameter hemispherical steel head was dropped from a height of 4.8 inches. C-scans of the damaged panels indicated that the damage was confined to a roughly circular area 0.5 to 0.6 inch in diameter.

The lightning strikes (for the -505, -507, and -509 CAI configurations shown in Figure 2-7) were conducted per MIL-STD-1757A, using the Zone II lightning attachment region requirements. The panels were subjected to a simulated two-component lightning strike. The first component represented a second high-peak-current return stroke, which attaches to the vehicle from ground. While this stroke is of high amperage, the charge transfer is small. Nevertheless, this high-peak-current phase can create large instantaneous vapor pressures, which, in confined regions, can create significant explosive damage. The second strike component represented the continuing current phase, which develops a considerably lower charge but lasts roughly 1,000 times as long. The result, then, is a high-charge transfer that can cause severe burning and eroding of the composite material. The compression panels (CAI) were subjected to a high-peak-current phase of 100,000 amperes with an action integral (a measure of the energy delivered) of $0.25 \times 10^6 \text{ A}^2 \text{ sec}$ and a continuing-current phase of 400 amperes for 400 msec.

Prior to being struck, the specimens were primed and painted. An unpainted panel of the -509 configuration (unprotected) was used for calibrating the lightning strike setup. Following calibration, the panels were loaded into the test frame with the painted side up. The lightning discharge electrode was centered over the strike target, and a steel ground plate was clamped to one end of the panel. A current probe located at the base of the test frame transmitted discharge measurements via an optical fiber cable (used to avoid electromagnetic interference) to oscilloscopes in an RF-shielded control room. A diagram of the test circuit is shown in Figure 4-2. After charging the capacitors in the high-current generator, the high-peak current and continuing current components of the simulated strike were delivered through the discharge electrode in rapid sequence. Typical measured waveforms for the two components are shown in Figure 4-3.

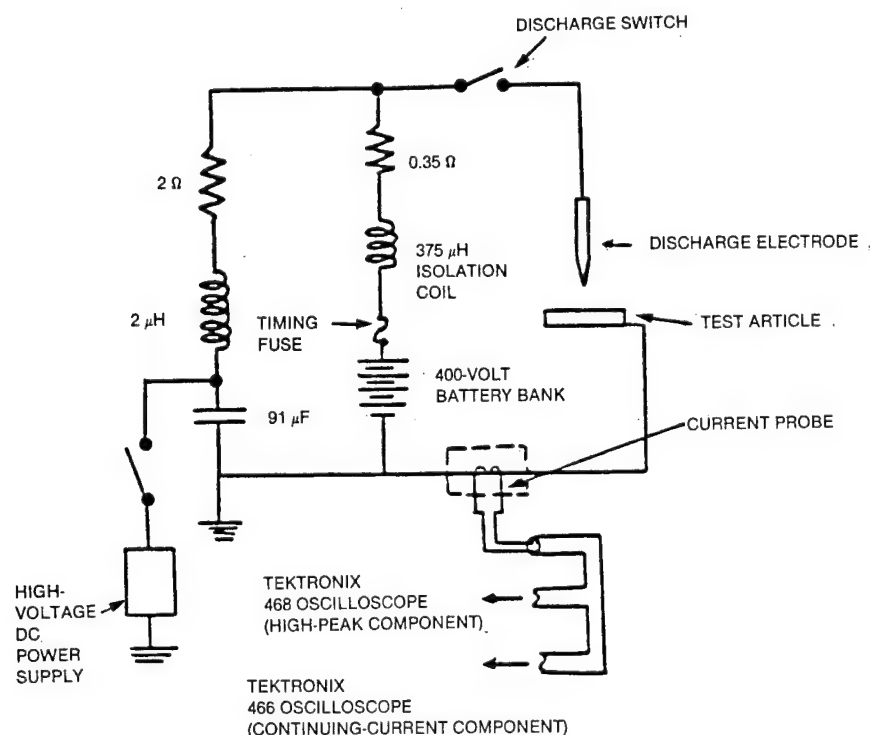
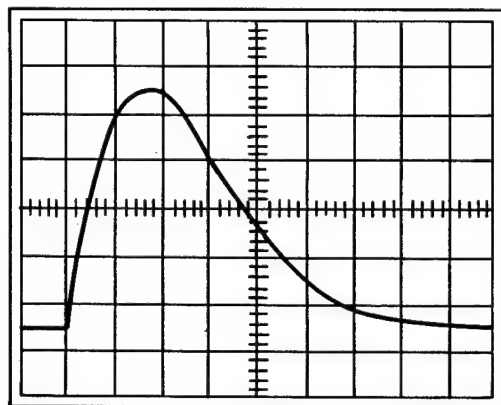
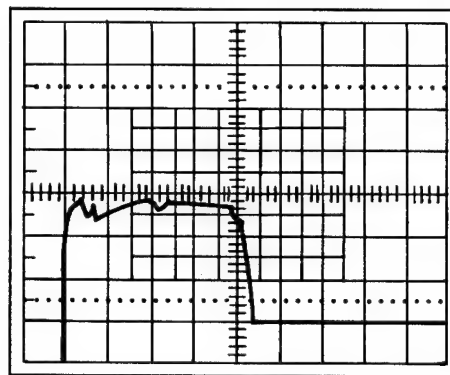


Figure 4-2. Test Circuit for Lightning Simulation



HIGH PEAK CURRENT
COMPONENT WAVEFORM
(KA VERSUS t)



CONTINUING
CURRENT COMPONENT
WAVEFORM (A VERSUS t)

Figure 4-3. Measured Waveforms for Simulated Lightning Strike Components

Table 4-1 gives actual discharge measurements for each of the specimens. Table 4-2 gives a detailed description of the damage sustained by each panel. The -505 panel (interwoven aluminum wire protection system) displayed the least damage (mainly top ply damage), while the unprotected panel displayed the most damage (penetration through all 12 plies). It should be noted here that the interwoven aluminum wire system was significantly thicker (cured thickness $\cong 0.021$ inch) than the nickel-coated graphite cloth system (cured thickness $\cong 0.011$ inch). X-ray photographs, showing the extent of damage to the nickel-coated fibers and the aluminum wires, are included for typical -505 and -507 panels in Figures 4-4 through 4-8.

Although it was not actually one of the CAI specimens, it is interesting to compare the behavior of the calibration panel (unpainted, unprotected) to that of the -509 panel (painted, unprotected). The calibration panel displayed damage to the top 4 to 5 plies with no through-penetration (in fact, no visible damage to the back). This is contrasted with the -509 panel, in which all 12 plies were damaged and there was noticeable penetration. It is suspected that the paint layer has the effect of confining the energy of the strike, resulting in explosive damage.

For the last of the Group A specimens (the biaxial stress specimens) load was applied simultaneously in two mutually orthogonal directions. These specimens were designed to simulate (in a simplified way) the biaxial state of stress that exists at a fuselage barrel splice. Circumferential hoop stresses are simulated by bypass loads supplied by an MTS machine, while longitudinal bolt loads are represented by loads applied by a specially designed fixture. This fixture (Figure 4-9) consists of a scissors mechanism driven by a manually operated hydraulic pump to produce the desired state of stress.

The biaxial specimens (BAS) were tested over a range of test conditions that varied from 100-percent bypass to 100-percent bearing. The -1, -2, and -3 specimens were first loaded into the MTS machine. Pump pressure was then increased to 250 psi (corresponding to a bolt load of just over 500 pounds). Bypass load (via the MTS machine) was then added until the specimens failed. The -4 and -5 specimens were tested using the same procedure, except the pump pressure was 500 psi (just over 1,000 pounds of

Table 4-1
Lightning Discharge Test Values

SPECIMEN ID	CHARGE TRANSFER (COULOMBS)	PEAK CURRENT (kA)	ACTION INTEGRAL (A ² s)	GENERATOR VOLTAGE (kV)	CIRCUIT RESISTANCE (OHM)
CAI-505					
-1	22	105	0.275×10^6	+37	0.23
-2	24	103	0.265×10^6	+37	0.24
-3	22	102	0.26×10^6	+36	0.23
CAI-507					
-1	21	95	0.23×10^6	+35	0.24
-2	20	103	0.265×10^6	+38	0.25
-3	17.5	102	0.26×10^6	+37	0.24
CAI-509					
-1	21	98	0.24×10^6	+40	0.30
-2*	21	—	—	+39	—
-3	20.5	101	0.255×10^6	+39	0.28

*MEASUREMENT SIGNAL FROM HIGH PEAK CURRENT COMPONENT WAS NOT RECORDABLE. HOWEVER, VOLTAGE, CHARGE TRANSFER, AND VISUAL DAMAGE ARE SIMILAR TO CAI-509-1 AND CAI-509-3.

Table 4-2
Lightning Damage

SPECIMEN ID	
WIRE-WOVEN CAI-505-1	PRINCIPAL DAMAGE AREA 0.6-1.2-IN. DIAMETER. DAMAGE EXTENDS THROUGH TOP PROTECTION PLY ONLY. TOP PLY WEAVE IS LARGELY INTACT IN DAMAGE AREA, THOUGH FIBERS HAVE NO RESIN AND ARE DELAMINATED FROM PLY BELOW APPROX. 0.4 IN. DIAMETER.
NICKEL-COATED CAI-507-1	PRINCIPAL DAMAGE AREA 1.75-2.0 IN. DAMAGE EXTENDS THROUGH TOP PROTECTION PLY, WITH RESIN ELIMINATED FROM 0.5-IN. DIAMETER IN SECOND PLY. TOP PLY WEAVE DESTROYED IN 1.0-IN.-DIAMETER AREA. TOP PLY DELAMINATION IN 2.9-IN.-DIAMETER AREA.
UNPROTECTED CAI-509-1	PRINCIPAL DAMAGE AREA 2.4-3.1 IN. PRINCIPAL DAMAGE AREA EXTENDS THROUGH 6-8 PLIES. 1/8-IN.-DIAMETER HOLE PENETRATES THROUGH ALL 12 PLIES. REAR PLY SPLINTERED OFF IN A 0.2 BY 6-IN. STRIP. TOP PLY BLOWN OFF IN APPROXIMATELY 0.70-IN.-WIDE STRIPS. BULGING OF TOP SURFACE, 3.00-IN. DIAMETER, 0.10 IN. HIGH.

*VISIBLE DAMAGE OF THREE STRIKES ON EACH PANEL IS SIMILAR; THEREFORE, DESCRIPTIONS HERE ARE REPRESENTATIVE OF ALL STRIKES ON A GIVEN PANEL.

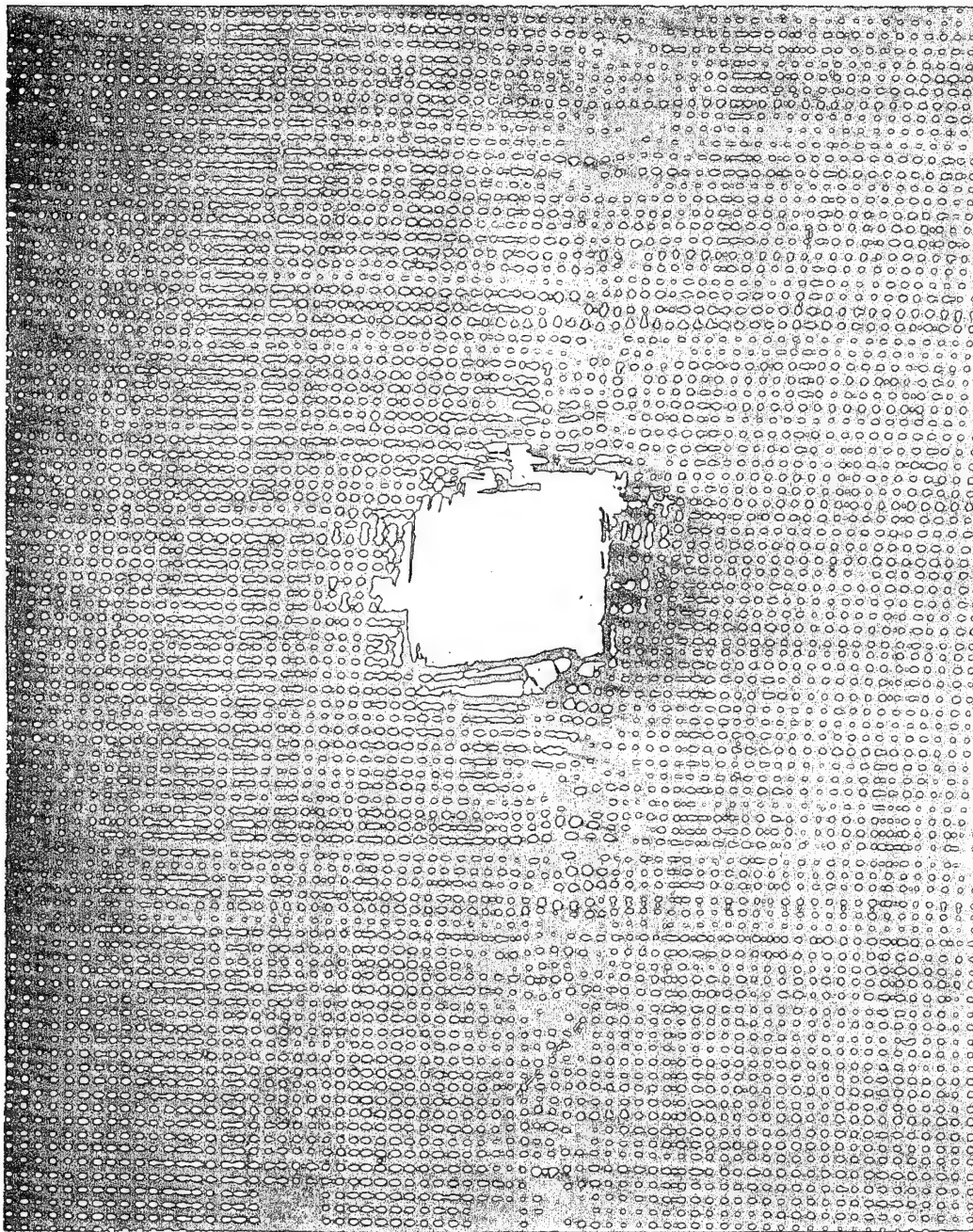


Figure 4-4. X-Ray of -505 CAI Specimen Showing Damage to Nickel-Coated Fibers

bolt load). The -6 and -7 specimens originally were to have been tested at 750 psi (using the same procedure). As the pump pressure approached 650 psi, however, a sudden drop in pressure occurred (indicative of bearing yield damage). Pump pressure was again increased to 650 psi (after several more minor drops) and then held while the bypass load was added. The -8 specimen was tested using a different procedure. In this case, the bypass load was applied first (20,000 pounds), and then the bearing load (pump pressure) was increased until the specimen failed. The -9 specimen was tested in a similar manner at a bypass load of 10,000 pounds. The -10 specimen was tested with no bypass load at all; pump pressure was simply increased until a bearing failure occurred. The -11 and -12 specimens were likewise tested with no bearing load; i.e., these specimens were simply loaded in tension using the MTS test machine.

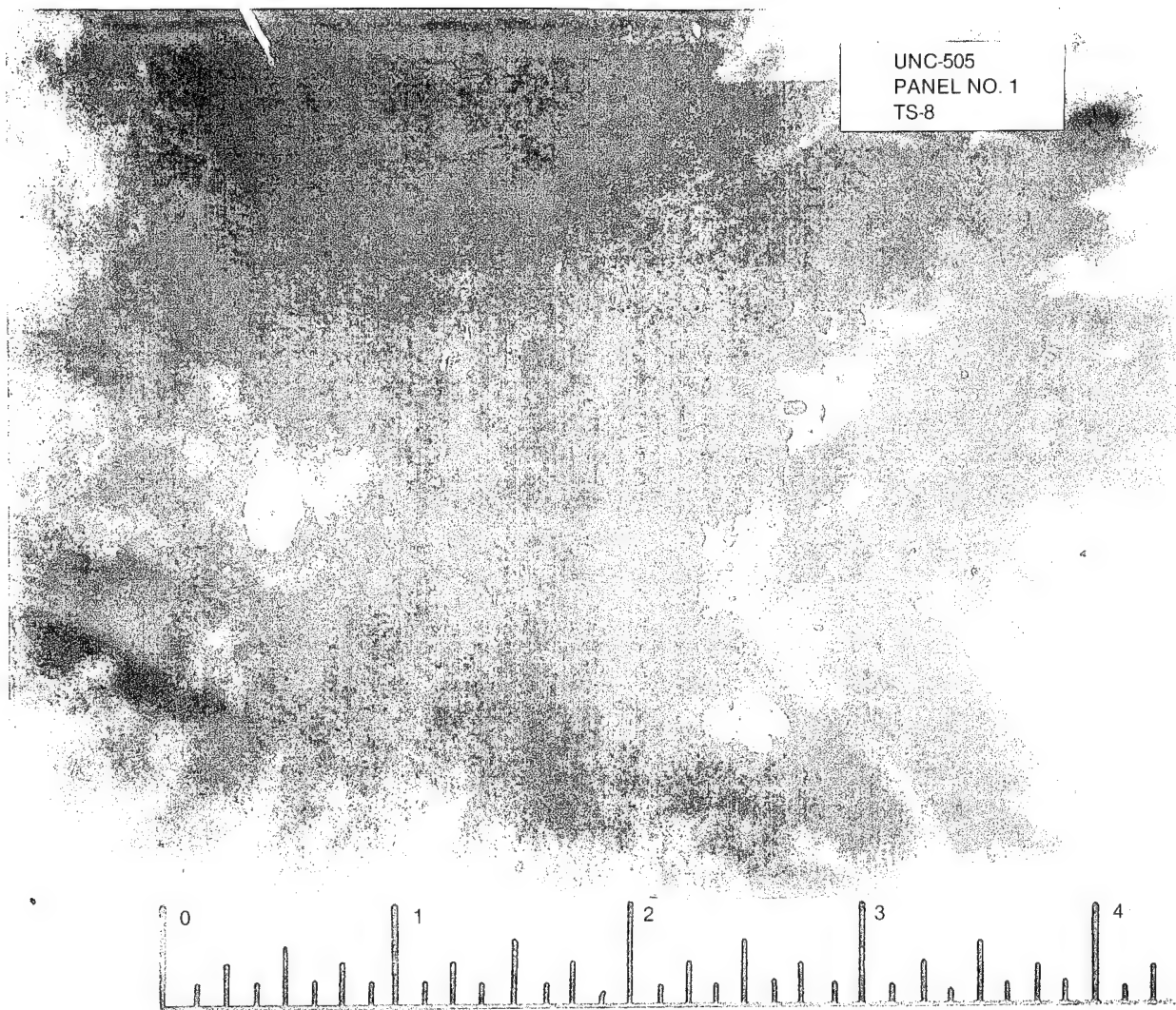


Figure 4-5. After Strike Damage on Wire-Woven Panel (UNC-505-2)

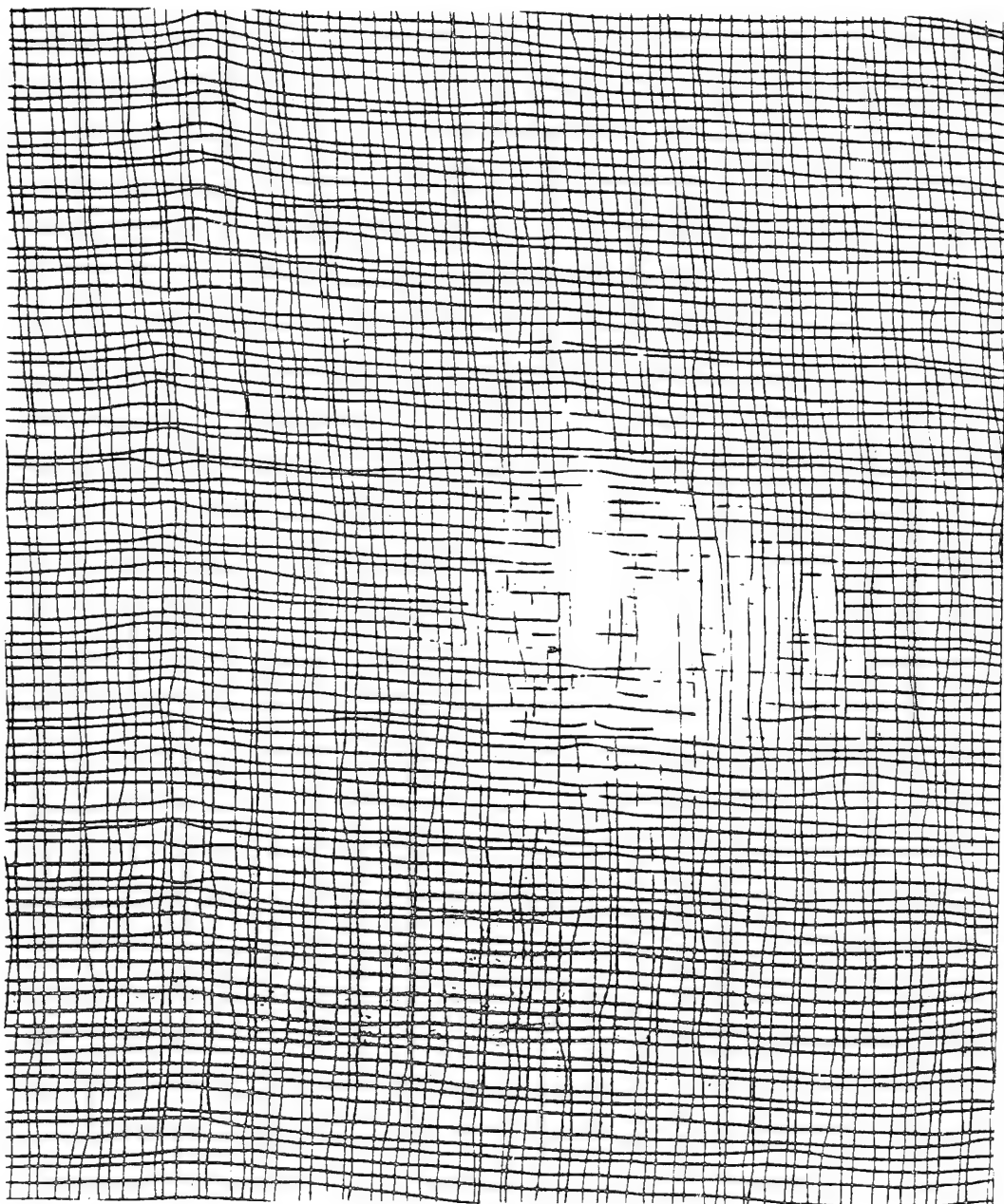


Figure 4-6. X-Ray of -507 CAI Specimen Showing Damage to Aluminum Wires

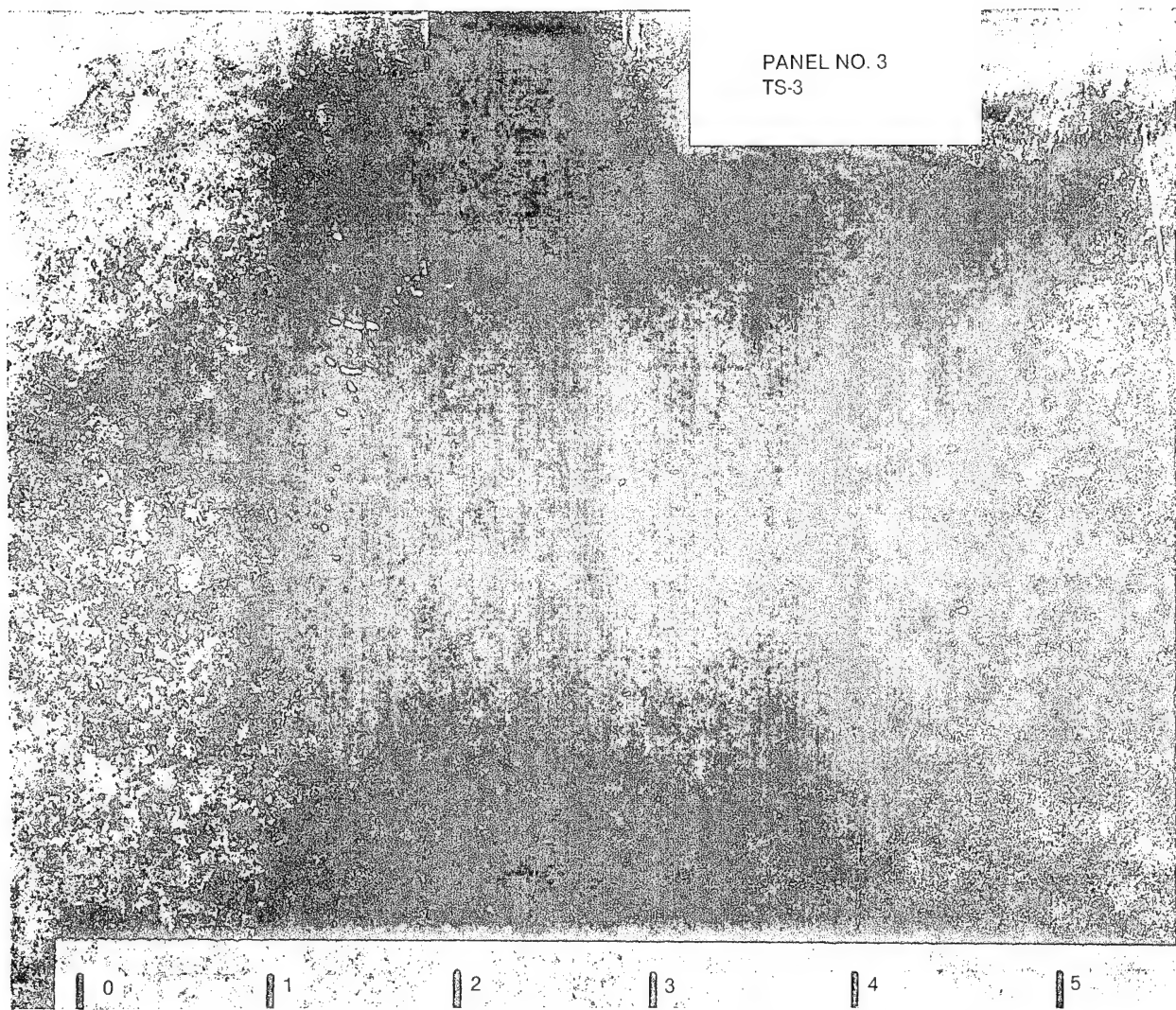


Figure 4-7. After Strike Damage on Nickel-Coated Panel (UNC-507-3)

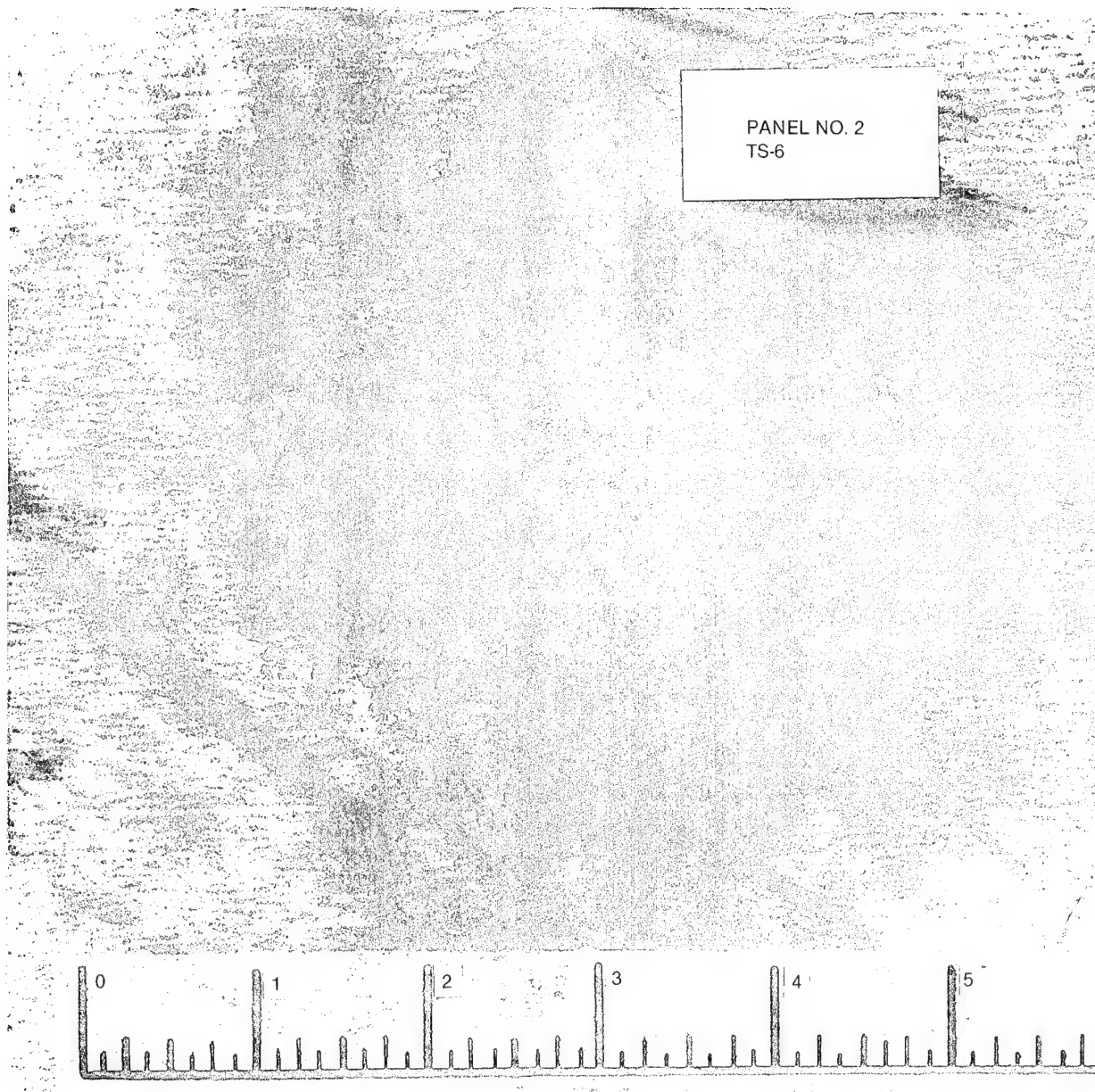


Figure 4-8. After Strike Damage on Unprotected Panel (UNC-509-3)

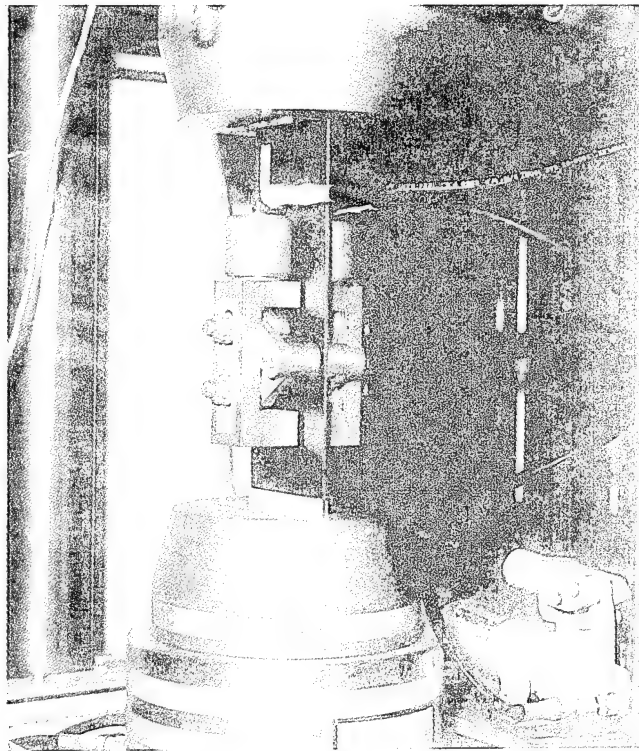


Figure 4-9. Test Setup for Biaxial Specimens (BAS)

4.2 GROUP B

The Group B tests included a number of specimens with large cutouts and the shear-tee pull-off specimens. All of the cutout specimens were tested in a four-posted, servohydraulic MTS test machine capable of delivering loads up to 220,000 pounds. Figure 4-10 shows a typical test setup for the tension panels. The testing of the shear panels required the use of a picture frame test fixture. The design of this fixture was based on research performed at Langley Research Center and the U.S. Army Aviation Research Development Command. The fixture is composed of two back-to-back picture frames (each composed of four rails connected with high-strength pins), which sandwich the test panel. The corner pins of the fixture are positioned so that their centerlines are coincident with the corners of the panel test section. This arrangement virtually eliminates corner stresses while applying a nearly uniform shear flow. The particular test fixture used was designed for a 2- by 2-foot test section. Typical strain gage locations for the shear cutout panels are shown in Figure 4-11.

In addition to strain gage data, photoelastic measurements were taken for three of the tension panels and all of the shear panels. (The two tension panels with E-glass softening were primarily intended for manufacturing and process development; nevertheless, the panels were tested with limited instrumentation, i.e., only six strain gages and no photoelastic film.) The specimens were loaded incrementally up to a safe maximum load (usually one-third of the predicted failure load). At each load increment, measurements of the principal shear strains (maximum positive and maximum negative) were taken using a Photoelastic Inc. 030 Series Reflective Polariscopes. Figure 4-12 shows the photoelastic measurements being taken for one of the shear panels.

The 18 shear-tee pull-off specimens were tested in a 10,000-pound-capacity Instron test machine. The loading fixture was designed to simulate the boundary conditions of the baseline aircraft under cabin pressure. This fixture consisted of a T-section base to which the skin was attached, and two aluminum plates that tied to the tee itself. The 12 close-tolerance fasteners that attached the skin to the base were carefully matched to the test fixture to ensure that membrane stresses were properly developed in the skins.

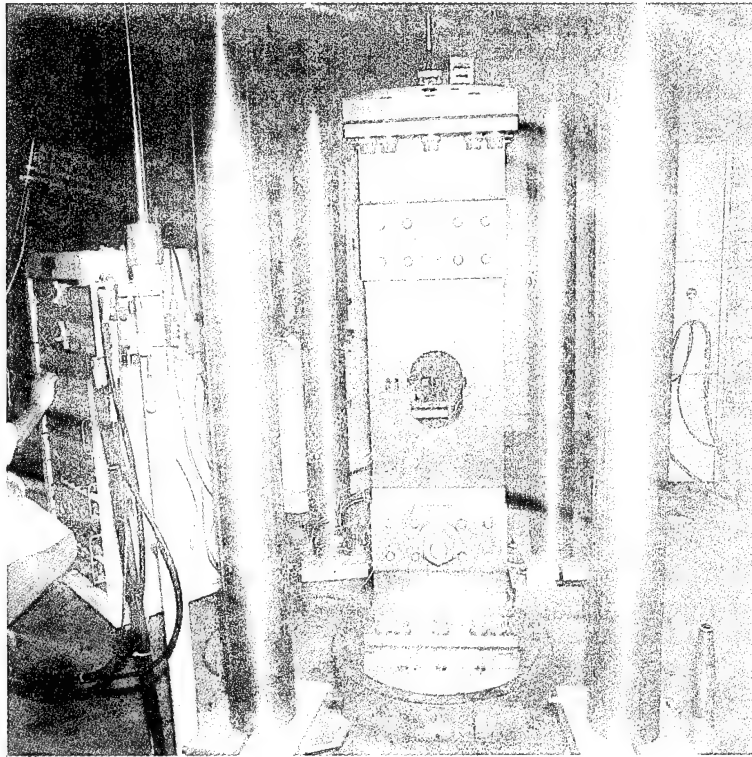


Figure 4-10. Typical Test Setup for Group B Tension Panel Test

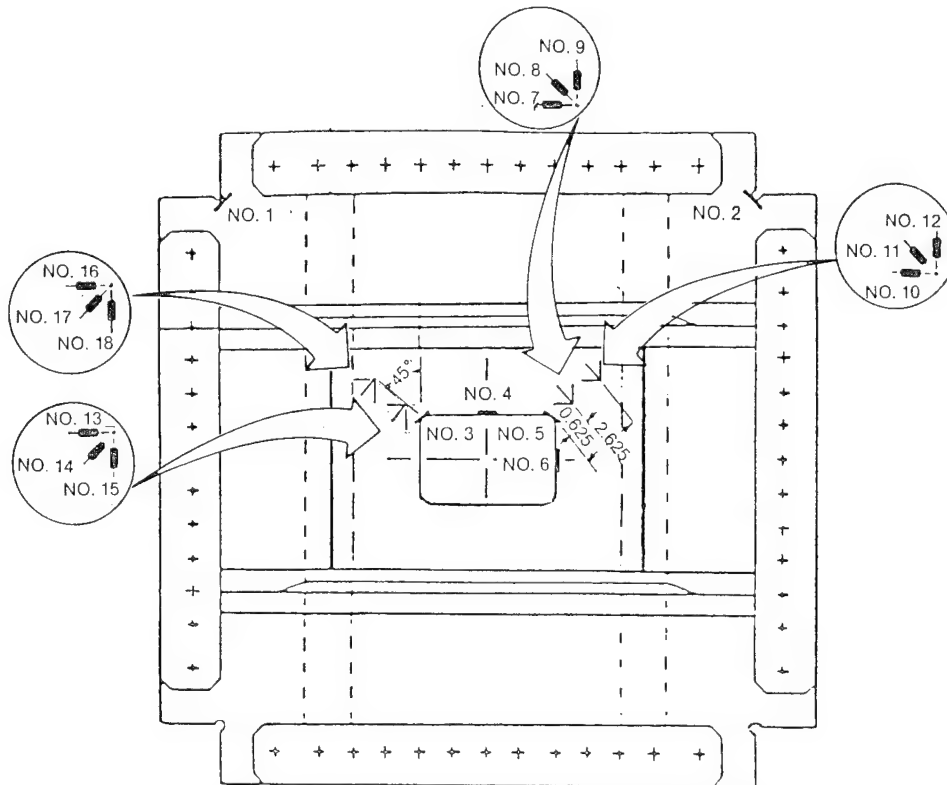


Figure 4-11. Typical Strain Gage Locations for Shear Cutout Panel (-501)

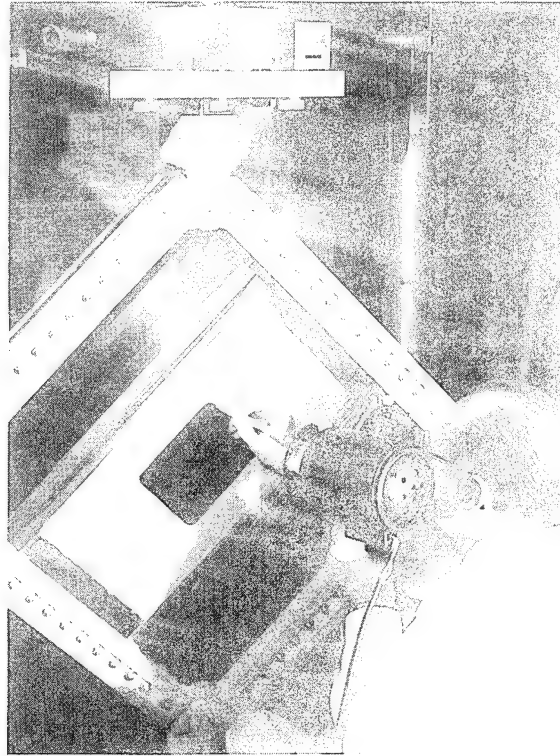


Figure 4-12. Photoelastic Measurements of a Group B Cutout Panel

Loading of the specimens was displacement-controlled at a rate of 0.050 inch per minute. At prescribed load levels, vertical displacement was measured at each of three locations. For the first specimen tested, displacement at the tee centerline was obtained by measuring the distance between the top of the tee and the fixture base. For subsequent specimens, this procedure was abandoned in favor of head travel plots. For all specimens, vertical displacements at the edges of the shear-tee flanges were recorded by measuring offsets from the fixture base using a dial caliper.

4.3 GROUP C

The Group C tests included the skin splice specimens, a longeron runout specimen, and two two-stiffener panels containing the transverse skin/longeron splice. The skin splice specimens were tested in a 100,000-pound-capacity MTS test machine outfitted with hydraulic grips. All specimens were tested in tension. The longeron runout specimen was tested in a four-posted, servohydraulic MTS test machine capable of delivering loads up to 220,000 pounds.

One transverse splice panel was tested in tension, the other in compression. These specimens were designed to represent a section of the transverse (barrel) splice and therefore required a special fixture to provide lateral support at the simulated frame stations. A schematic of the fixture designed for this purpose is shown in Figure 4-13. The two frames were designed to slide in the supporting C-channels to avoid picking up any longitudinal load (see detail in figure). Connections to the simulated frames were through representative shear-tees and clips.

Strain gage locations for each of the Group C specimens are given in Figures 4-14, 4-15, and 4-16.

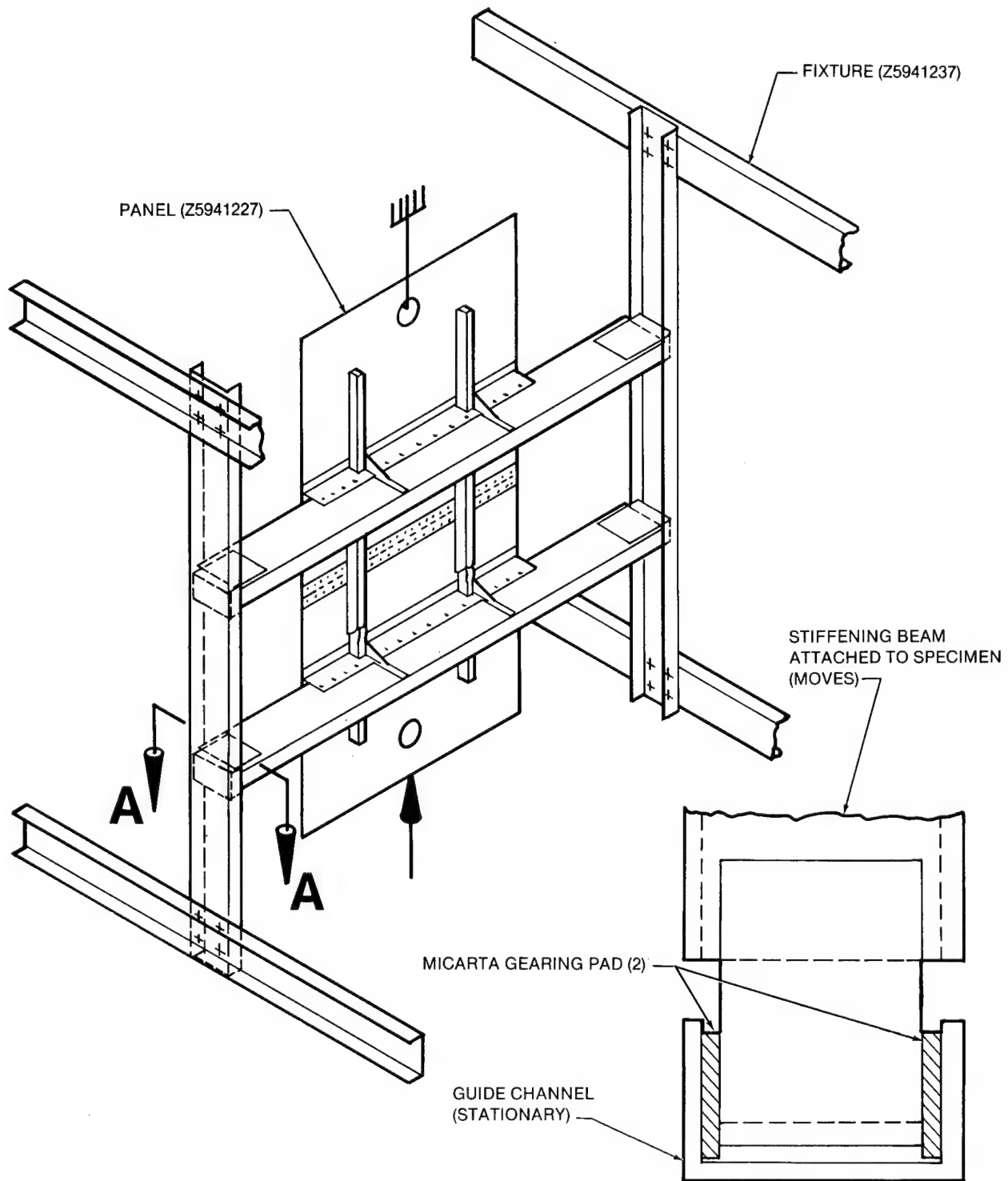


Figure 4-13. Schematic of Test Fixture for Transverse Splice Panels

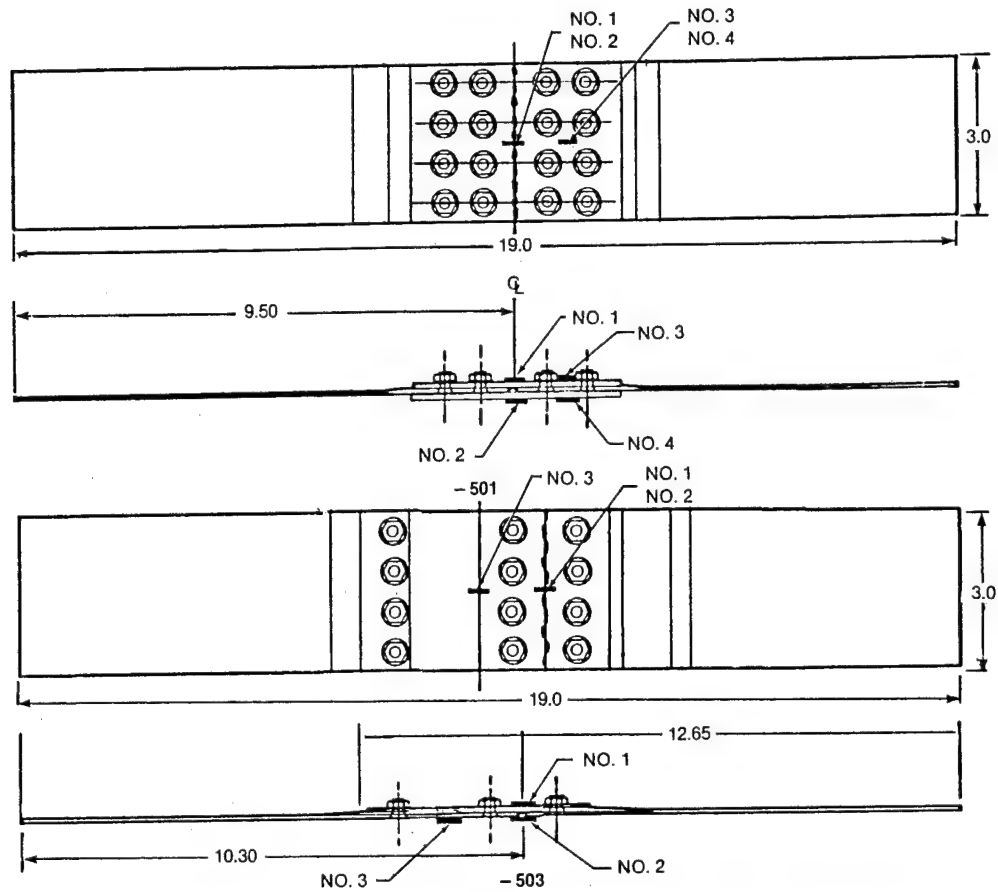


Figure 4-14. Longitudinal Skin Splice Strain Gage Locations

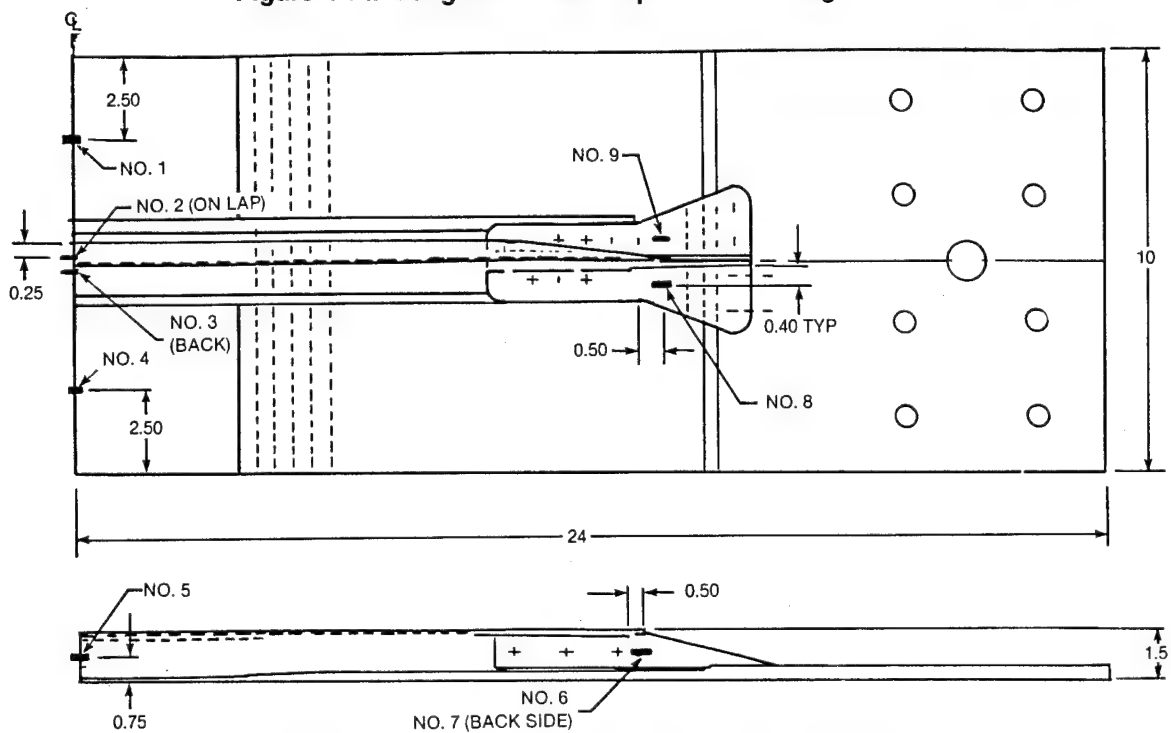


Figure 4-15. Longerons Runout Strain Gage Locations

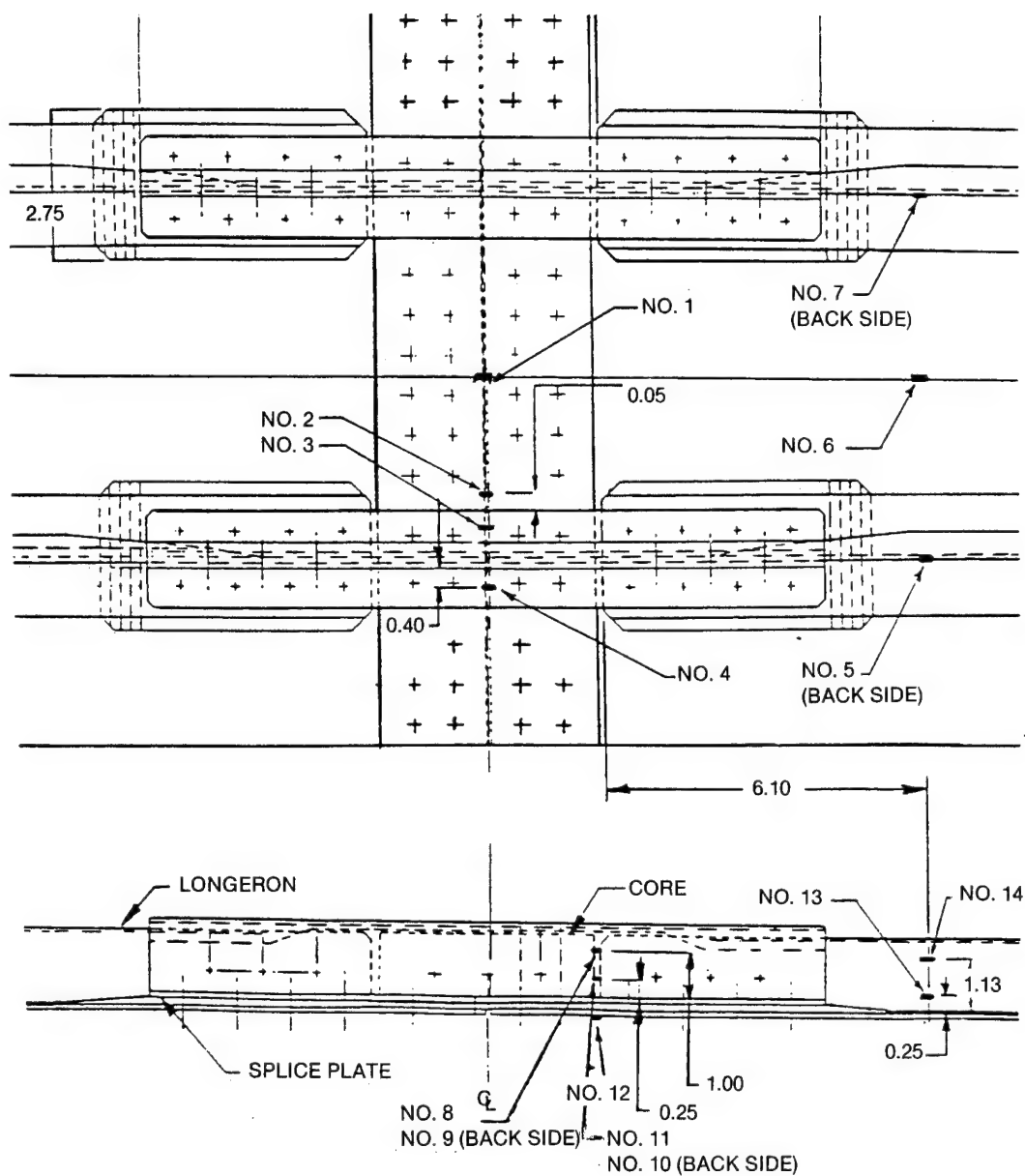


Figure 4-16. Transverse Splice Panel Strain Gage Locations

4.4 GROUP D

Testing of the two Group D panels was accomplished in an existing Douglas test fixture, which was capable of applying both shear and compression loads. This fixture (Figure 4-17) consists of three large members connected to one another and the fixture base by four links. For compression loads, the upper and lower members are drawn together by the four compression actuators. The panels are effectively isolated from the rest of the fixture by the nature of the linked connections and the use of corrugated steel panels in the bays on either side of the test panels. The corrugations are quite capable of transferring shear loads.

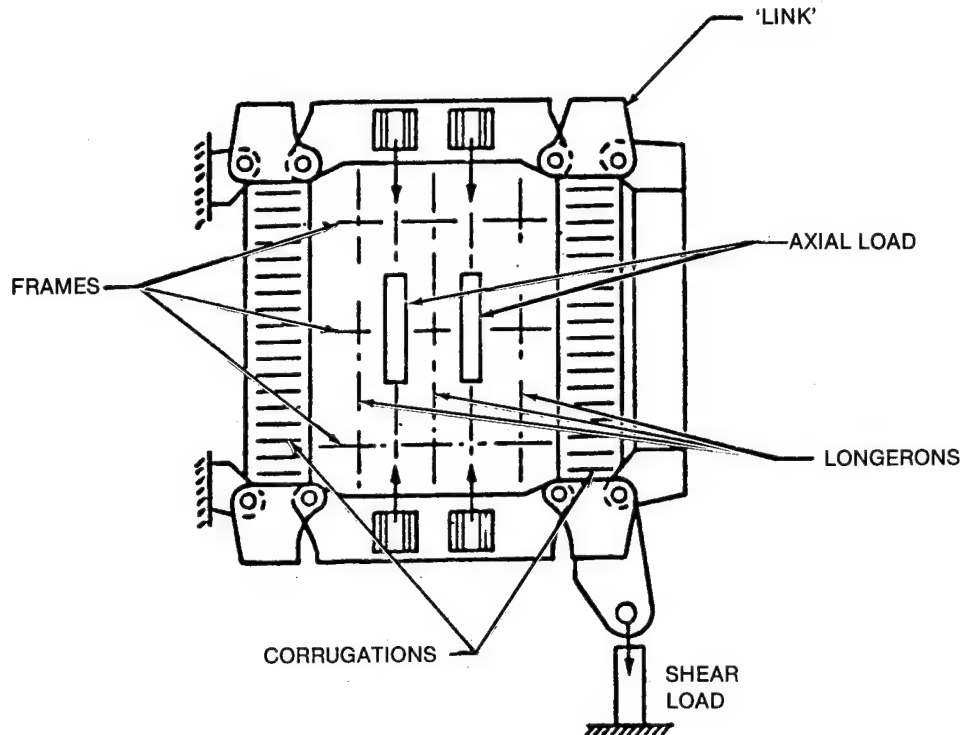


Figure 4-17. Shear/Compression Interaction Test Fixture

Compression loads were applied by four 20-square-inch actuators; shear loads were applied by a single 100-square-inch actuator. Prior to installation of the test panels, the steel corrugated side panels were calibrated. The corrugations were installed in the fixture without a test panel and loaded with the compression actuators. Load-versus-deflection data were taken over a range of deflections from 0.0 to 0.35 inch. These data indicated that the corrugations picked up roughly 25,000 pounds of compression load per inch of deflection.

Instrumentation on the transverse splice panel included 12 axial strain gages (Type EA-06-125AC-350) and 4 rosettes (Type EA-06-125RS-350) (Figures 4-18 and 4-19). Instrumentation for the window-belt panel included 16 axial gages and 3 rosettes of the same types (Figure 4-20). In-plane deflections of the load fixture were measured using 10 linear deflection transducers. Data were recorded on a Tektronix 4054 Graphic and Data Acquisition System capable of single-point or continuous-read sampling of strain gage, deflection transducer, and load cell output. Data were displayed scan by scan at the Tektronix terminal when in the single-point mode.

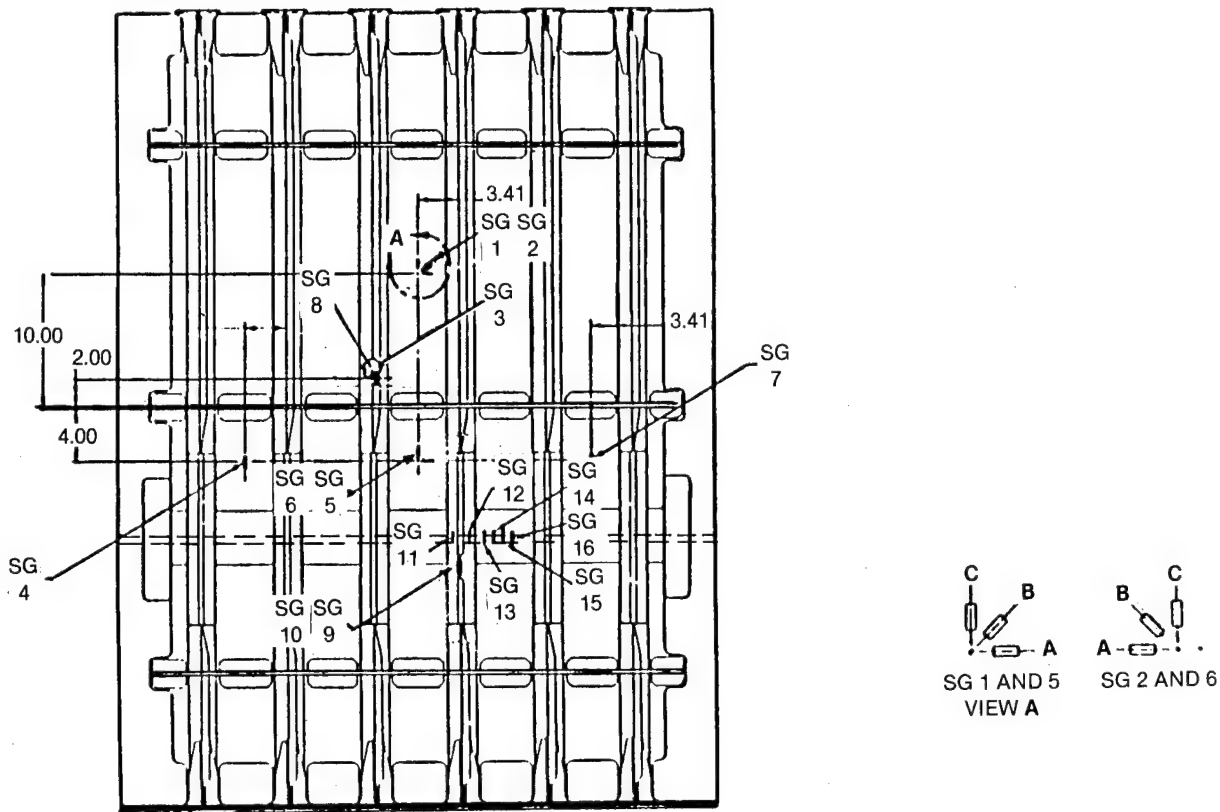


Figure 4-18. Transverse Splice Panel Strain Gage Locations

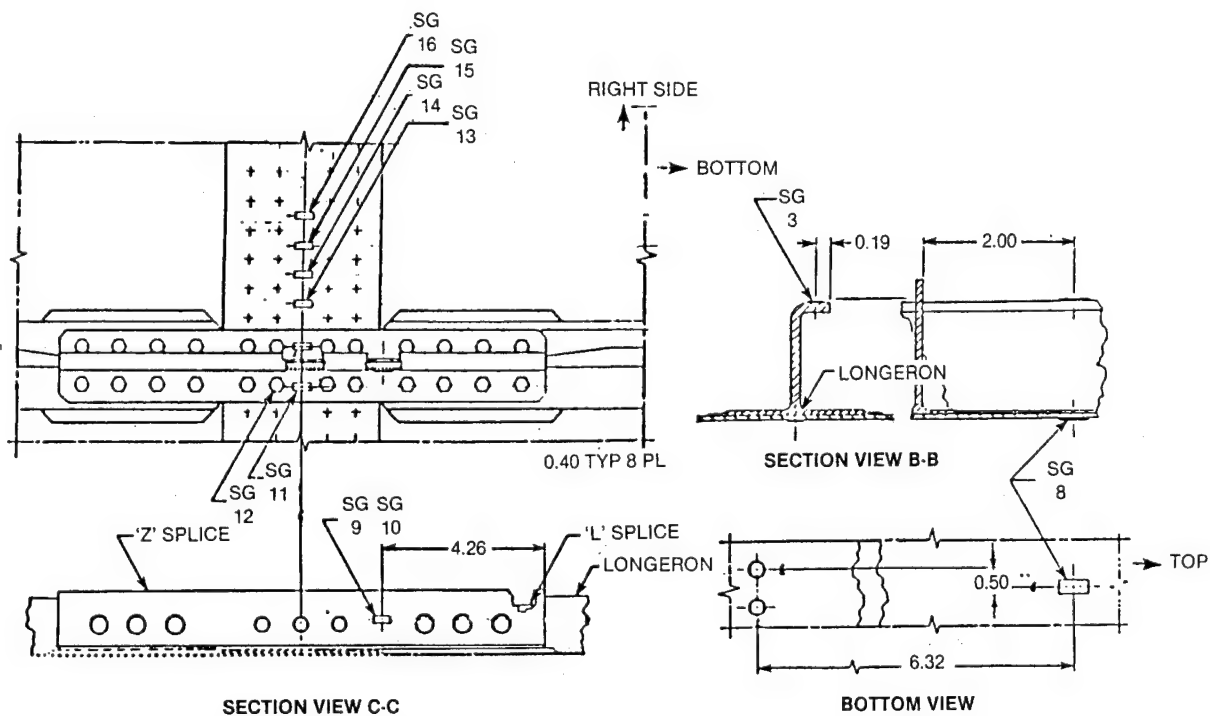


Figure 4-19. Transverse Splice Panel Strain Gage Locations Additional Detail

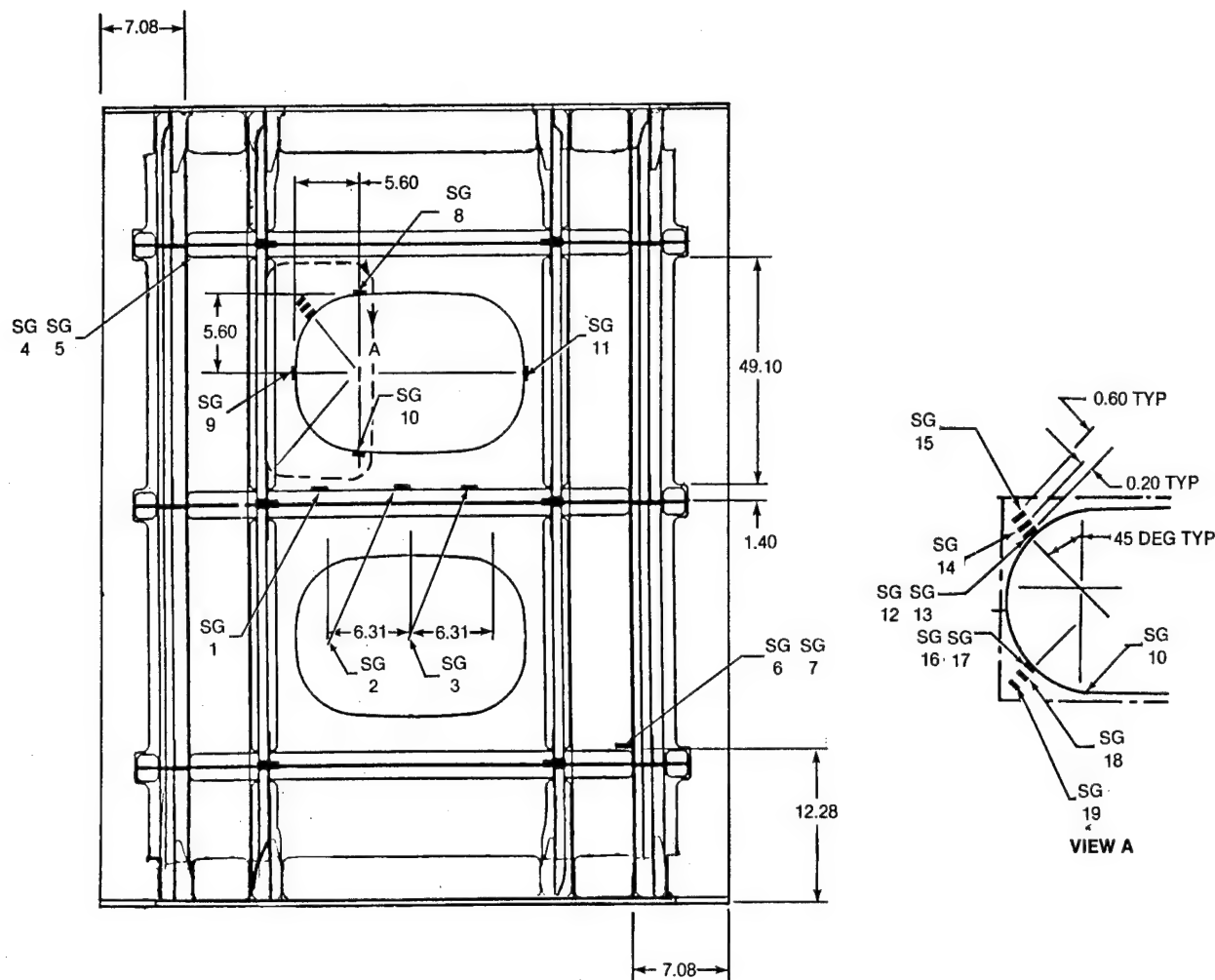


Figure 4-20. Strain Gage Locations, Window Belt Panel

A shadow moiré grid was used for a qualitative assessment of the out-of-plane deflections of the transverse splice panel, primarily for visual determination of the onset of buckling. Changes of the moiré fringe pattern were also used to observe changes in buckling mode shape as various combinations of shear and compression were applied. Even though the panel was curved, the grid was flat. This was acceptable, however, since no quantitative measurements were taken. The grid had 52 lines per inch. It was placed approximately 1 inch from the specimen with a light source and camera angle set at roughly 45 degrees from the perpendicular.

Photoelastic techniques were used to examine the distribution of load around one of the cutouts in the window-belt panel. The photoelastic coating consisted of a two-part liquid epoxy system — Ciba 502 resin and 951 hardener — which was poured onto a flat surface, allowed to partially cure, and then applied to the curved test specimen. While the specimen was under load, the photoelastic coating was observed using a Photoelastic Inc. 030 Series Reflective Polariscopes. The instrument has a resolution of 0.01 fringes. Readings were taken at the edge of the cutout where maximum tension and compression fringes were found.

SECTION 5 TEST RESULTS

5.1 GROUP A

The Group A tests were structured to provide monolayer and laminate elastic properties and allowables, joint characterization data (for both tension and compression, double and single shear, and biaxial conditions), and a limited amount of damage tolerance data (from compression panels). Specimen descriptions are given in Sections 2 and 3. Data given in this section are generally averages of three test results.

Monolayer testing was conducted for four material systems: F584/IM6 unidirectional tape, F584/IM6 five-harness satin weave cloth, F584/E-glass 120-weave cloth, and F584/S2-glass unidirectional tape. A summary of the monolayer properties calculated from these tests is given in Table 5-1. All elastic and strength properties were calculated using nominal specimen thicknesses. Longitudinal and transverse elastic moduli were extracted from strain gage data from the monolayer tension tests. Strain gages were not used for the monolayer compression tests. In-plane shear properties were obtained from tension tests of ± 45 -degree laminates using the methodology explained in Figure 5-1. Two shear moduli are given: the initial tangent modulus, and the secant modulus at $\gamma \cong 30,000$ microstrain. (The choice of 30,000 microshear-strain arises from the nature of the failure criterion used to calculate laminate allowables, and the longitudinal strain-to-failure of the carbon and E-glass materials.)

**Table 5-1
Monolayer Properties**

MATERIAL	t_{nom} (IN.)	E_L (MSI)	E_T (MSI)	ν_{LT}	G_{LT0} (MSI)	G_{LT1} (MSI)	F_{Lt} (KSI)	F_{Lc} (KSI)	F_{Tt} (KSI)	F_{Tc} (KSI)	F_{SH} (KSI)
F584/IM6 TAPE	0.0057	23.0	1.29	0.37	0.63	0.36	343.0	203.0	7.2	37.4	20.2
F584/IM6 CLOTH	0.0170	10.1	10.3*	0.06	0.53	0.32	144.0	86.8	144.0*	86.8*	16.7
F584/E GLASS (NO BLEED)	0.0060	2.1	2.1*	0.15	—	—	29.7	66.4	29.7*	66.4*	14.1
F584/E GLASS CLOTH (BLEED)	0.0051	2.6	2.6*	0.14	0.48	0.31	48.3	—	48.3*	—	15.9
F584/S2 GLASS TAPE (NO BLEED)	0.0082	4.9	—	0.34	—	—	147.0	—	—	—	—
F584/S2 GLASS (BLEED)	0.0060	6.3	—	0.29	0.69	0.32	211.0	171.0	—	—	17.5

* TRANSVERSE PROPERTY ASSUMED EQUAL TO LONGITUDINAL PROPERTY FOR CLOTH LAMINATES

G_{LT0} IS THE INITIAL TANGENT MODULUS

G_{LT1} IS THE SECANT MODULUS AT $\gamma_{LT} = 30,000$

Unnotched tension (UNT) and compression (UNC) tests were conducted in the 0-degree (X) direction for the four laminates. Two additional UNT configurations were included to determine the effect of the lightning protection systems on the elastic and strength properties of the basic fuselage skin laminate. Figure 5-2 summarizes the unnotched tension and compression test results. Comparisons with the laminate properties estimated from the monolayer data are also shown. Predicted elastic properties are based on traditional laminate theory; predicted strength properties are based on the Ashizawa-Black failure criterion (Reference 2).

Two sets of unnotched tension specimens were fabricated and tested. The original specimens were "dog-boned" in an attempt to avoid failures at the grips of the test machine. None of these specimens, however, actually failed at the minimum cross section (Figure 5-3). The redesigned specimens were simply 7.50-inch by 1.12-inch strips with no dogbone or doublers. It was observed that there was only a slight increase in the ultimate tension strength of lay-ups No. 2, 3, and 4. Lay-up No. 1, however, showed a substantial increase in strength of just over 37 percent. In an attempt to reconcile this discrepancy, specimens from both sets were inspected for thickness, ply count, and ply orientation, but no anomalies were discovered.

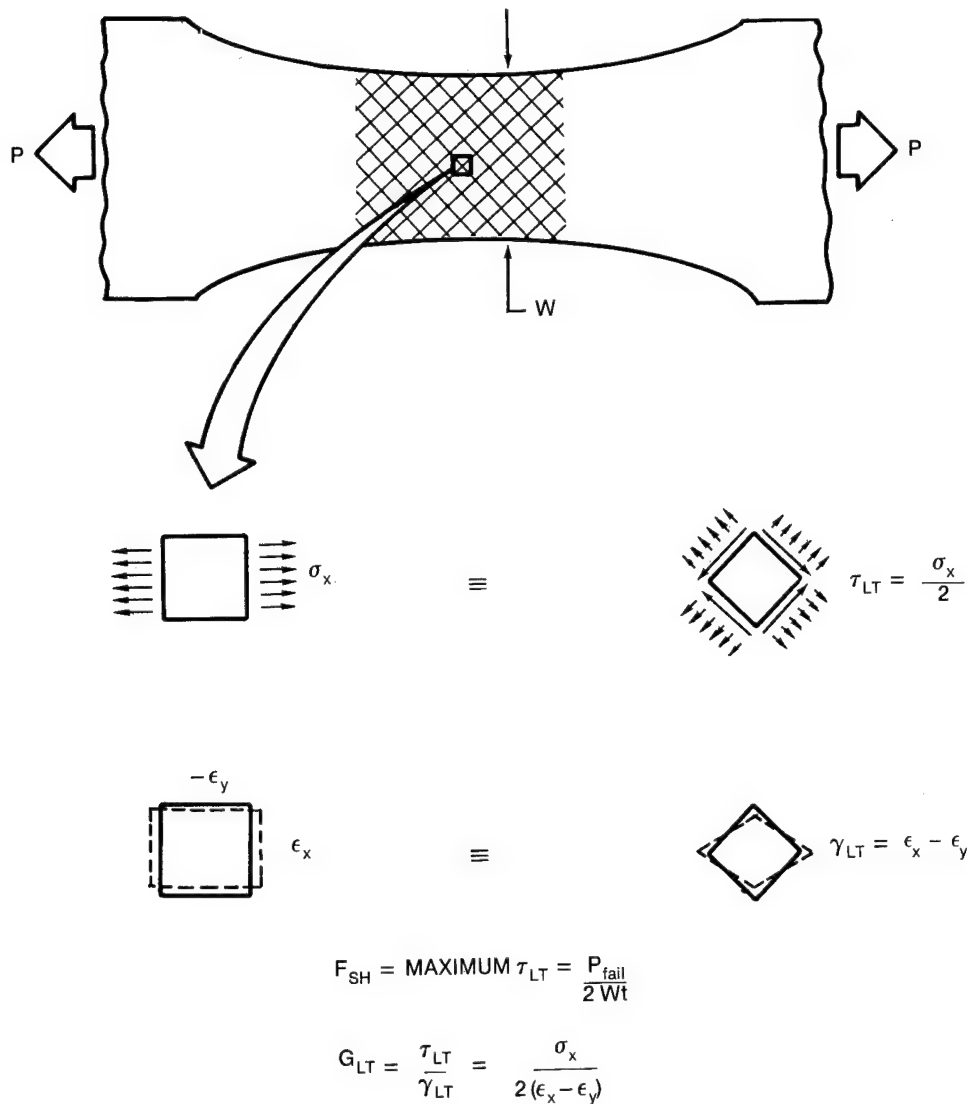


Figure 5-1. Method for Calculating Monolayer Shear Properties

Figure 5-4 summarizes the unloaded hole tension (ULT) results (excluding those of the -507 configuration, discussed later). Gross-section stresses were calculated from measured widths and nominal thicknesses. Gross-section strains were calculated from the gross-section stresses and the measured moduli from the unnotched tension tests. Comparisons are shown to the gross-section stresses which would be predicted assuming isotropic, linear elastic stress concentrations and using the unnotched tension allowables from the UNT tests. The higher test values are indicative of some form of a relief mechanism which lessens the effective stress concentration at failure. The work performed under the NASA-sponsored Critical Joints Program (NAS1-16857) (Reference 3) suggests the unloaded-hole C-factor as the appropriate empirical constant to be calculated from these results. These values are given in Figure 5-4 for lay-ups No. 2 and 4. No C-factor is given for lay-up No. 3, which demonstrated seemingly complete relief (i.e., showed no evidence of any stress concentration whatsoever).

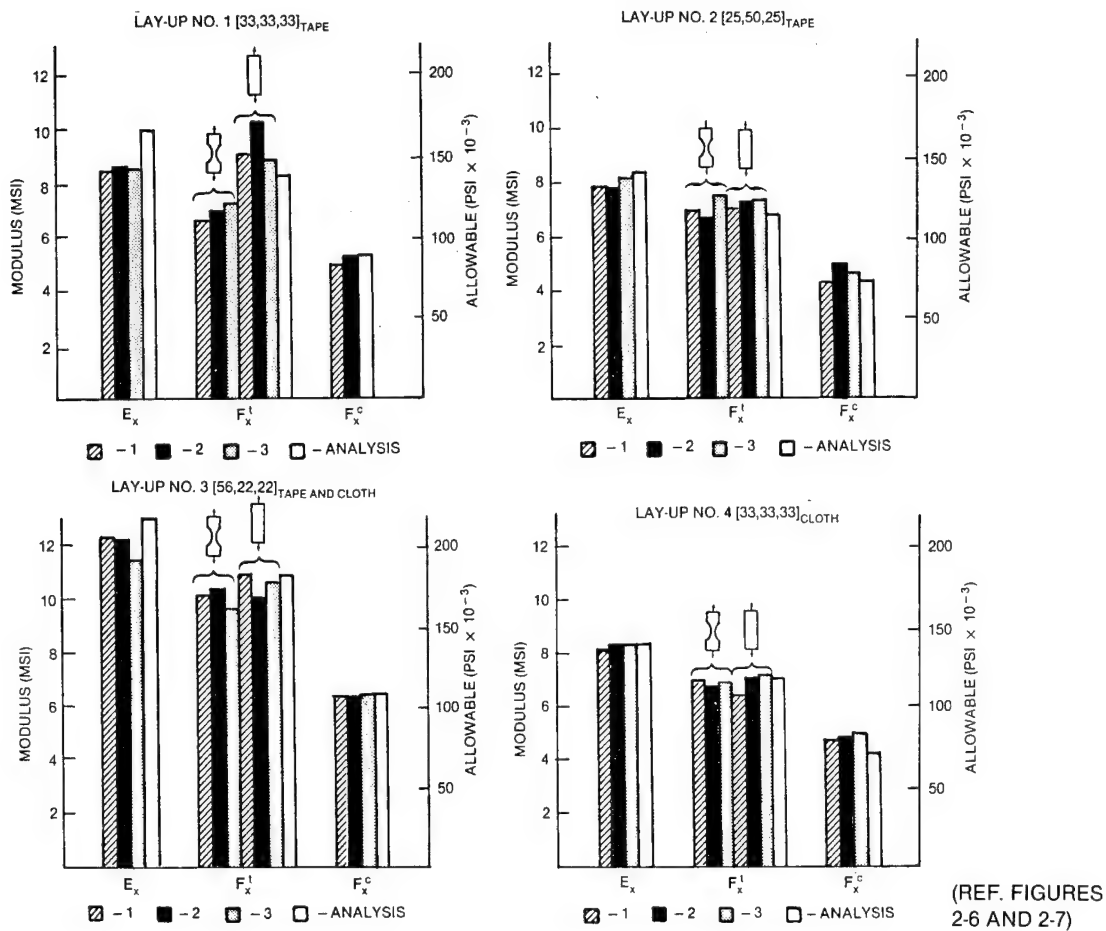


Figure 5-2. Unnotched Tension and Compression Specimen Test Results

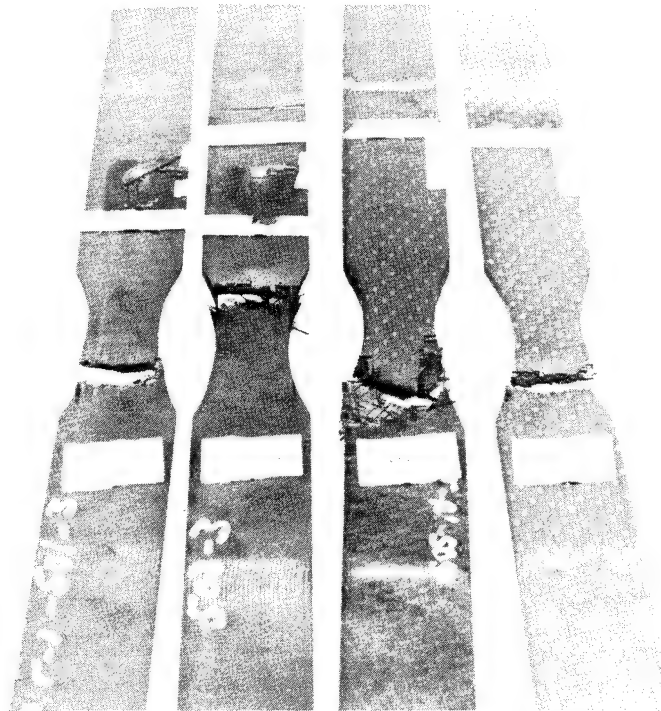


Figure 5-3. Failures of the Dogboned UNT Specimens

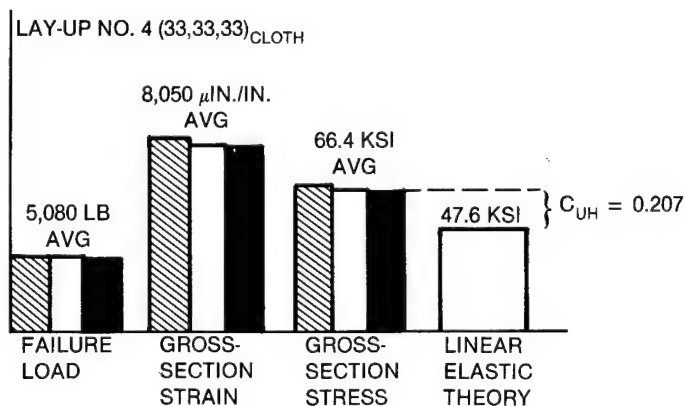
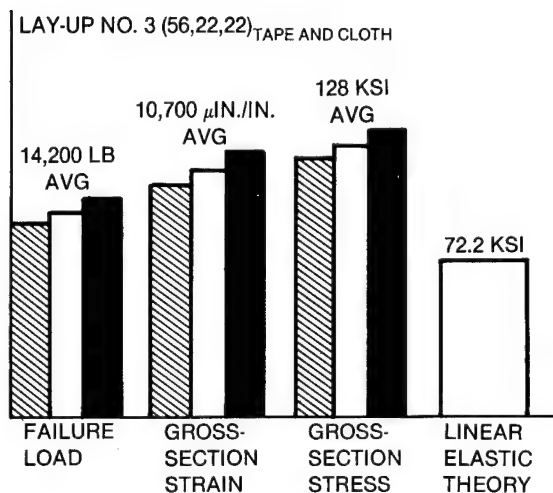
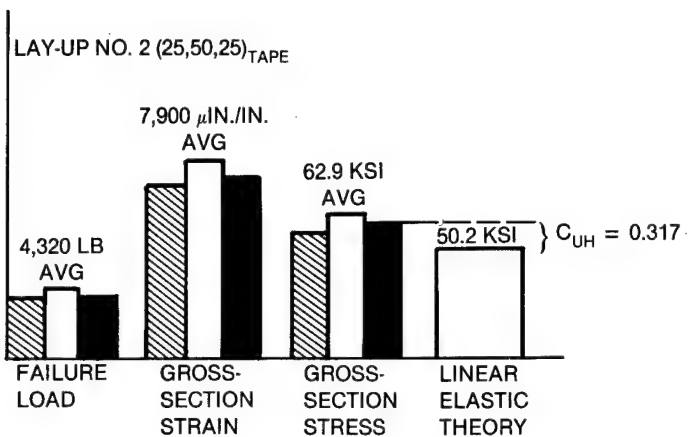
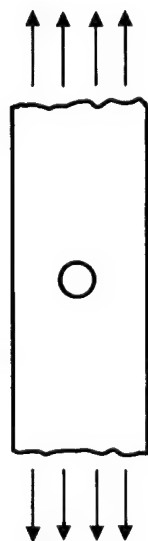


Figure 5-4. Unloaded-Hole Tension Specimen Test Results

The double-lap tension (DLT) tests were based on 3/16-inch-diameter fasteners. Two sets of specimens for each lay-up pattern were tested: one with a nominal width of 0.563 inch ($w/d = 3$) and one with a nominal width of 1.13 inch ($w/d = 6$). The wider specimens were designed to fail in bearing, the narrow ones in net-section tension. Two configurations (-525 and -527) were tested with countersunk fasteners.

A similar relief effect occurs for net-section tension failures of the narrow DLT specimens (also referred to as loaded-hole tension specimens) as occurs for the ULT specimens. Figure 5-5 summarizes these results and again shows comparisons to theoretical strengths assuming isotropic, linear elastic stress concentrations. Loaded-hole C-factors are given (for lay-ups No. 2 and 4) as the empirical constant which quantifies the relief effect. Again, the test results for lay-up No. 3 are unique. The narrow specimens failed in a shearout mode rather than in net-section tension.

Load/deflection characteristics, or spring rates, for each of the fastener/laminate combinations were also measured. Specifically, the relative displacement of the specimen edges (inner member relative to the two outer members) at the centerline of the fastener were recorded using special fixtures. These spring rates are used for determining load sharing among fasteners in a multirow bolted joint (essential for the analysis of composite joints).

The wide DLT specimens were tested to determine bearing "yield" and bearing ultimate stresses for lay-ups No. 2, 3, and 4 (for double-shear, tension loads). Load/deflection properties were used to determine the loads at which joint performance became nonlinear. This onset of nonlinearity is then reported as the bearing yield stress. Bearing ultimate stress was determined from the maximum load obtained (regardless of the hole deformation).

Figure 5-6 shows typical failures for each of the three wide DLT configurations. The -509 configuration (lay-up No. 2) clearly failed in bearing. The failure zone of the -507 configuration (lay-up No. 4) extends to the edge of the specimen, indicating edge effects could have been significant. (Edge distance for all of these specimens was 0.625 inch, which is just over $3d$). The -511 configuration (lay-up No. 3) appears to have failed in a shearout mode. Figure 5-7 summarizes the results of the bearing tests. Note that the narrow DLT configuration for lay-up No. 3 (-505) is included because of the similarity in failure mode with the -511 configuration.

The ULT tests and the double-lap tension specimens were designed to yield empirical engineering constants to be used in the analysis of double-shear tension joints. Analysis of compression joints is less well understood. Nevertheless, a number of specimens were designed to provide some insight into the behavior of compression joints. These included the unloaded-hole compression (ULC) specimens and the double-lap compression specimens (DLC). Again, configurations of three laminates were tested (lay-ups No. 2, 3, and 4).

The ULC specimens were similar to the ULT specimens except that fasteners were used to fill the holes during the tests. Two sets of ULC specimens were tested for each lay-up: one set with 5/32-inch bolts, the other with 3/16-inch bolts. Two specimens (-525 and -527) were tested with countersunk holes. These tests are discussed later in this section.

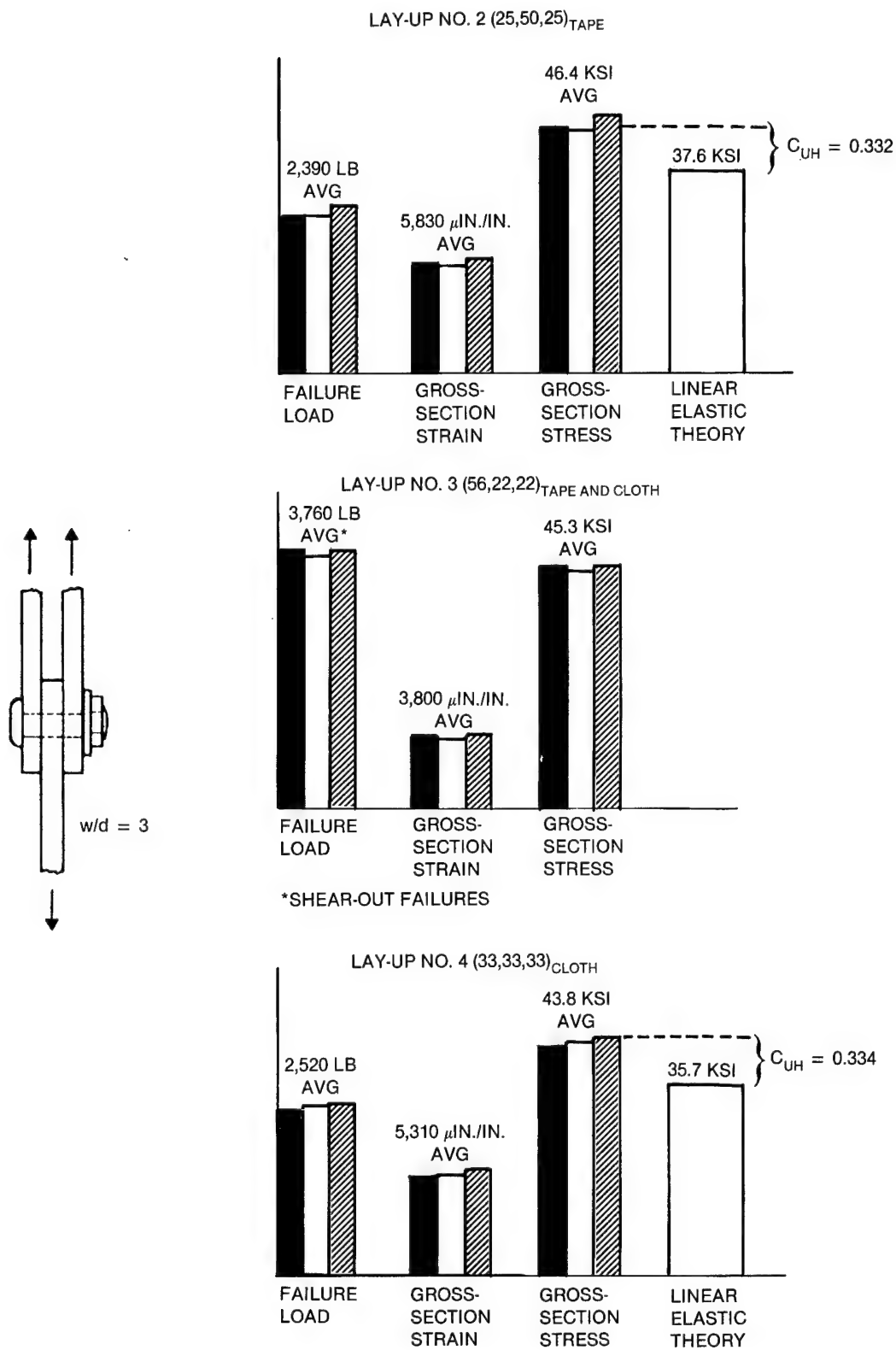


Figure 5-5. Narrow DLT Specimen (Loaded Hole) Test Results



Figure 5-6. Bearing and Shear-Out Failures of Wide DLT Specimens ($W/D = 6$)

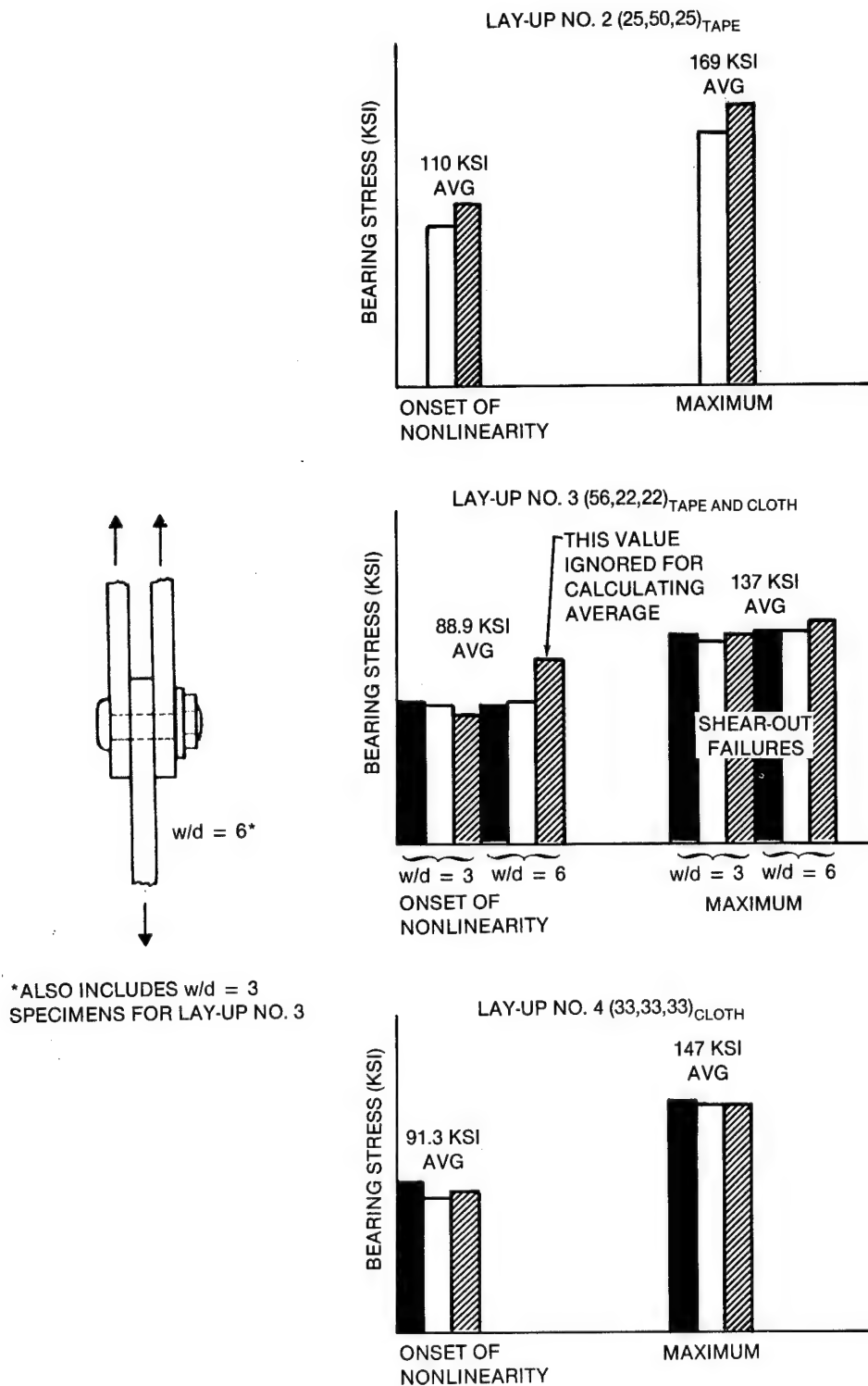


Figure 5-7. DLT Specimen Test Results (Bearing and Shear-Out Failures)

A summary of the failure loads, gross-section stresses, and gross-section strains for the ULC specimens is given in Figure 5-8. Failures of the specimens tested with 5/32-inch fasteners tended to exhibit more damage through the hole. Failures of the specimens tested with 3/16-inch fasteners tended to show less damage at the hole, but tended to broom or buckle in front of the fastener (Figure 5-9).

Like the DLT specimens, two sets of DLC specimens were tested for each lay-up pattern: one with a w/d of 3, and one with a w/d of 6. The wider specimens were expected to fail in bearing and thus yield a comparison of bearing strengths for tension and compression loading. Figure 5-10 summarizes the DLC test results for both the narrow and wide DLC specimens. Typical failures for the narrow DLC specimens tended to occur in front of the fastener or, in some cases, a considerable distance away from the fastener (Figure 5-11).

Several of the specimens were designed to look at countersunk bolt holes and countersunk fasteners and their effects on joint performance. These included unloaded hole tension and compression specimens (ULT-507, ULC-525, and ULC-527) as well as double-lap tension and compression specimens (DLT-525, DLT-527, DLC-529, and DLC-531). All of these specimens were fabricated from lay-up No. 2.

The results of the ULT-507 configuration tests are presented in Figure 5-12. Comparisons are shown between this configuration and its noncountersunk counterpart (ULT-503). As indicated, failure load and gross-section stress are down by an average of 22 percent. Net-section stress, however, shows considerably less reduction (only 8 percent).

The results of the countersunk ULC tests are presented in Figure 5-13. The -515 and -521 ULC specimens were tested with 5/32-inch and 3/16-inch protruding head fasteners to simulate loose fit and net fit bolts, respectively. The -525 configuration was tested *without* a fastener and the -527 configuration with a 3/16-inch countersunk bolt to simulate the same situations for countersunk fasteners. Comparisons of the failure loads of the -525 and -515 configurations again reveal an average drop of about 22 percent. Likewise, net-section stress comparisons show a much smaller drop: about 9 percent. Similar comparisons for the -527 and -521 configurations indicate the countersinks have less effect for the net fit case, demonstrating drops of 19 percent and 4 percent, respectively, for the average gross-section and net-section strengths. Figures 5-14 and 5-15 show typical failures for the two countersunk ULC configurations.

All of the DLT and DLC specimens failures occurred in the center member rather than in either of the splice plates. Therefore, the effect of using countersunk fasteners would be expected to be minimal. Figure 5-16 gives a comparison of countersunk and noncountersunk test results for both the narrow and wide DLT specimens. As can be seen, virtually no change in strength was evidenced for the narrow specimens (which failed in net-section tension). Bearing strengths on the other hand (from the wide DLT specimens), demonstrated a reduction of about 12 percent when countersunk fasteners were used. Figure 5-17 presents a similar comparison for the DLC specimens.

The single-lap tension specimens (SLT) were designed to provide coupon level data for single shear joints. Figure 5-18 summarizes the SLT test results. All of the narrow specimens failed in net-section tension at one of the "bearing + bypass" locations. In the case of the -507 configuration, the net-section stresses shown account for the area removed by the countersink. (This was the only configuration that was countersunk at the failure location.)

Comparison of the data from the -501 and -507 configurations reveals an overall drop in strength of almost 36 percent (or a reduction in net-section strength of about 14 percent) due to simply flipping the fasteners. The critical location in one case (-501) was through a noncountersunk hole, and, in the

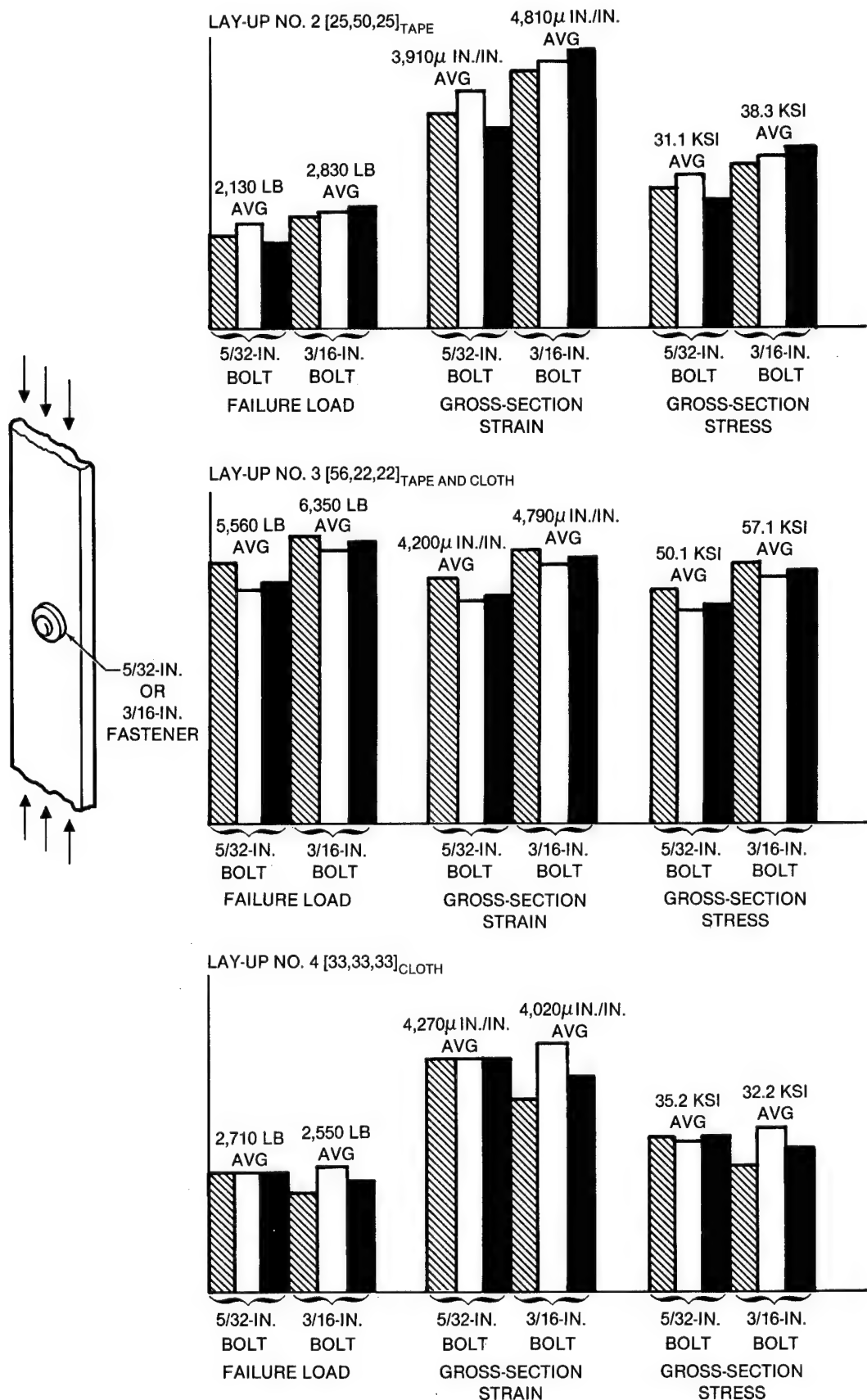


Figure 5-8. Unloaded-Hole Compression Specimen Test Results

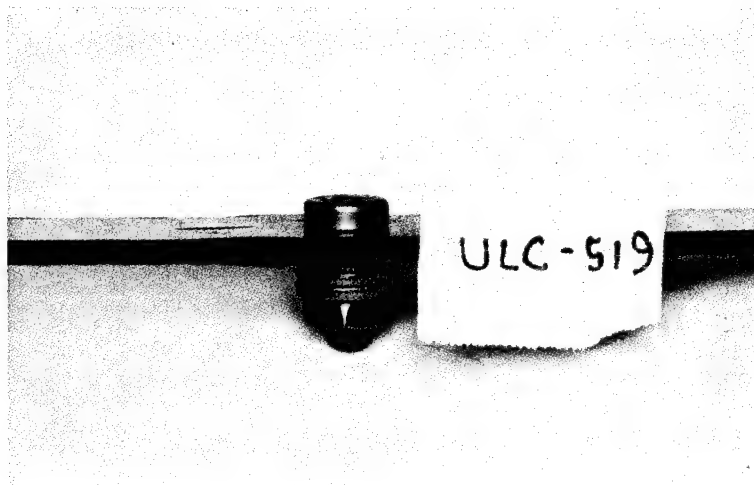


Figure 5-9. Typical Failure of ULC Specimen with 3/16-Inch Fastener (Lay-Up No. 4)

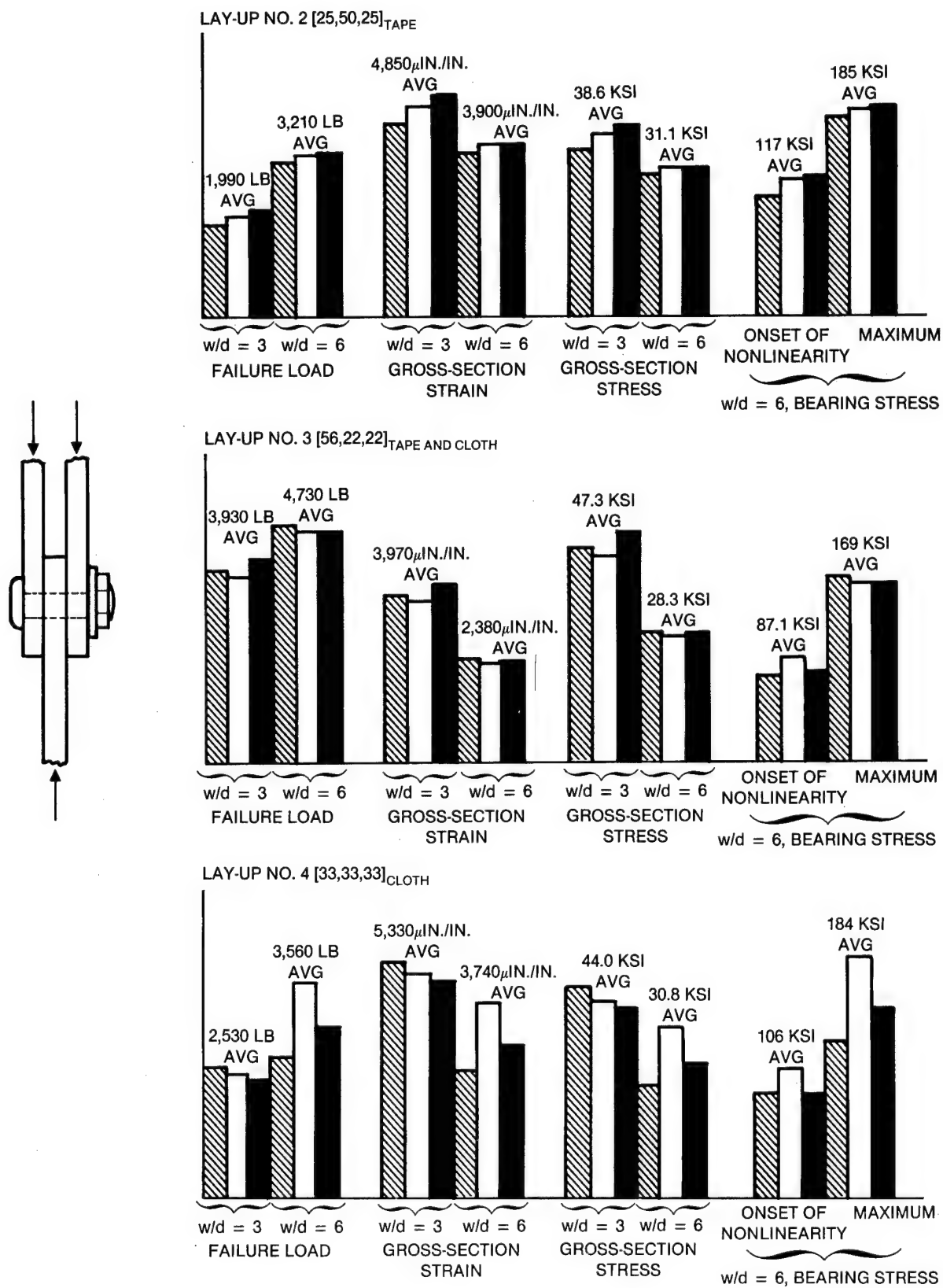


Figure 5-10. Double-Lap Compression Specimen Test Results

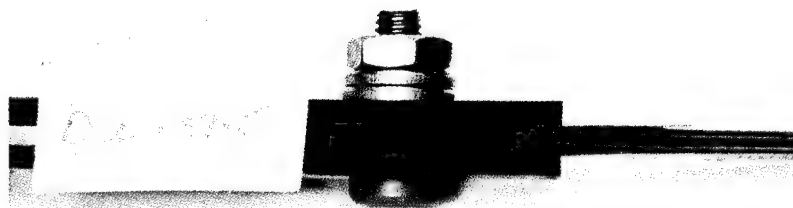


Figure 5-11. Typical Failure of Narrow DLC Specimen (Lay-Up No. 2)

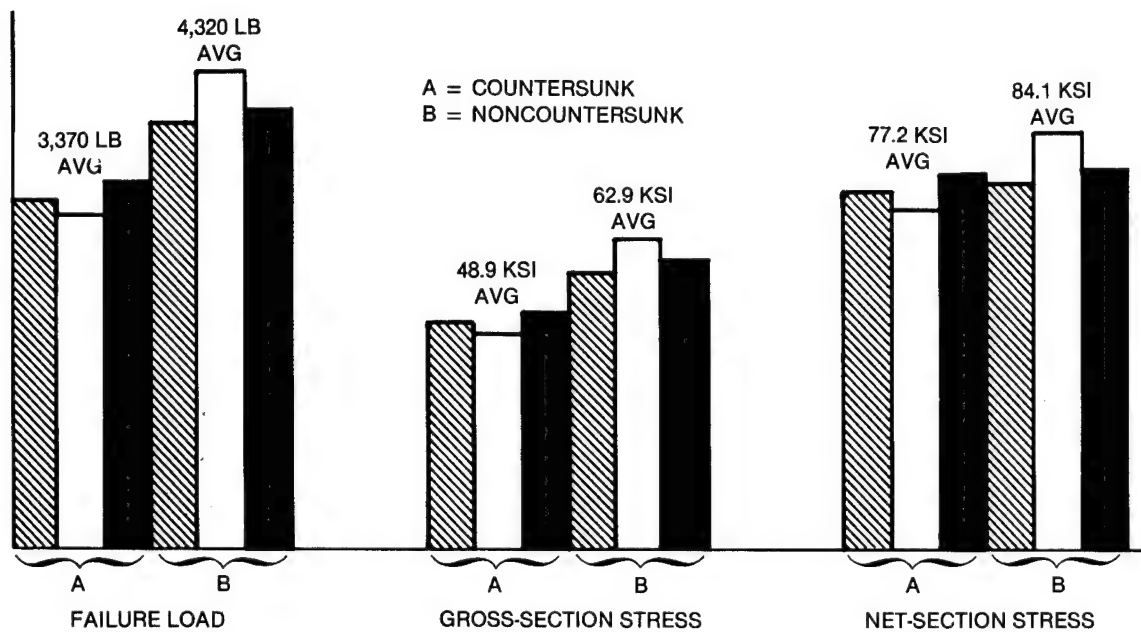


Figure 5-12. Unloaded-Hole Tension Specimen Results (Lay-Up No. 2, Countersunk)

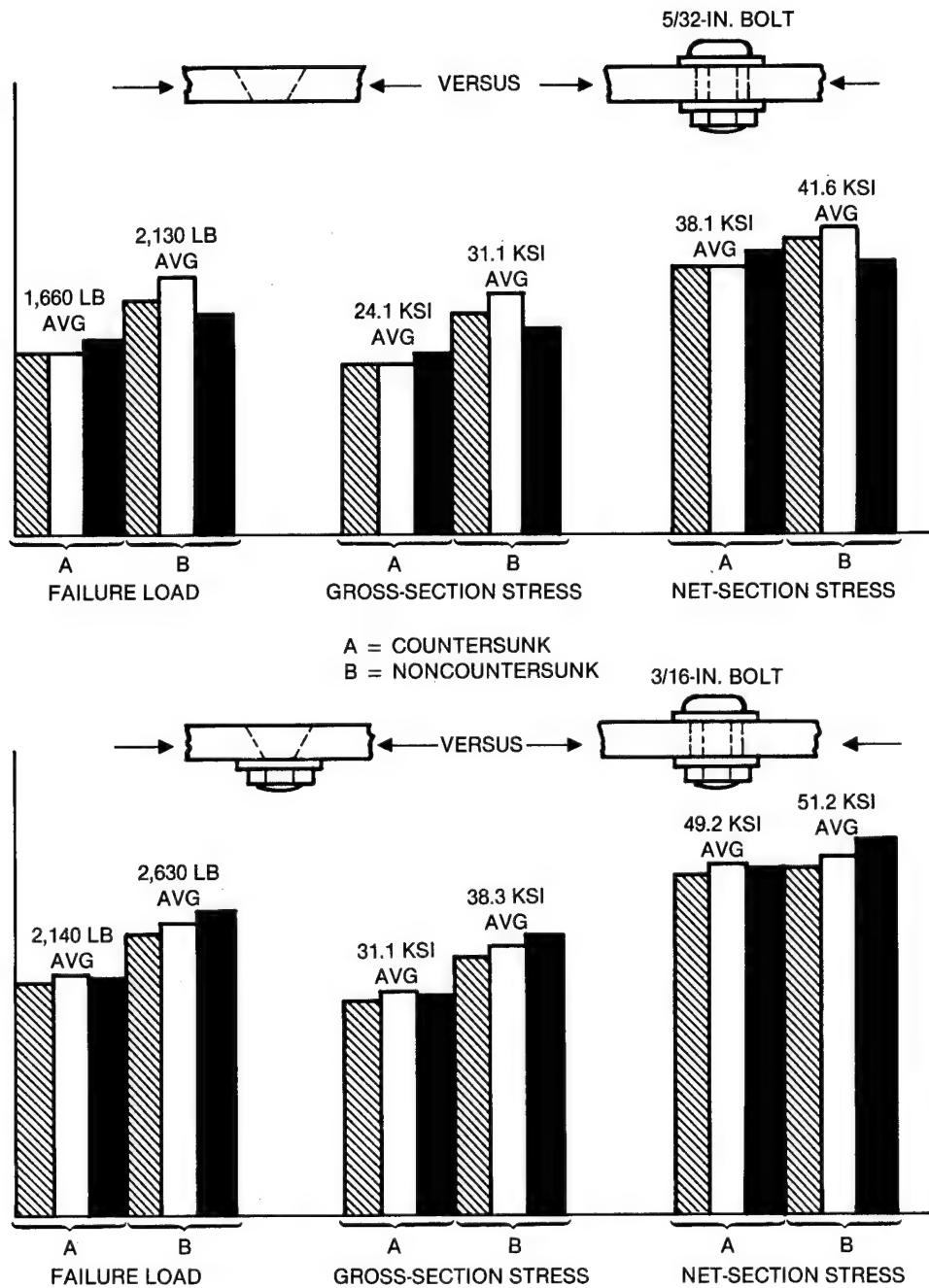


Figure 5-13. ULC Specimen Test Results (Lay-Up No. 2, Countersunk)



Figure 5-14. Typical Failure of Countersunk ULC Specimen (Tested Without Fastener)

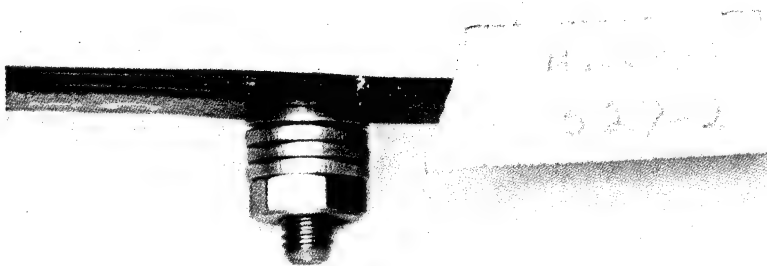


Figure 5-15. Typical Failure of Countersunk ULC Specimen (Tested With Fastener)

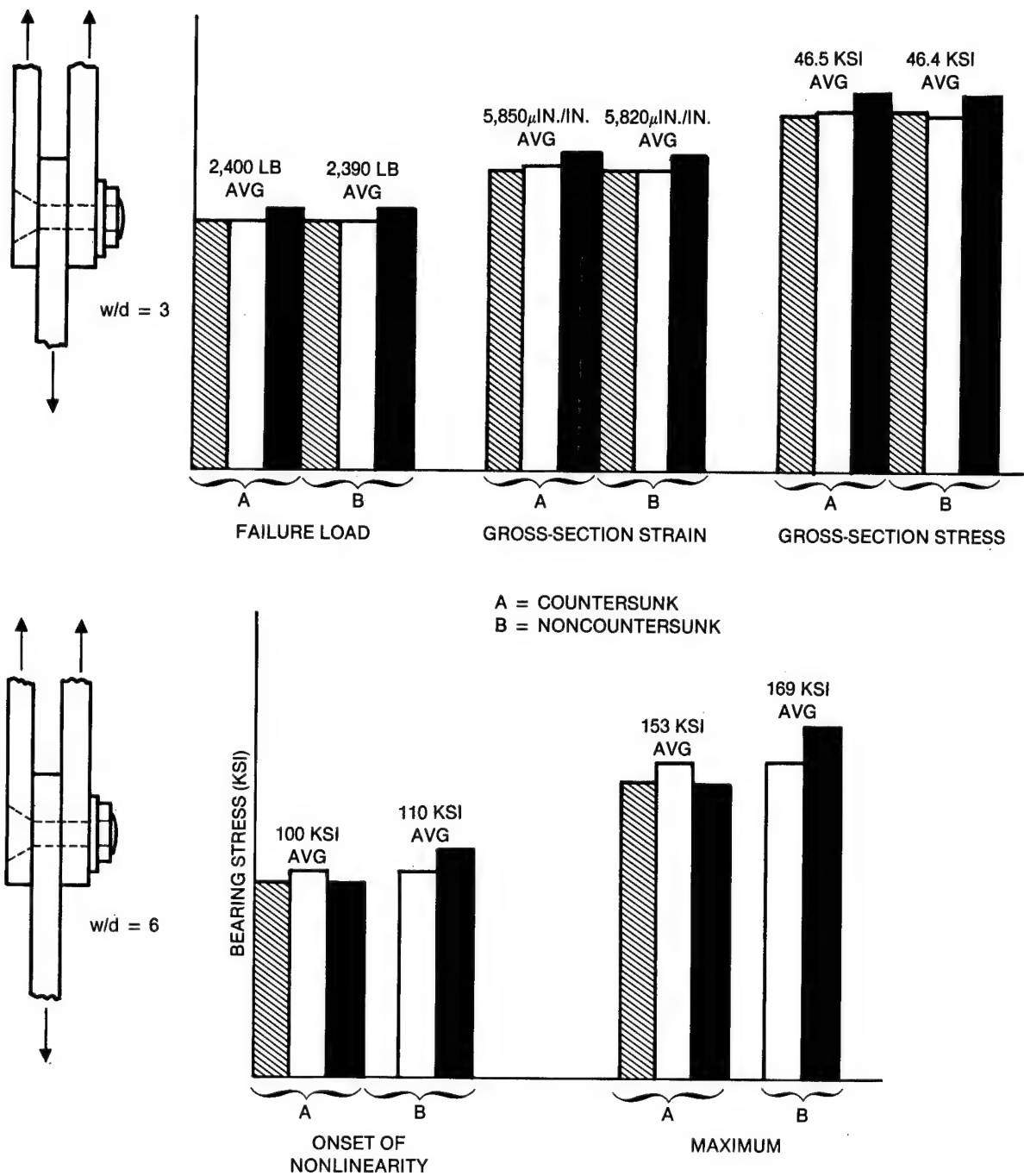
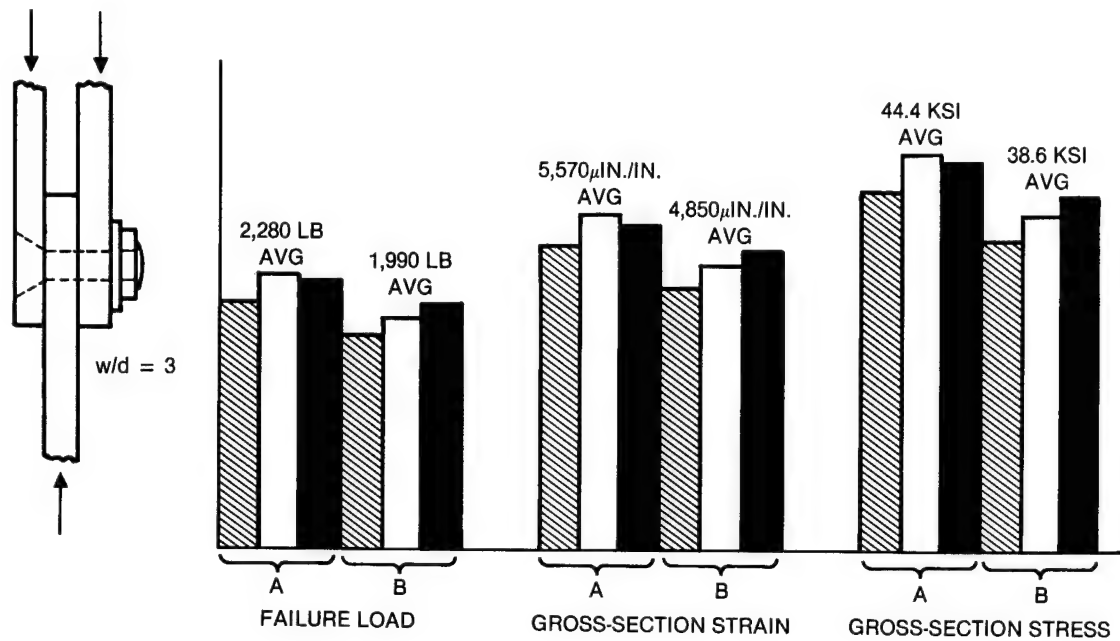


Figure 5-16. DLT Specimen Test Results (Lay-Up No. 2, Countersunk Fastener)



A = NONCOUNTERSUNK
B = COUNTERSUNK

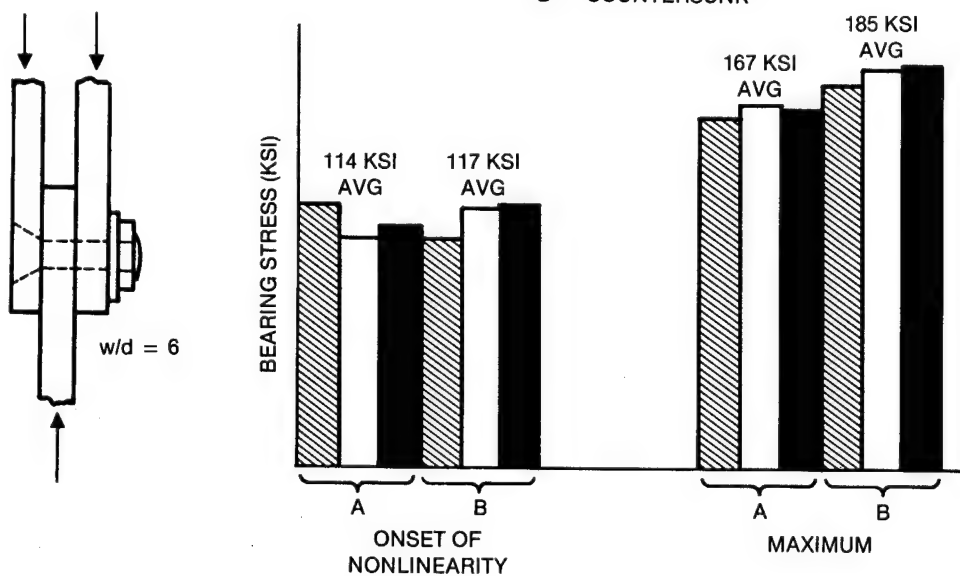


Figure 5-17. DLC Specimen Test Results (Lay-Up No. 2, Countersunk Fastener)

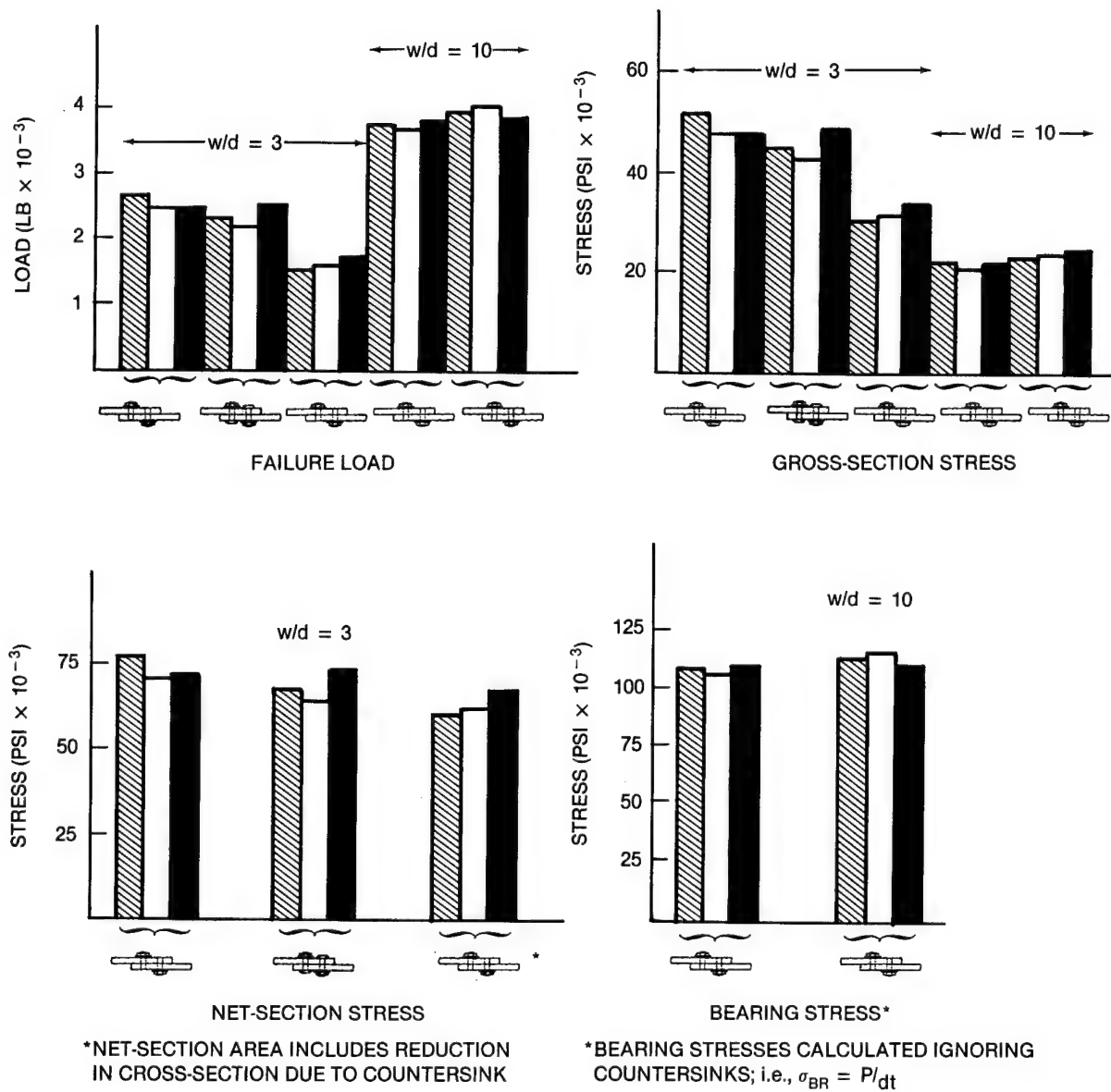


Figure 5-18. SLT Specimen Test Results

other, (-507) was through a countersink. Comparison of the -501 and -505 data suggests the countersunk configuration is actually stronger than the noncountersunk configuration (again, as long as the critical "bearing + bypass" location is not in a countersunk member). This is thought to be a result of the reduced eccentricity of the countersunk connection. The test results of the -503 and -509 (wide) SLT configurations were very similar. These specimens failed as a combination of the fasteners pulling through the laminate and failure of the fastener heads. Considerable fastener rotation and hole deformation was also evident. Although the failures were not pure bearing failures (like those seen for the wide DLT and DLC specimens), Figure 5-18 includes nominal bearing stresses (ignoring the countersinks) for reference and comparison. Load/deflection properties were also recorded for the -501, -503, and -505 configurations.

The last of the coupon-level joint specimens were designed to investigate the effects of biaxial loading (orthogonal bearing and bypass components) on joint performance. The 12 biaxial stress specimens (BAS) were nominally identical but tested with varying combinations of bearing loads and bypass loads.

The results of the biaxial tests are summarized in Figure 5-19. These data indicate that bearing stresses of up to 60 ksi had virtually no effect on the orthogonal bypass strength. Likewise, specimens 6 and 7 show only a small loss in bypass strength at 80 ksi bearing. Specimen 9 indicated that an orthogonal bypass load of 2,500 lb/in. (roughly 3,300 $\mu\text{in./in.}$ gross-section strain) had no effect on either the onset of non-linearity (bearing yield) or the ultimate bearing strength. The only specimen which demonstrated any significant interaction was specimen 8, and this is at levels of bearing (140 ksi) and bypass (6,500 $\mu\text{in./in.}$ gross-section strain).

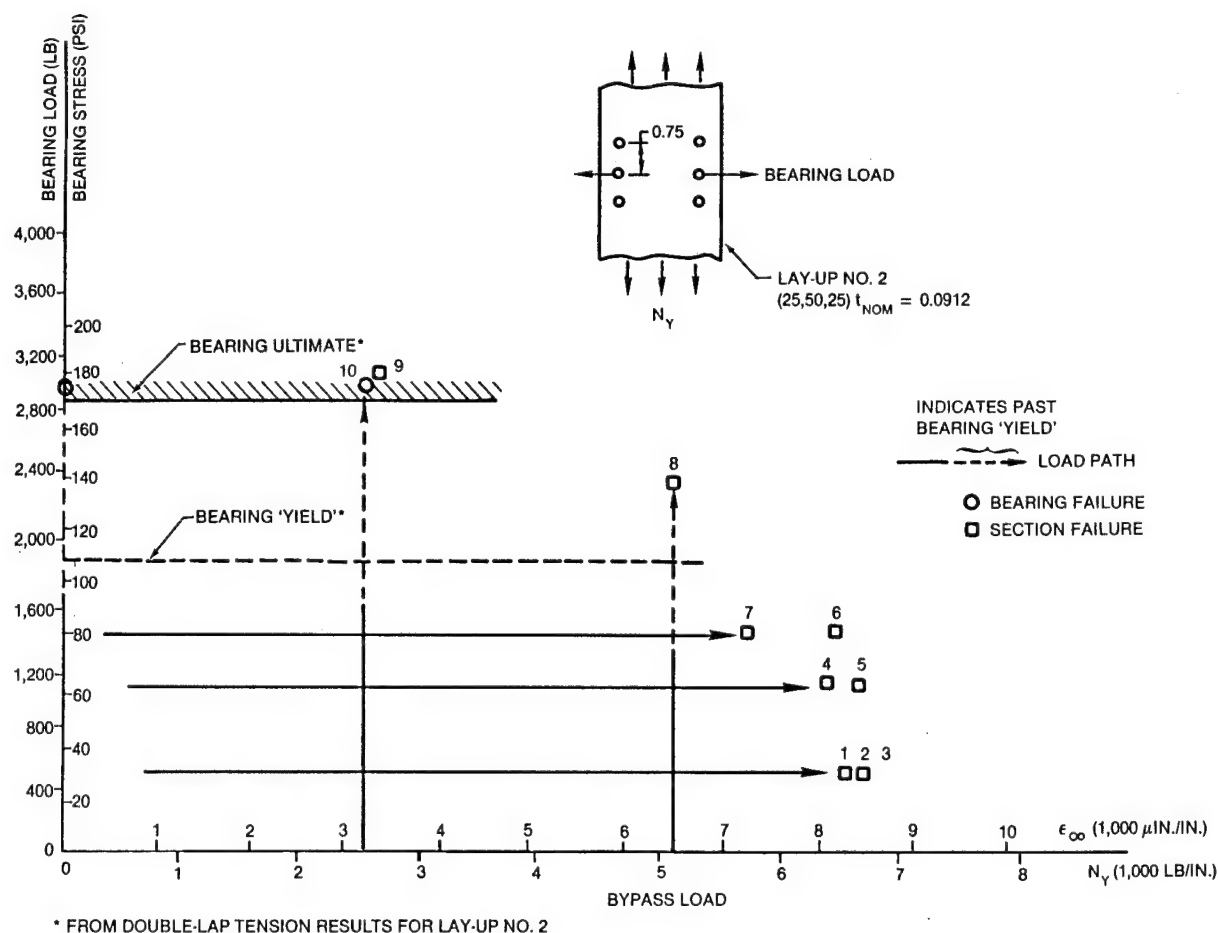


Figure 5-19. BAS Specimen Test Results

It should be reiterated that only the middle of the three rows of fasteners was loaded in bearing. Thus, the effective bolt spacing for bearing loads was closer to $8d$ than $4d$. This, of course, would have the effect of encouraging bearing failures for those tests dominated by loaded hole stress fields (specimens 9 and 10 in Figure 5-19). The concern lies, however, in the reduced tangential tension stresses (at the top and bottom of the loaded holes) and the (perhaps reduced) interaction with the peak tangential tension stresses from the bypass load (along the sides of the bolt holes). Calculations indicate, however, that the reduction in effective peak tangential stress for the bearing loads was only on the order of 6 or 7 percent (assuming the loaded-hole C-factor from the DLT testing). It is concluded, therefore, that the effect of loading all three rows of fasteners would be minimal.

The last of the Group A specimens were the compression-after-impact or CAI panels. The results of these tests are summarized in Figure 5-20. The highest strength loss observed was for the unprotected panel subjected to lightning strike, followed by the panel with a 1/2-inch-diameter hole. However, the impacted panel and the protected panels subjected to lightning strike all exhibited strengths greater than 39 ksi (the stress corresponding to the design ultimate strain of $4,500 \mu\text{in./in.}$).

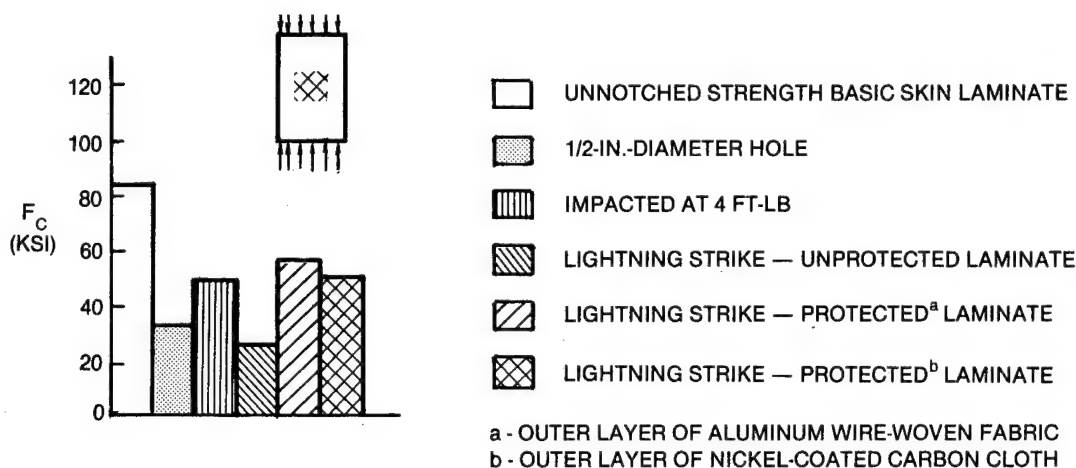


Figure 5-20. CAI Specimen Test Results

5.2 GROUP B

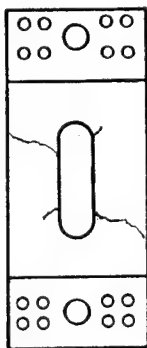
The Group B tests included tension and shear panels containing large cutouts, and the shear-tee pull-off specimens. Specimen descriptions are given in Sections 2 and 3. The ultimate failure loads for the five tension panel configurations are given in Table 5-2. The two panels softened with E-glass failed at lower loads than the baseline. The panel with the graphite doubler and the panel softened with S2-glass both showed improvement (up to 66 percent and 26 percent, respectively). Failure locations for the panels are illustrated in Figure 5-21.

All of the panels except the -505 (with the thick graphite doubler) buckled at the top and bottom of the cutout at load levels varying from 18 to 25 kips. This behavior is quite obvious from the strain gage data taken for the -501 and -509 panels, each of which had a strain gage positioned at the top of the cutout. There was no gage at this location for the two E-glass panels; however, the buckling load was estimated from the change in slope of the data from the strain gages along the side of the cutout.

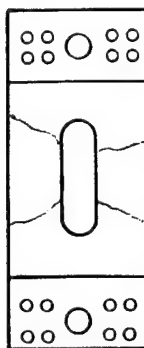
**Table 5-2
Tension Cutout Test Results**

CONFIGURATION	DESCRIPTION	NONLINEARITY STARTED AT (LB)	FAILURE LOAD (LB)
- 501	BASILINE LAY-UP NO. 2 (25, 50, 25) $t^* = 0.0912$	25,000	54,000
- 503	PARTIALLY SOFTENED WITH E-GLASS IN 0/90 DIRECTIONS $t^* = 0.0864$	25,000	50,000
- 505	BUILDUP AROUND THE CUTOUT $t^* = 0.2280$ IN.	LINEAR TO FAILURE	90,000
- 507	FULLY SOFTENED WITH E-GLASS $t^* = 0.0960$	25,000	38,610
- 509	PARTIALLY SOFTENED WITH S2 TAPE GLASS IN 0/90 DIRECTIONS $t^* = 0.0936$	15,000	68,310

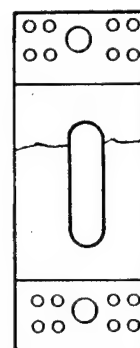
*THICKNESS AT THE CUTOUT



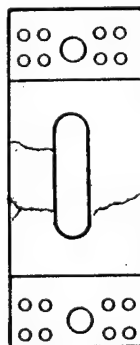
BASILINE
(- 501)



E-GLASS SOFTENED (0s AND 90s)
(- 503)



E-GLASS SOFTENED
(- 507)



GRAPHITE DOUBLER
(- 505)



S2-GLASS SOFTENED
(- 509)

Figure 5-21. Failure Locations for Group B Tension Cutout Panels

The baseline panel (-501) was the only one to buckle in opposite directions at the top and the bottom of the cutout. This is illustrated in Figure 5-22 by the asymmetry of the photoelastic fringe pattern at 31 kips. Although difficult to discern, the top of the cutout buckled toward the camera, producing tensile strains on the surface being viewed, which subtract from the membrane compressive strains to produce a black, or zero-principal-strain, region. Likewise, the buckle at the bottom of the cutout is away from the camera, producing bending strains which add to the compressive membrane strains. Typical plots of strain gage and photoelastic data are shown in Figures 5-23 and 5-24.

A summary of the failure loads for the shear panel tests is given in Figure 5-25. All three panels failed initially at the top and bottom corners of the cutout. These localized failures did not result in the collapse of the panels, however. As indicated, the ultimate failure of the -505 panel was precipitated by a partial failure of the picture frame load introduction fixture. Strain gage data indicated that the panel was close to failure before this occurred.

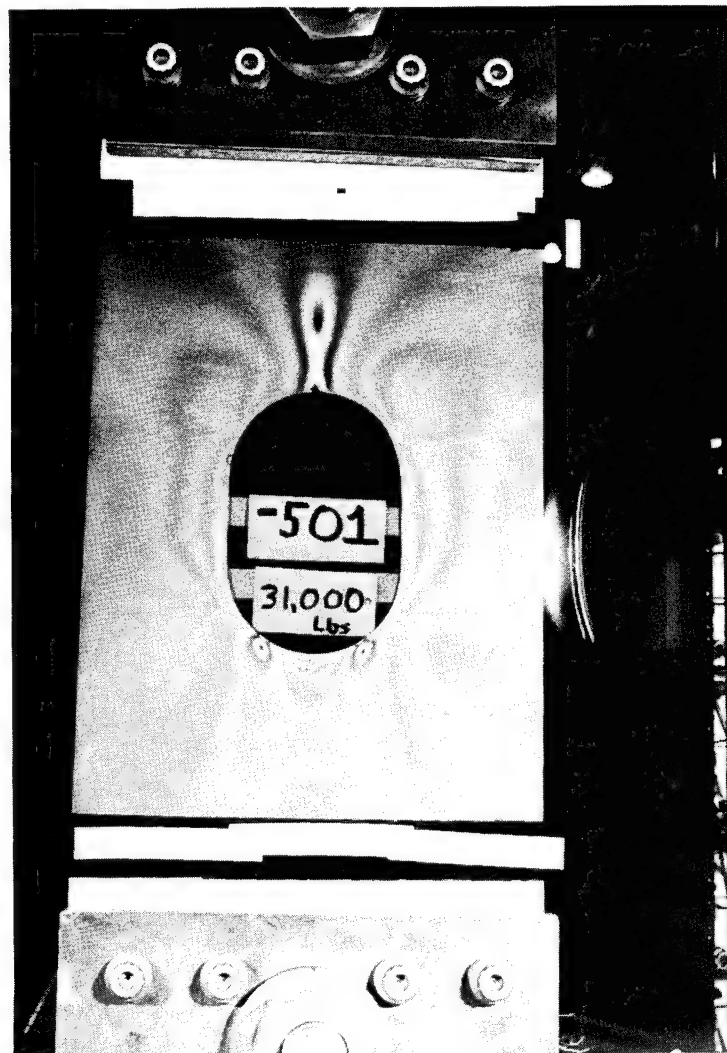


Figure 5-22. Photoelastic Fringe Pattern for -501 Tension Cutout Panel

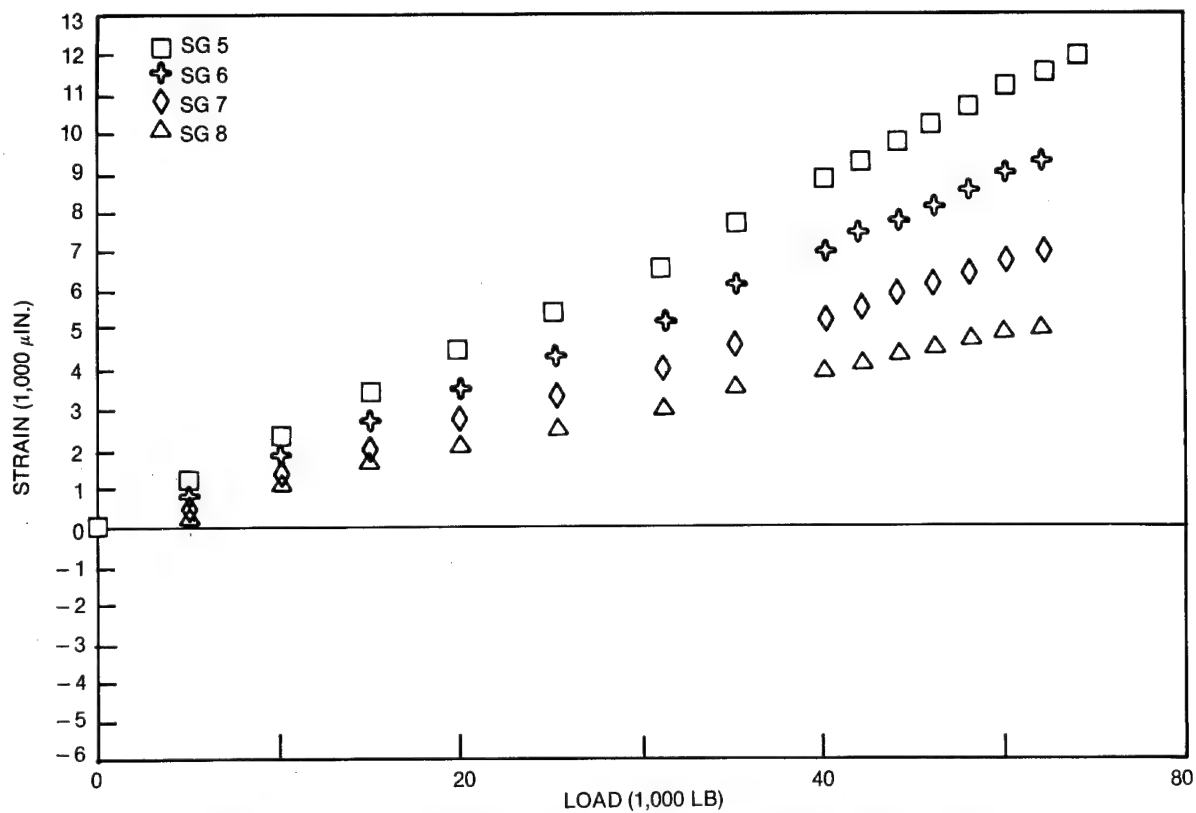


Figure 5-23. Typical Strain Gage Data for Tension Cutout Panel (-501)

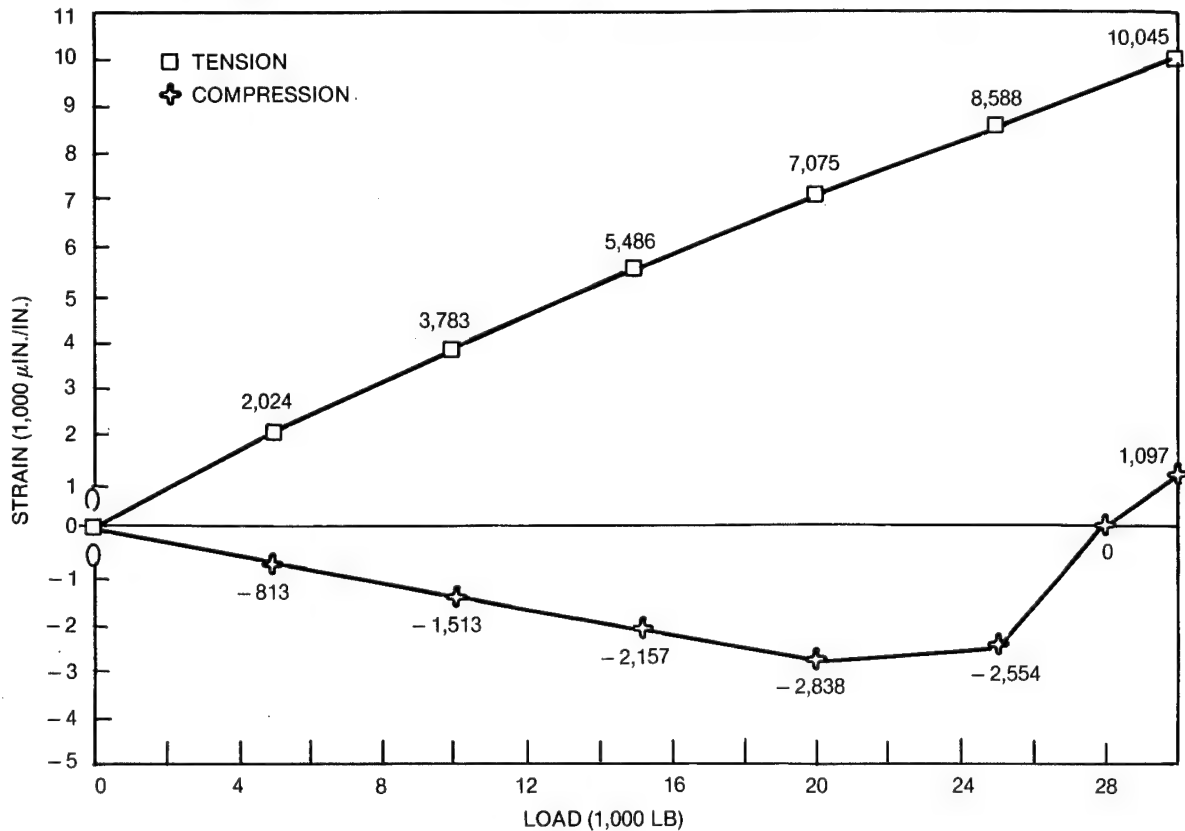


Figure 5-24. Typical Photoelastic Data for Tension Cutout Panel (-501)

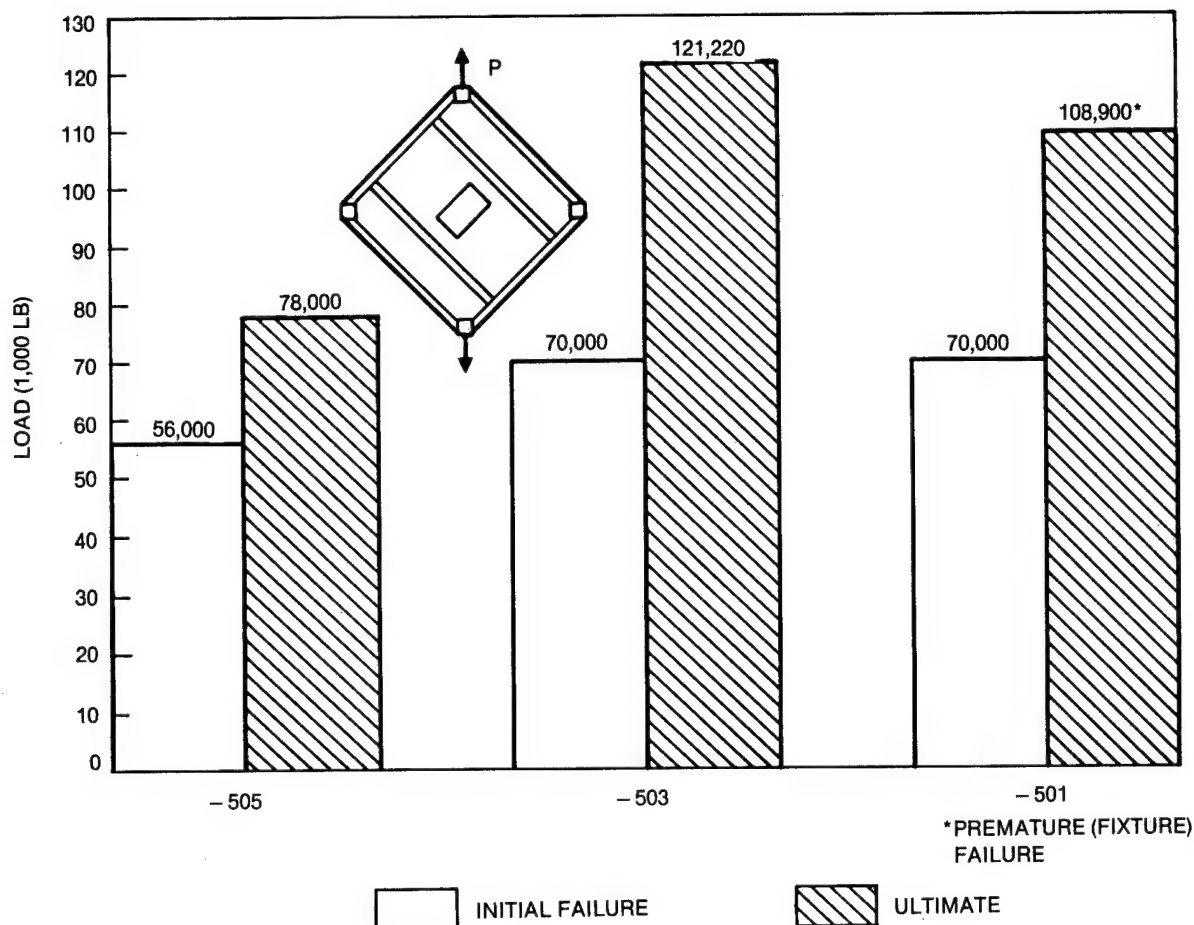


Figure 5-25. Failure Loads for Group B Shear Cutout Panels

A sketch of the failed baseline panel (-501) is included as Figure 5-26. Strain gage data (Figure 5-27) taken at the top corner indicate a moderate change in slope at about 30 kips and a marked nonlinear behavior beginning around 50 kips. While holding the load at 56 kips, a loud noise was heard, and while holding at 58 kips, a drastic drop in measured strain at the top corner ($-9,830$ to $-2,632 \mu\text{in./in.}$) was observed. Inspection of the test article revealed delaminations at the cutout on both compression diagonals (top and bottom corners). As the load was increased, these delaminations were observed to progress toward the intersections of the stiffeners. Panel failure occurred while holding at 78 kips. Ultimate failure appears to have resulted from the stiffeners having disbonded from the panel, thus effectively eliminating the last remaining load path for the diagonal compression load.

As noted in Figure 5-26, there was also some very slight damage observed on the tension diagonals, as well as some slight brooming at the ends of the stiffeners, indicating that they had been end-loaded by the thick steel doublers bonded to the periphery of the panel. The loads carried by the latter, however, are not considered to have been significant.

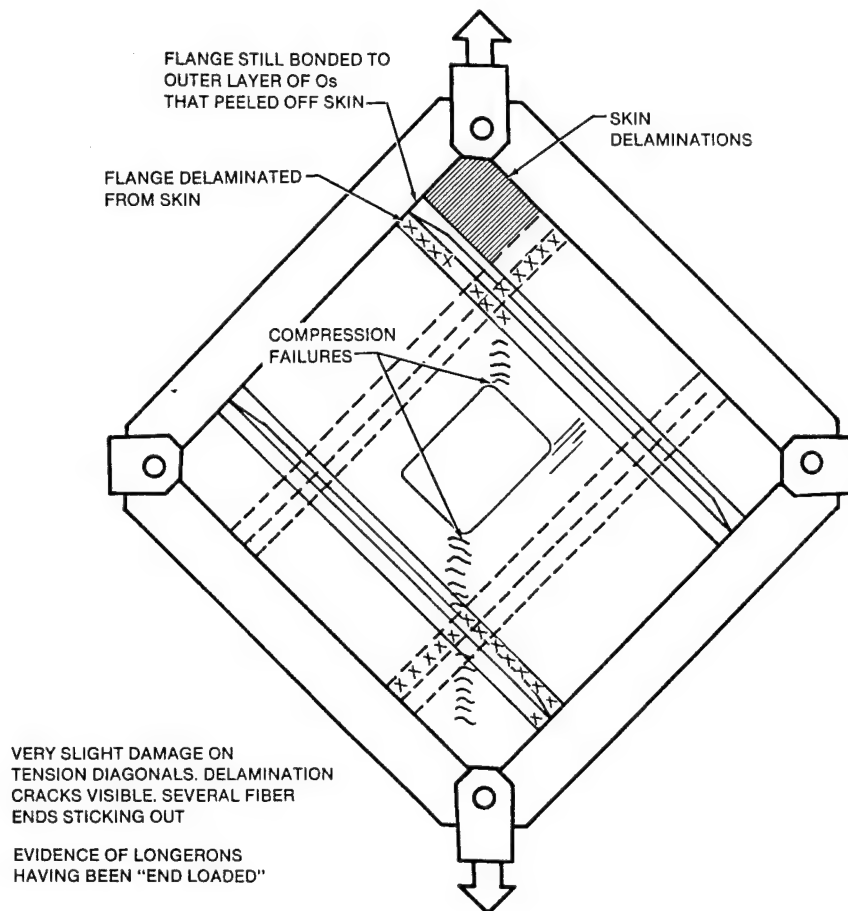


Figure 5-26. Failure Locations for -501 Shear Cutout Panel

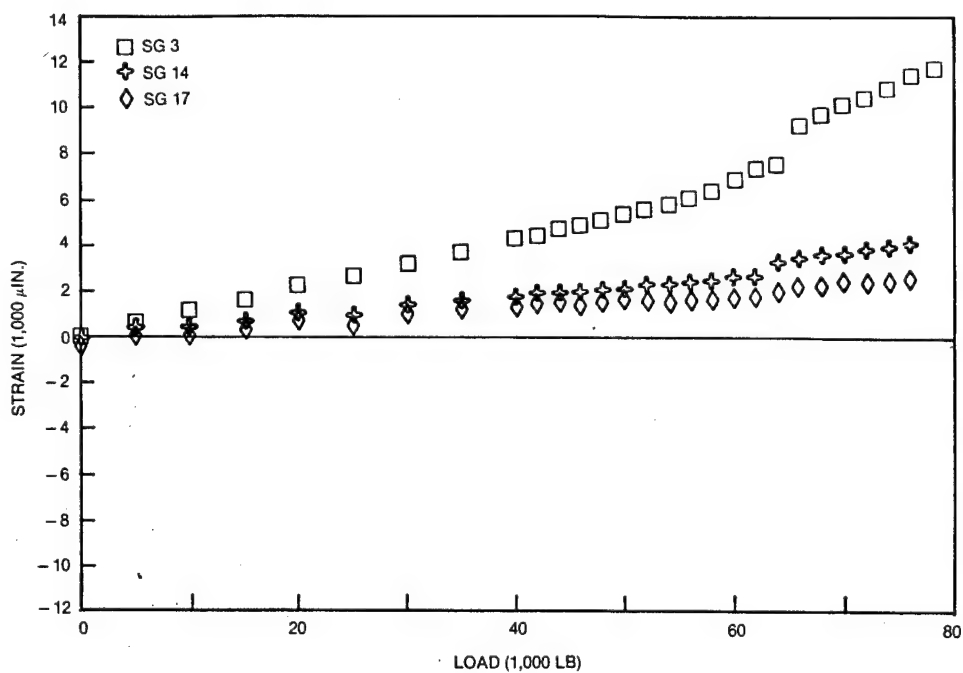


Figure 5-27. Strain Gage Data at Top Corner of Shear Panel Cutout (-501)

Figure 5-28 is a sketch of the softened panel (-503) after failure. Strain gage data taken at the bottom corner indicate roughly linear behavior to about 60 kips. At 70 kips, measured strains at the bottom corner began to drop off rapidly with increasing load (down from $-11,629 \mu\text{in./in.}$ at 70 kips to $-5,360 \mu\text{in./in.}$ at 80 kips). Visual examination revealed very localized delaminations in both compression corners. These delaminations occurred on the side of the panel with the photoelastic film only a few layers from the outside surface. They were also located very close to the points of tangency of the corner radii to the straight sides. The load was then increased to 100 kips. Unlike the -501 (baseline) panel, very little growth of the delaminations was detected as the loads were increased to panel failure, which occurred at 121,110 pounds.

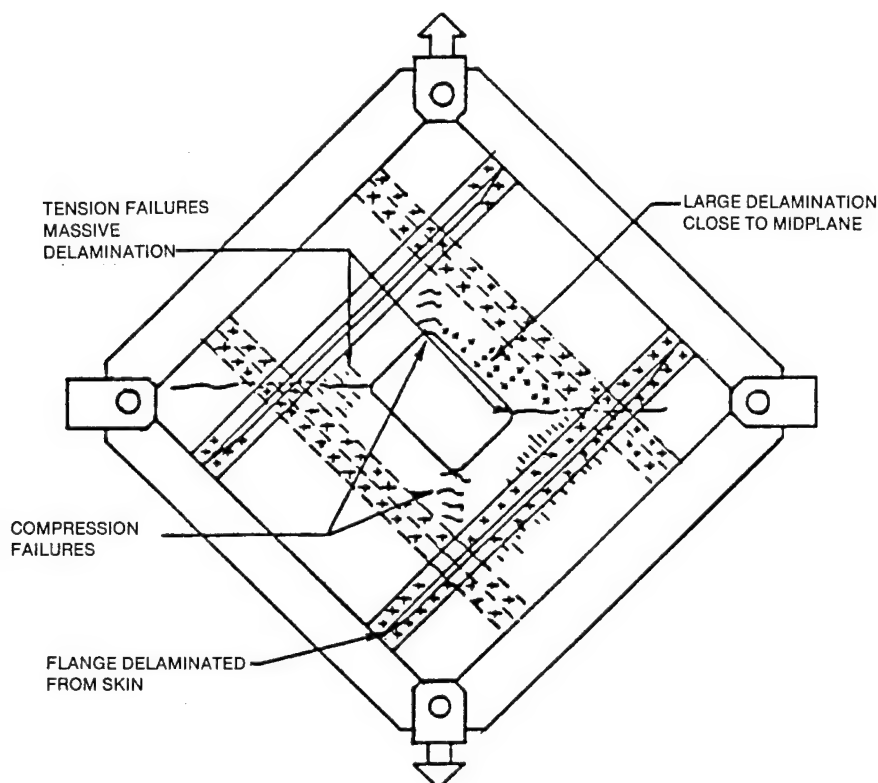


Figure 5-28. Failure Locations for -503 Shear Cutout Panel

It was not obvious whether the final failure was precipitated by the rapid spread of delamination on the compression diagonals, coupled with the eventual disbonding of the stiffeners, or by failures across the tension diagonals. However, given the lack of appreciable observed delamination just prior to failure, and the extensiveness of the damage on the tension corners, it is thought that the tension failures occurred first, with the subsequent deformations producing the compression damage. It should also be noted that the disbonding of the stiffeners was not actually a failure of the bondline, but rather delamination between the first and second plies of the skin.

As previously noted, the ultimate failure of the -505 shear panel was precipitated by a partial failure of the test fixture. Strain gage data taken at the bottom (compression) corner indicated very low strains and became nonlinear very quickly (at about 30 kips). Photoelastic measurements indicated higher strains, which remained roughly linear over the range of loads surveyed (0-30 kips). Strain gage data taken at the left (tension) corner remained linear to about 60 kips. While holding the load at 70 kips, a loud noise was heard. Delaminations in both the compression corners were observed. At 108,900 pounds, the load fixture failed, loading the panel eccentrically and forcing a premature failure. Figure 5-29 shows stiffener separation (note the outer layer of 0s which peeled from the skin and are still attached to the stiffener) and the massive delaminations which occurred at the cutout.

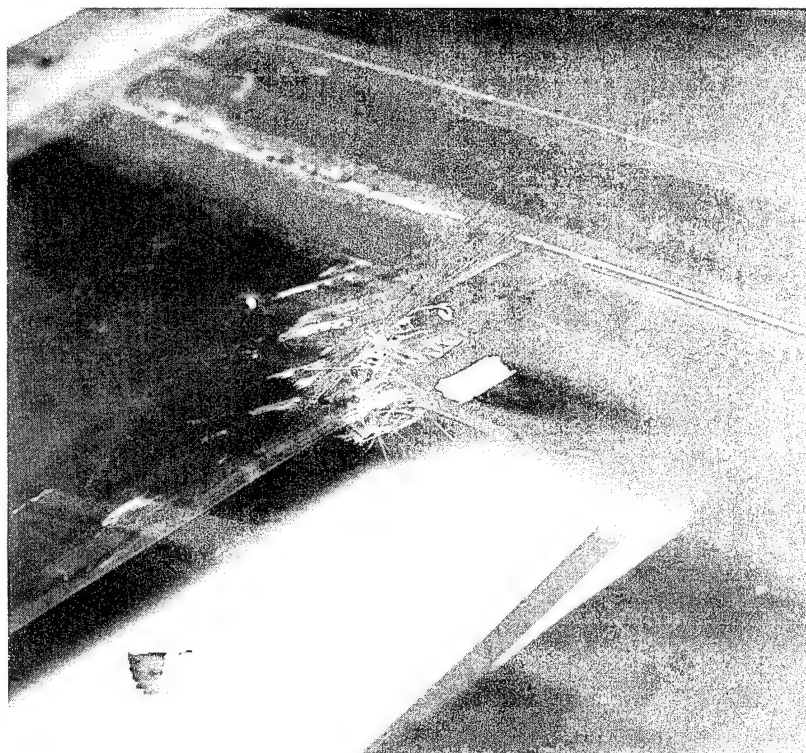


Figure 5-29. Posttest Photograph of Shear Cutout Panel (-505)

Six configurations of the shear-tee/skin intersection were examined. The results of these tests are summarized in Table 5-3. The -503, -509, and -511 configurations all yielded similar results, indicating that neither the alternate adhesive nor the presence of the imbedded hoop plies in the skin had a significant effect on the pull-off strength. The gradual tapering of the shear-tee flange (-505) did, however, result in a noticeable increase in the pull-off load (up to about 425 lb/in.). The worst performers were the -501 and -507 configurations (at about 250 lb/in.), indicating that either adding a ply to connect the tee flanges or thinning/softening the tee as a whole can reduce the pull-off strength dramatically. Figure 5-30 depicts what is thought to be the failure sequence for the shear-tee pull-off specimens. During testing, a loud sound was heard at anywhere from 10 percent to 40 percent of the ultimate failure load (depending on the configuration). As the load continued to increase, a crack was sometimes visible in the region from A to C. These cracks are thought to have originated in the vicinity of A and tended to spread both upward toward B and through the filler material toward either of the C points. Eventually, the cracks would reach a critical length and the specimens would fail suddenly. Examination of the failed specimens revealed adhesive on both the (now separated) tee and skin elements in areas to either side of center. This indicates a cohesive bondline failure in this area (corresponding to the area between points C and D. To either side of this region, there is very little adhesive visible; instead, 0-degree strands are observed on both elements, indicating an interlaminar failure in the first ply of the skin. The -501 specimens, however, showed no sign of any adhesive or 0-degree tape on the failure surface. Instead, there was the very distinct pattern of the 0/90-degree cloth, indicating an interlaminar failure in the tee assembly.

Relating the apparent failure sequence back to the specimens provides some insight into their relative performance. The -503, -509, and -511 specimens all had identical tee elements. Apparently, neither the alternate adhesive, nor the increased stiffness of the skin under the tee, had any significant effect on the peel stress at point C once the crack had propagated to that point. The higher strength of the -505 configuration was likely due to a reduction in this peel stress, effected by the tapered flanges flexing with the

Table 5-3
Shear-Tee Pull-Off Test Results

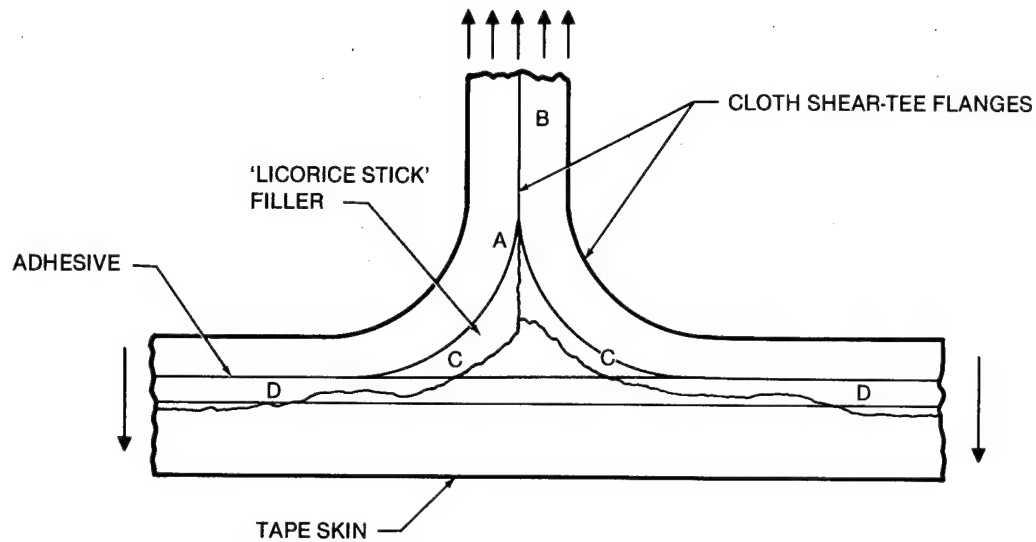
CONFIGURATION		NOISE HEARD AT (LB)	CRACK OBSERVED AT (LB)	FIRST LOAD DROPPED AT (LB)	FAILURE LOAD (LB)	AVERAGE FAILURE LOAD (LB)
- 501	- 1	400	800	600	1,120	1,127
	- 2	200	900	600	1,145	
	- 3	200	800	500	1,115	
- 503	- 1	350	—	450	1,738	1,666
	- 2	—	—	700	1,590	
	- 3	300	—	620	1,670	
- 505	- 1	200	—	600	1,980	1,900
	- 2	—	1,200	600	1,830	
	- 3	200	900	600	1,890	
- 507	- 1	200	—	600	1,160	1,150
	- 2	—	—	500	1,175	
	- 3	200	—	500	1,115	
- 509	- 1	300	800	600	1,570	1,640
	- 2	300	500	500	1,820	
	- 3	300	600	500	1,530	
- 511	- 1	300	500	400	1,460	1,587
	- 2	300	800	600	1,630	
	- 3	300	600	600	1,670	

skin. Although the soft flanges of the -507 configuration certainly conformed to the deflection of the skin (probably more so than for the -505), the stiffness of the flanges at the base of the tee was much less than that for any of the other configurations. This apparently increased the peel stress considerably. The lower strength of the -501 configuration is attributed to the lower peel strength of the brittle matrix at point C when compared to that of the adhesive.

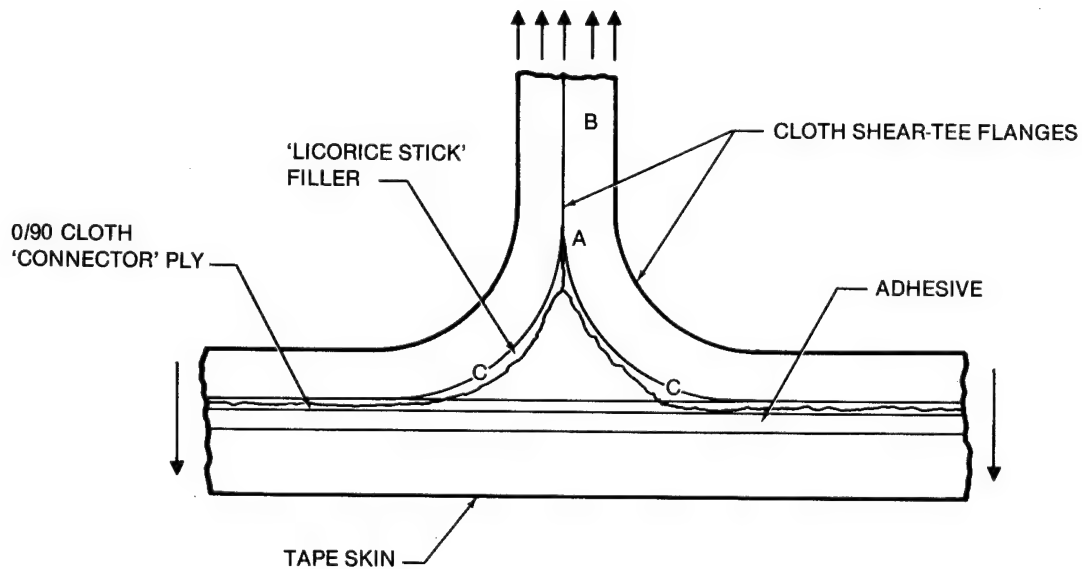
5.3 GROUP C

The Group C tests included longitudinal and transverse skin splice specimens (two configurations of each), a longeron runout specimen, and two 2-stiffener panels (longeron/skin splices). One of the longeron/skin splices was tested in tension, the other in compression. Specimen descriptions are given in Sections 2 and 3.

The results of the skin splice tests are summarized in Figure 5-31. All of these specimens were fabricated from the basic skin laminate (0.0684 inch nominal thickness) to which four plies of 45 were added at the splice region to yield the reinforced skin laminate (0.0912 inch nominal thickness). Gross-section stresses are based on the built-up thickness. Gross-section strains can be obtained by dividing by measured modulus of elasticity for lay-up No. 2 (7.96 Msi). The first replicate of each of the skin splice configurations was tested with faying surface sealant while the second and third were tested without. The presence of the sealant had little effect on the strength of the longitudinal skin splices. The strengths of the transverse splices were more noticeably affected (reduced) by the presence of the sealant. This reduction is generally attributed to the increased eccentricity of these single-shear joints due to the added thickness of the sealant.



A. -503, -505, -507, -509, & -511 SPECIMENS



B. -501 SPECIMEN

Figure 5-30. Apparent Failure Sequence for Shear-Tee Pull-Off Specimens

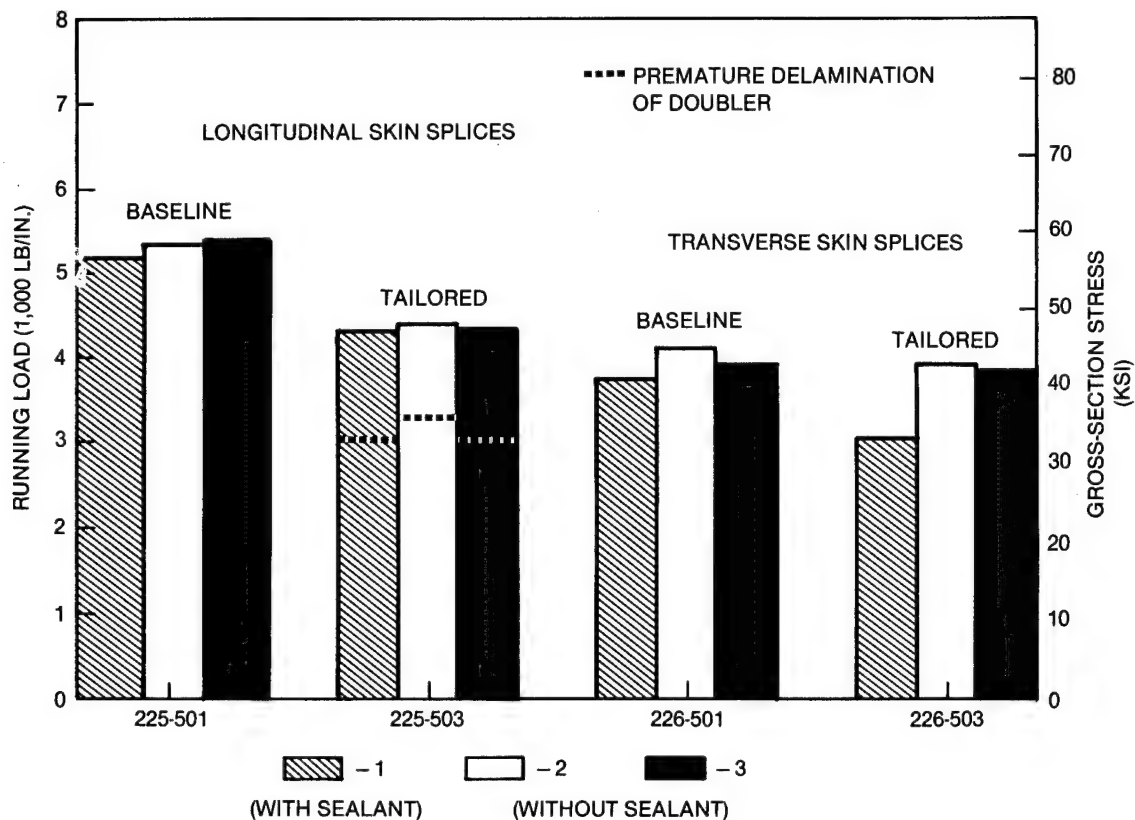


Figure 5-31. Failure Loads for Group C Skin Splice Specimens

The failure mode of the baseline longitudinal splice specimens was net-section tension in the center (skin) member at one of the two outermost rows of fasteners. These specimens also contained delaminations in the basic skin (prior to the build-up at the splice) on the opposite side of the net-section failure. These are thought to have been secondary failures.

The tailored longitudinal splice specimens experienced premature doubler delaminations prior to failure. Figure 5-32 illustrates the location of the initial delamination as well as that of the ultimate (net-section tension) failure. The taper angle of the small doubler bonded to the left-hand skin was apparently too steep to allow it to conform adequately to the deformed curvature of the skin. The resultant peel force at the end of the doubler thus precipitated the premature delamination. (Note that this was not a bondline failure, but rather was an interlaminar failure in the first ply of the skin.) With the doubler separated from the skin, the ultimate failure occurred in the countersunk skin at the outermost fastener.

Figure 5-33 shows the failed baseline transverse skin splice specimen. The failure mode was net-section tension through the countersunk skin at one of the outermost rows of fasteners. Fastener rotation and bearing damage was minimal at the other three rows. This was typical of the two specimens assembled without sealant. The failed -1 specimen (assembled with sealant) appeared quite different, however. The ultimate failure apparently was partially tension through the outermost row of fasteners, and partially a combination of fastener failure and fastener pull-through. In addition, all four rows of fasteners exhibited significant fastener rotation with the accompanying bearing damage.

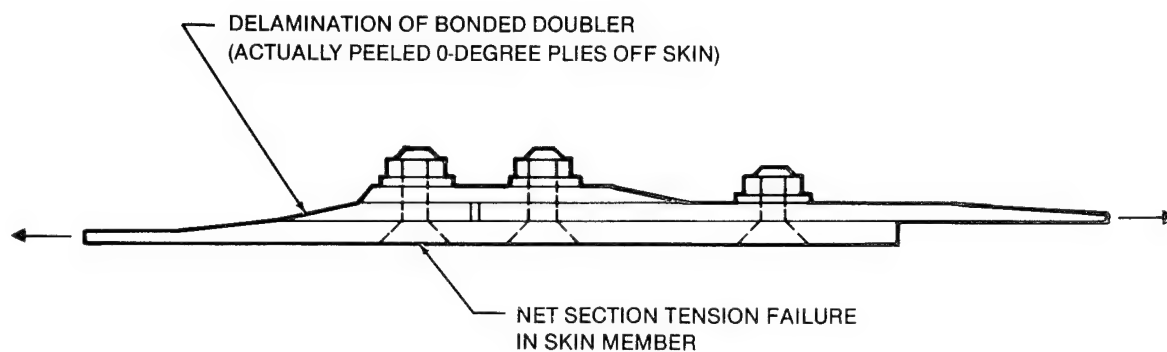


Figure 5-32. Failure Mode of Tailored Longitudinal Splice Specimens

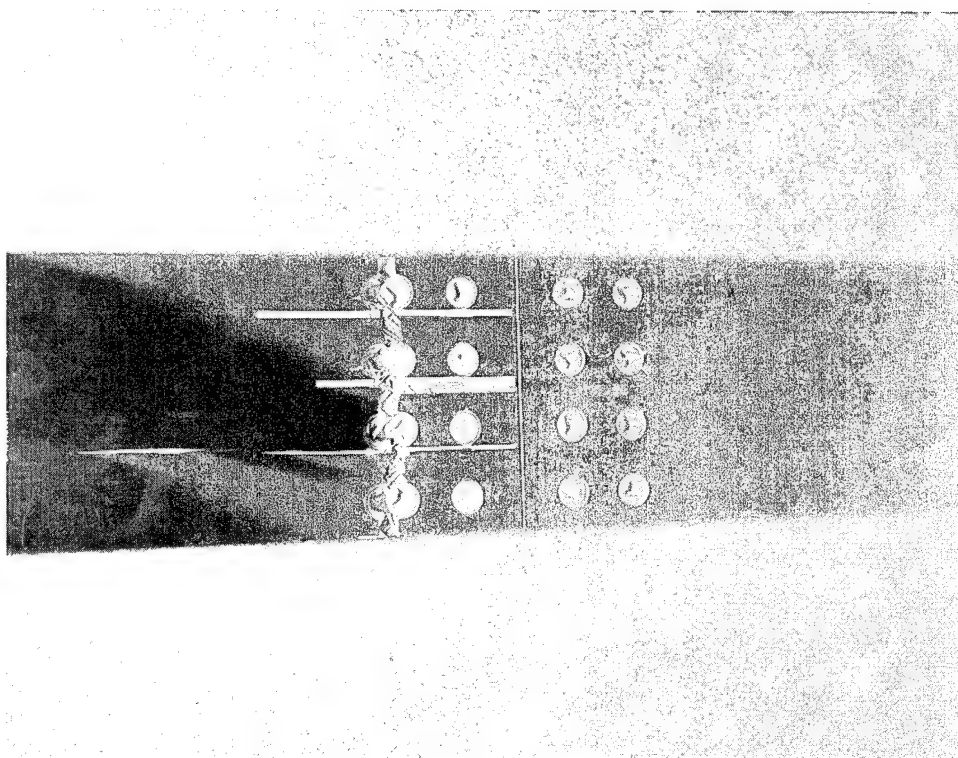


Figure 5-33. Failed Baseline Transverse Skin Splice Specimen

Failure of the tailored transverse skin specimens is illustrated in Figure 5-34. The ultimate failure mode was fastener pull-through or fastener failure at one of the inside rows of fasteners. A large amount of bearing deformation (up to 1/8 in.) was evident in the splice member at the outer rows of fasteners. Fastener rotation was apparent at all four rows of fasteners although significantly more noticeable at the two inner rows. Both of these suggest that a large portion of the load transfer was occurring at the inner rows of fasteners.

The presence of the sealant (for the -1 specimen) significantly reduced the strength of the tailored transverse splice specimen. The failure mode, for the most part, appears very similar to that of the -2 and -3 specimens (i.e., extensive bearing damage in the splice member at the outside rows of fasteners with the ultimate failure occurring at one of the inside rows due to fastener failure). Fastener failure for the specimens tested without sealant always occurred at the fastener head, through the tri-wing recess. Fastener failures for the -1 specimen, however, occurred at the opposite end near the first thread.

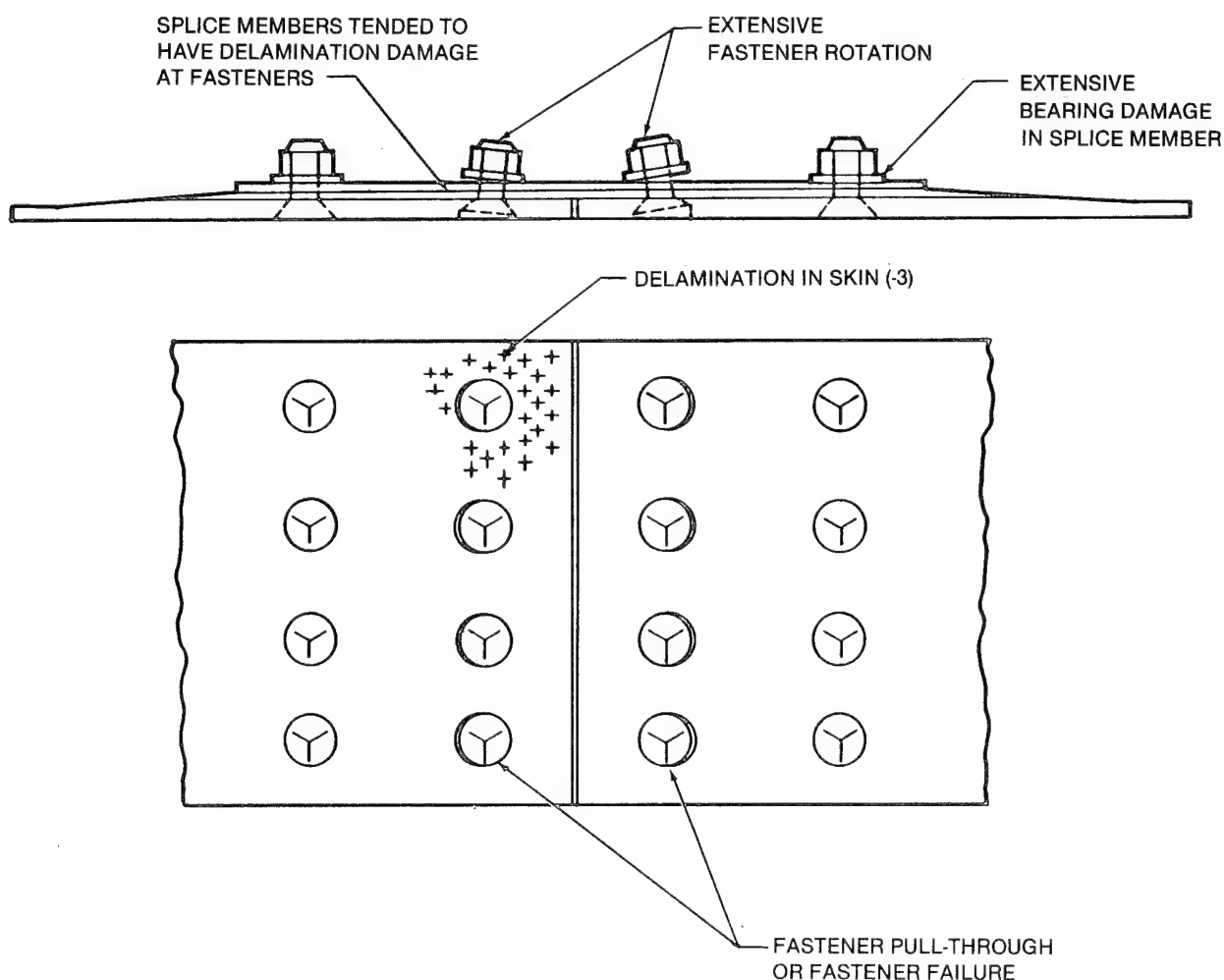


Figure 5-34. Failure Mode for Tailored Transverse Skin Splice Specimens

The longeron runout specimen failed at a tension load of 85,140 pounds. This corresponds to a running load of 8,514 lb/in. and a gross-section failure strain (P/EA at the center of the panel) of almost 11,000 $\mu\text{in./in.}$ Figure 5-35 shows the failed specimen. Three failure locations are noted: one through the skin before the thickness increase, and two through the stiffener. The stiffener failures were (1) at the first row of bolts tying the stiffener to the end clips, and (2) at the center of the panel. It is obvious that the stiffener separated from the skin because the failure locations were different for the two elements. The ramp angle where the skin buildup occurs (close to the net-section skin failure) could have contributed to this delamination.

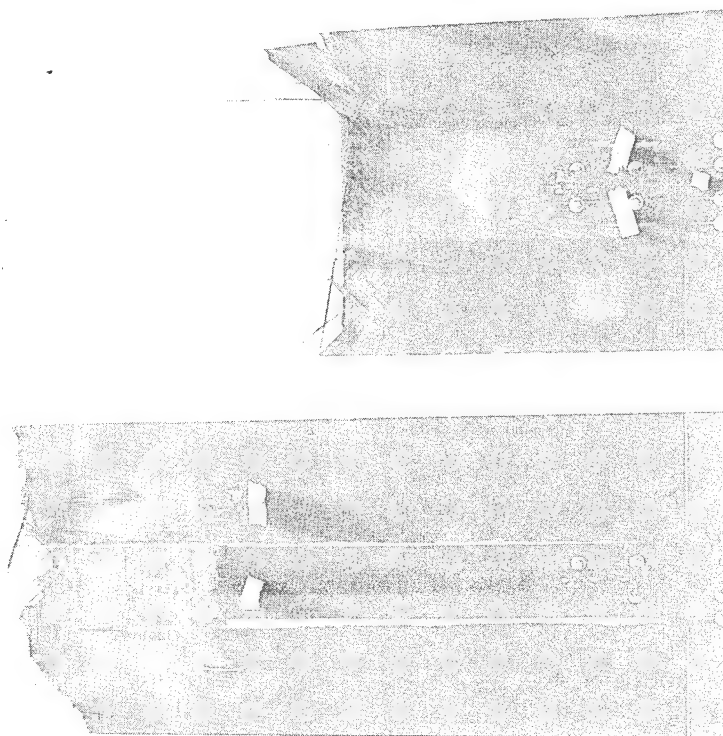


Figure 5-35. Failure of Longeron Runout Specimen

Strain gage data indicated very high strains at the center of the panel and very low strains in the end clips. A small amount of bending, due to the overall eccentricity of the test specimen, was also detected from the strain gage data. It is suspected that the initial failure was in the skin. Delamination of the stiffener from the skin likely occurred next. The reason for the longeron then failing in two places is not known.

The first of the two stiffener longeron/skin splice panels failed at a tension load of 68,310 pounds. This corresponds to a running load of 4,921 lb/in. and a gross-section failure strain (P/EA away from the joint area) of just over 4,400 $\mu\text{in./in.}$

Strain gage data taken in the vicinity of the splice was noticeably nonlinear. This geometric nonlinear behavior (a result of the eccentricity of the single-shear skin splice) is especially notable in the data from strain gage No. 1 (Figure 5-36). This gage, located in the center of the skin-splice plate, initially read negative even though the applied load was tension. The strain readings leveled off quickly, however, and eventually became positive at about 45 kips. Considerable local bending of the skin and skin-splice members was also visually confirmed during the test. Although not visually detectable, the strain gage data also indicated a degree of eccentricity in the longeron splice, with the strains generally higher in the L-member than in the Z.

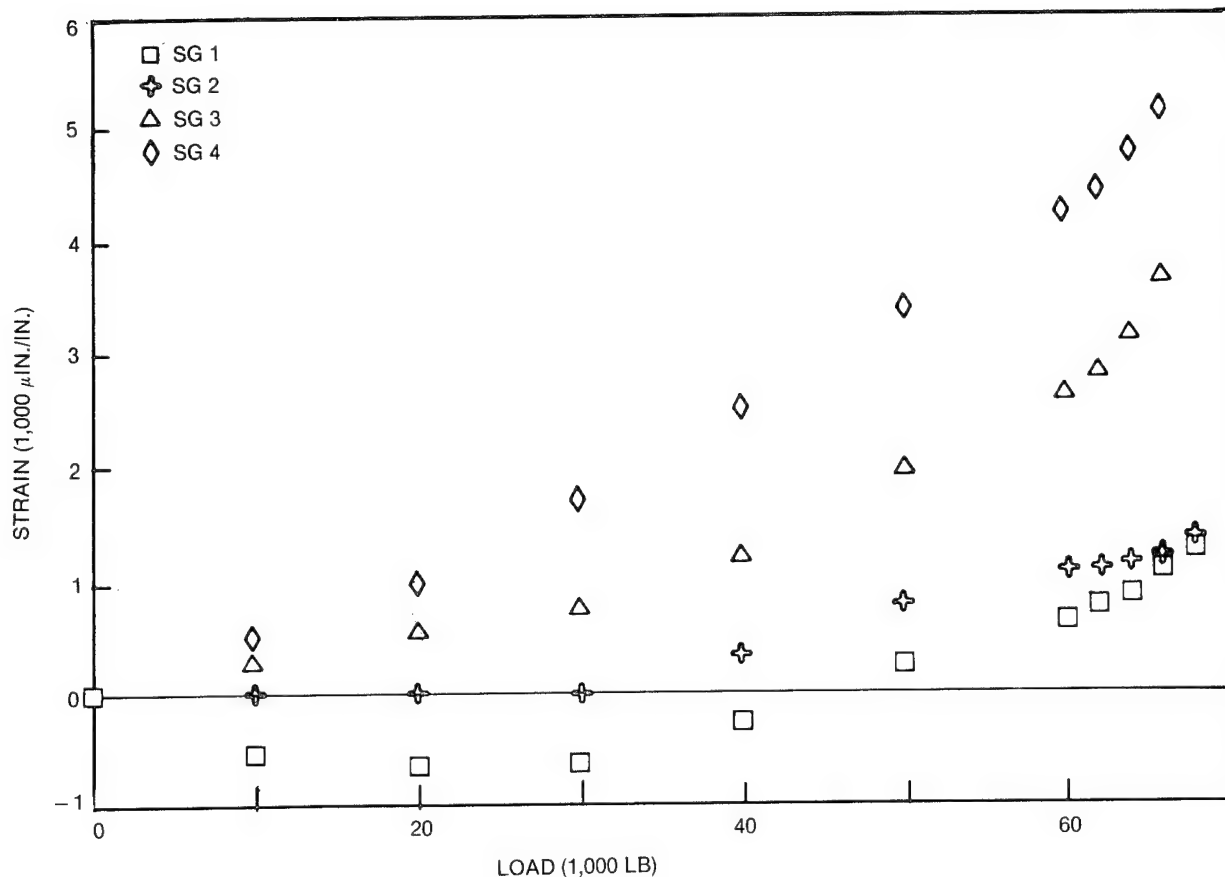


Figure 5-36. Transverse Skin/Longeron Splice Typical Strain Gage Data (Tension)

The apparent failure mode of the skin splice was a combination of fastener failures and fastener pull-through. It is observed that more of the failures in the outer row were by pull-through, while more of those in the inner row were failures of the fasteners themselves. Failure mode of the stiffener splice was a combination of net-section tension and shear-out. This failure mode, typical of both the L and Z splices, is illustrated in Figure 5-37. The shear-out failure, just above the line of 1/4-inch fasteners which attached the splice plates to the stiffener web, was typical of the failures experienced with the highly orthotropic reinforced longeron laminate (lay-up No. 3) in the Group A testing. The stiffener webs, as well as the Z and L splices were fabricated from this (54,23,23) laminate. The lower half of each splice, however, failed in net-section tension. This failure, through the innermost fastener attaching the splice flange to the longeron flange, was unique in that it was the only loaded-hole test for this laminate that failed in any mode other than shear-out. (See the discussion of the DLT test results from Group A.)

The second of the two-stiffener longeron/skin splice panels was tested in compression and failed at 46,310 pounds. This corresponds to a running load of 3,336 lb/in. and a gross-section failure strain (P/EA away from the joint) of approximately 3,000 $\mu\text{in./in.}$ Like the tension test, strain gage data as well as visual observations indicated a considerable amount of bending and nonlinear behavior. Edge deflections for this panel were limited, however, by the special fixturing. Nevertheless, the maximum transverse displacements appeared to be at the panel edges. Unlike the tension test, strain gage data indicated virtually no eccentricity in the stiffener splice (equal strains in the Z and L splice members).

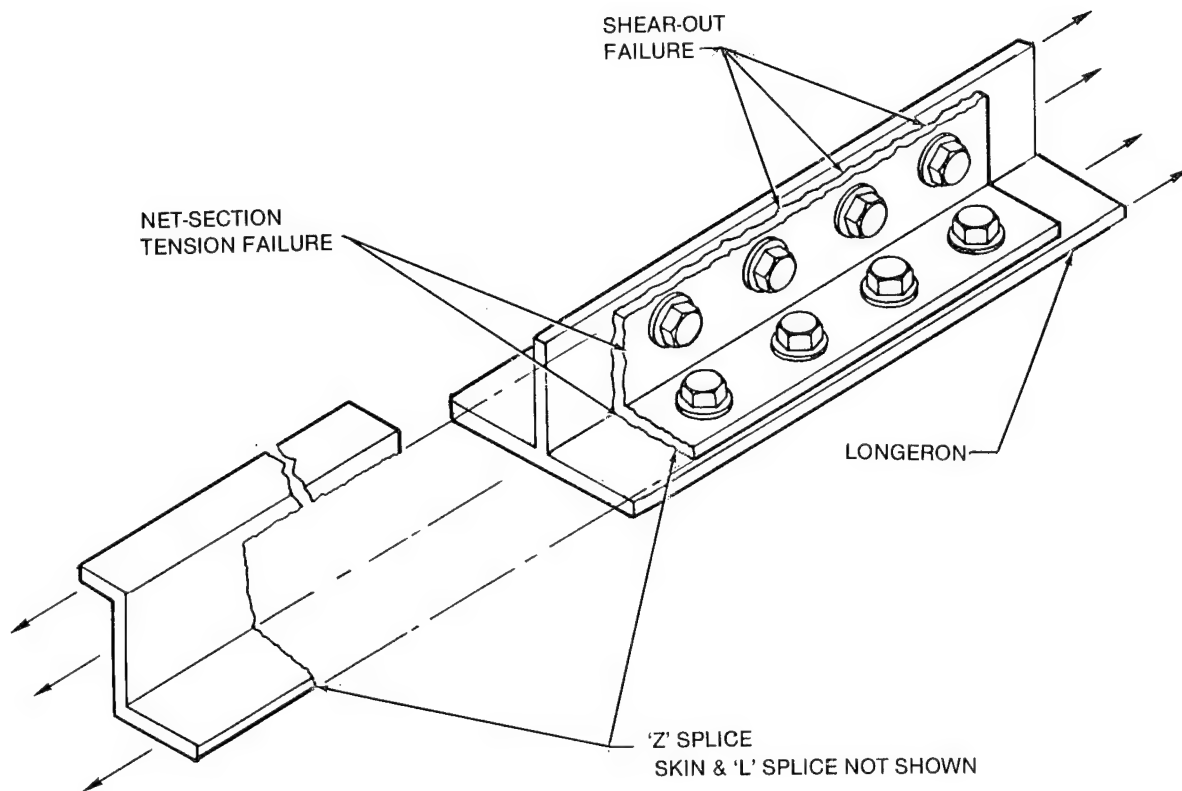


Figure 5-37. Failure Mode of Longeron Splices (Tension Specimen)

Figure 5-38 shows the compression panel during testing at roughly limit load with the skin buckling evident just "outside" of the splice bay (above and below the simulated frame supports).

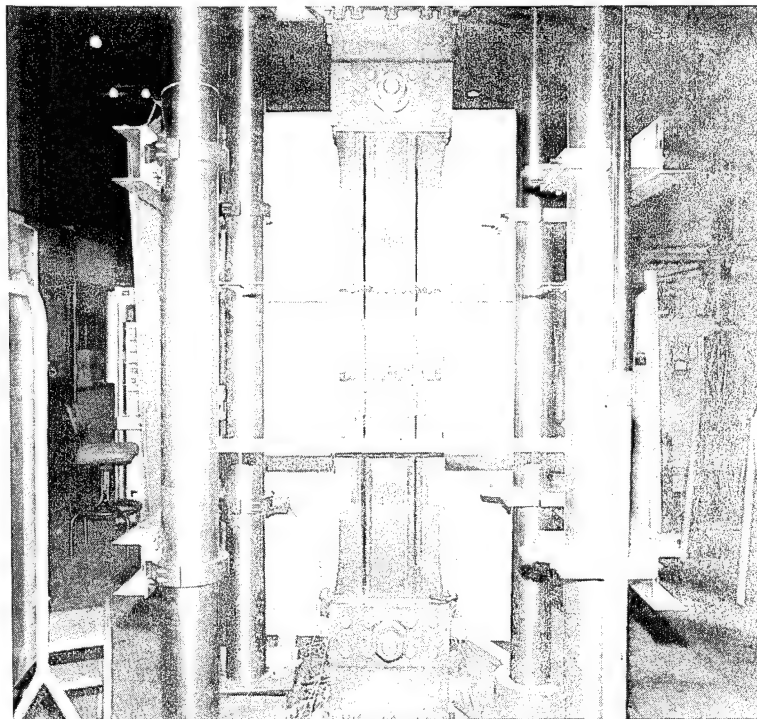


Figure 5-38. Longeron/Skin Splice Panel (Compression Specimen) Under Load

Figures 5-39 through 5-41 show several views of the specimen after failure. The skin failure (best seen in Figure 5-39) did not occur through the skin splice. The damage did, however, go through several of the fasteners which attached the skin/longeron flange combination to the Z and L stiffener flanges. At the panel edges (Figure 5-40), the skin failure was just below the splice plate, and just above the edge support. Failure of the Z and L splice plates (Figure 5-41) likewise did not occur through the longeron splice. The splice plates failed through two fastener holes; however, the load transfer at these fasteners should have been minimal. (These attachments were simply designed to stabilize the Z and L splice members where they bridge the stiffener load across the skin splice.)

Again, the exact failure sequence is not clear. A likely candidate for the initial failure is the skin failure at the edge of the panel due to the unrealistically sharp curvature induced at that point by the edge support system. Pull-through of the fastener heads after delamination of the skin and stiffener could also have contributed to the skin failure. After skin failure, all the load would have to be carried by the Z and L splice members. The attachments mentioned above (designed to stabilize the splice members) would likely have picked up significant loads. These factors, coupled with the added eccentricity of the partially failed joint, would cause failure of the stiffener splice elements.

5.4 GROUP D

Two 4- by 5-foot curved panels comprised the Group D tests. The first was a three-frame, six-stiffener panel which contained a transverse (barrel) splice. The second contained two large passenger window cutouts. Both of these panels were tested in a special fixture which allowed the simultaneous application of compression and shear loads. This test fixture is described in detail in Section 4. Specimen descriptions are given in Sections 2 and 3.



Figure 5-39. Failure of Longeron/Skin Splice Panel (Compression Specimen)

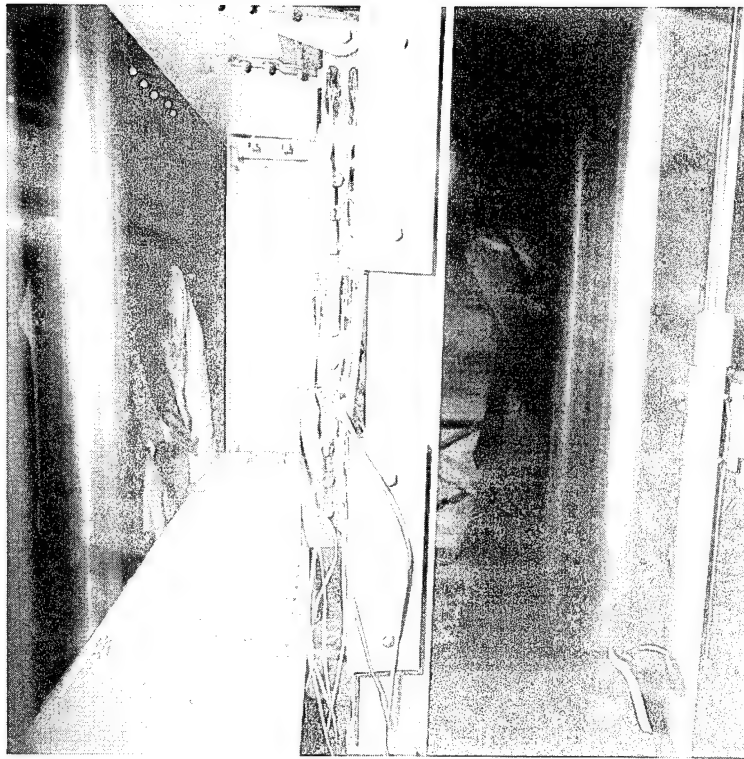


Figure 5-40. Failure of Longeron/Skin Splice Panel (Compression Specimen)



Figure 5-41. Failure of Longeron/Skin Splice Panel (Compression Specimen)

Load schedules for the two panels were similar (see Figure 5-42). In both cases, a series of load envelopes (combinations of shear and compression) was defined. Five points on each of these envelopes were designated as test conditions. Condition 1 was the first condition tested for a given envelope and was a 100-percent-shear load condition. After having successfully reached Condition 1, the shear load was decreased to that of Condition 2, which was a shear/compression load combination with a relatively low compression component. The compression load was then increased to that of Condition 2. The same pattern was followed to arrive at Conditions 3, 4, and 5, which were combinations of successively lower shear and higher compression components. Condition 5 was, in fact, a 100-percent-compression condition.

The load schedule for the transverse splice panel was structured around preliminary estimates of initial shear and compression buckling loads. A buckling envelope was established which included these two values and was based on an $R_c + R_s^2 = 1$ interaction formula. The load schedule for this panel was then defined as a series of envelopes that were scalar multiples (from 0.50 to 3.50) of the buckling envelope. For Series 1 through Series 4 (the 50-, 75-, 100-, and 125-percent envelopes), data were recorded in the point data mode (i.e., one scan was taken for each load condition). For the higher load level envelopes, data were recorded continuously (approximately one scan every two seconds).

The load schedule for the window-belt panel was based on a failure envelope determined by a preliminary finite-element analysis. This analysis assumed that failure of the panel would initiate at the edge of one of the cutouts. The test envelopes were then set up as scalar multiples (from 0.15 to 1.00) of the predicted failure envelope. Like the transverse splice panel, point data were taken for the lower load level envelopes (in this case, at 15, 20, 25, and 30 percent of the failure prediction), while continuously read data were obtained for higher load levels.

Shear buckling of the transverse splice panel was observed in the upper skin bays (away from the panel splice) at the maximum shear condition for Series 4 (125 percent predicted buckling) at a shear load of 32 kips, or a shear flow of roughly 530 lb/in. Southwell plots of the continuously read strain gage data from subsequent series were not conclusive (because of the sparsity of the data), but suggested initial buckling loads of from 30 to 38 kips. No buckling was detectable at the maximum-compression/zero-shear condition for this series.

The first notable acoustic emissions came while holding at the maximum shear load (Condition 1) for Series 7 (250 percent predicted buckling). This corresponded to a shear load of 64 kips and a shear flow of just under 1,100 lb/in. The panel completed the seventh series without further emissions.

While increasing the shear load to Condition 1 for the eighth series (76 kips), noticeable emissions began again at about 70 kips, continued while holding at the condition, and then eventually subsided. Again, the series was completed without further significant noises.

While increasing the load from 64 kips to 89 kips (Condition 1 for Series 9), acoustic emissions began again and continued until failure at 84,100 pounds (shear only). Although the panel underwent considerable deformation and appeared severely damaged, it continued to hold the load above 80 kips until the load was removed. The failure load corresponded to a shear flow of roughly 1,400 lb/in., an average shear stress of 20,500 psi., and an average shear strain of 8,500 micro-strain. The photograph at 64 kips captured the panel prior to complete failure. This photograph (Figure 5-43) shows a crease forming in the bay just to the left of the strain gage as well as a partial failure of the adjacent longeron.

The apparent failure mode was separation of the stiffeners and the skin. Very little damage was evident after the load had been removed from the panel. Some fiber breakage, as well as a small amount of damage to two longerons, was visible. Nondestructive testing of the panel revealed the true extent of the

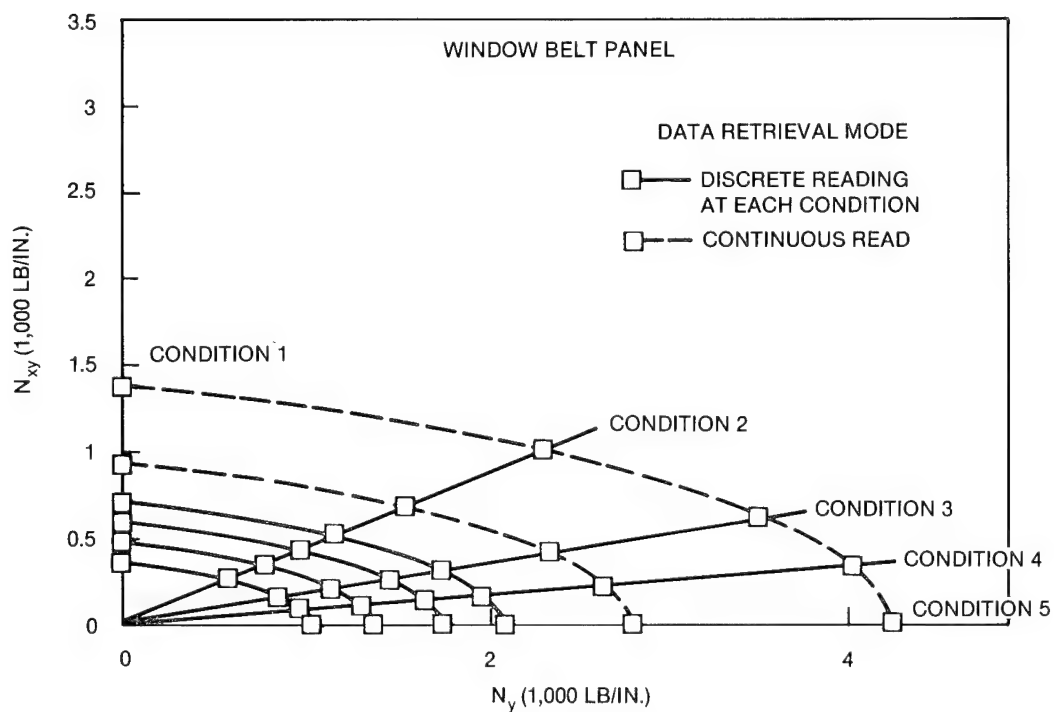
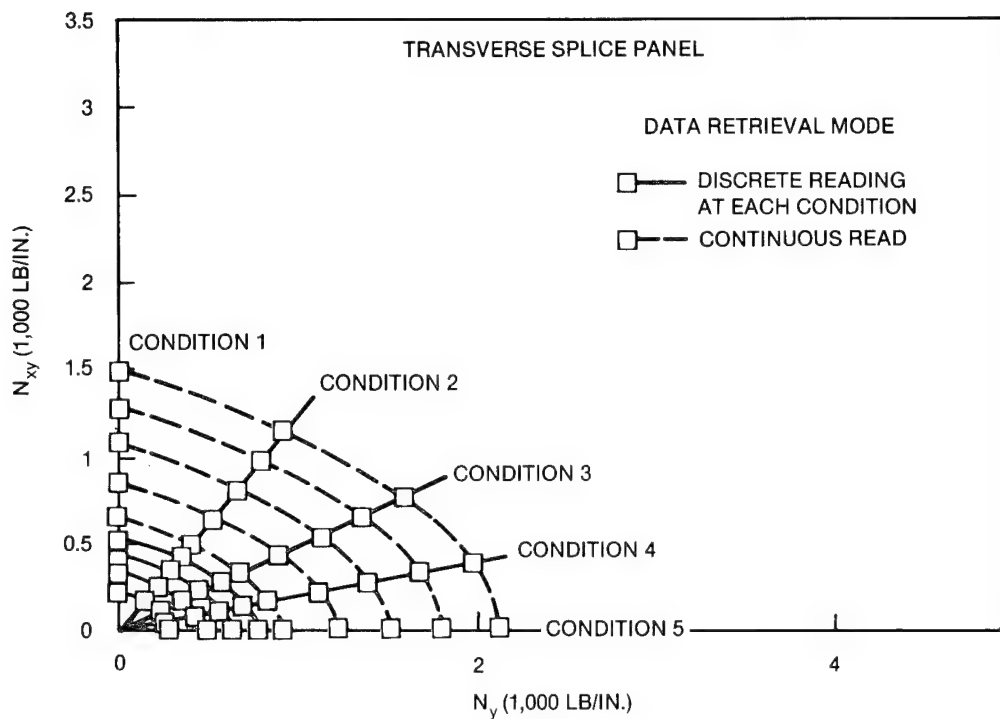


Figure 5-42. Load Schedules for the Group D Panels

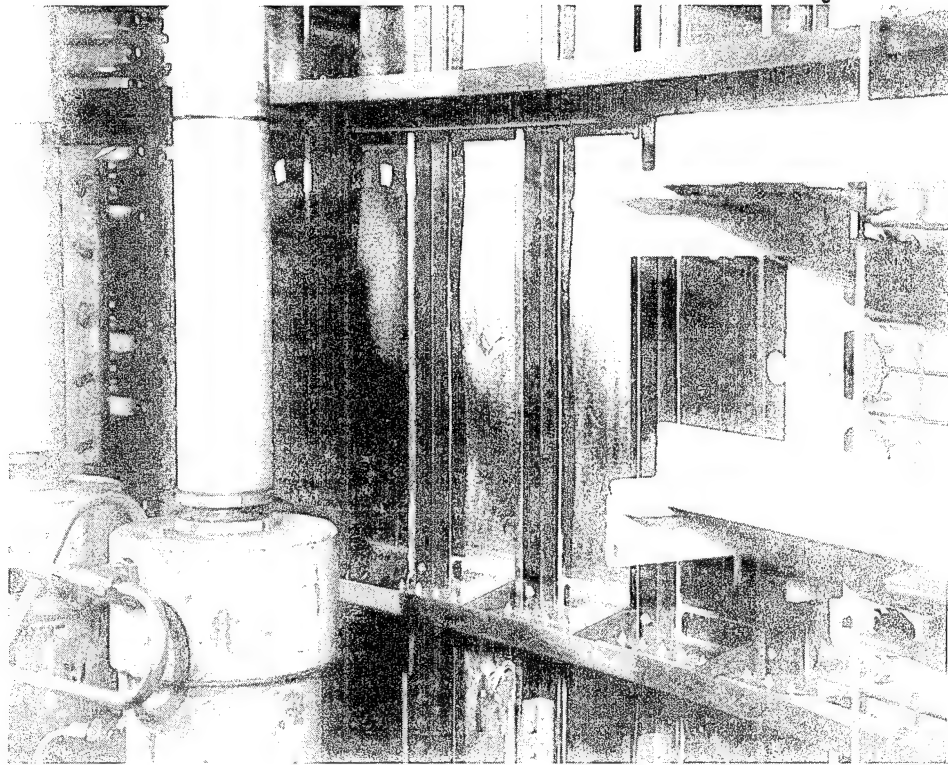


Figure 5-43. Group D Transverse Skin Splice Panel — Partially Failed

delamination. The marked areas in Figure 5-44 show that the skin and longerons were separated over a considerable portion of the stiffener length (especially the third longeron from the left).

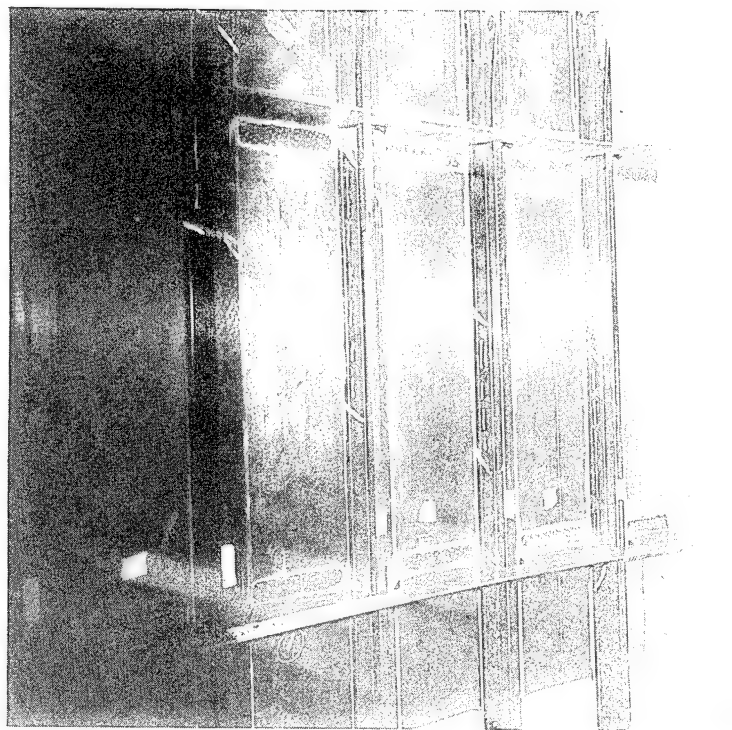


Figure 5-44. Areas of Delamination of Transverse Skin Splice Panel (from NDI)

Strain gage data for this specimen (see Figure 5-36) provided information concerning skin buckling and the behavior of the transverse splice. The continuously read data for the shear-only conditions (discussed above) are presented in Figure 5-45. The data and the failure load of 84.1 kips suggest a post-buckling ratio for this panel of between 2.5 and 3.0 (depending on the choice for the initial buckling load). Strain gage data from the small skin bay just above the splice (strain gages No. 5 and 6) indicate a small amount of curvature, which suggests a very shallow buckle present here also. (Skin thickness in this bay was nominally 0.0912 in.). Strain gages at the joint indicated behavior similar to that of the two-stiffener transverse splice panel loaded in compression (i.e., nearly equal strains in the Z and L splice members, and tensile strains on the inside surface of the skin splice plate). The strains at the joint were generally quite low due primarily to the fact that the highest compression load applied was 75 kips, corresponding to a running load of about 1,800 lb/in. (this to be contrasted with the failure load of the two-stiffener panel of 3,336 lb/in.).

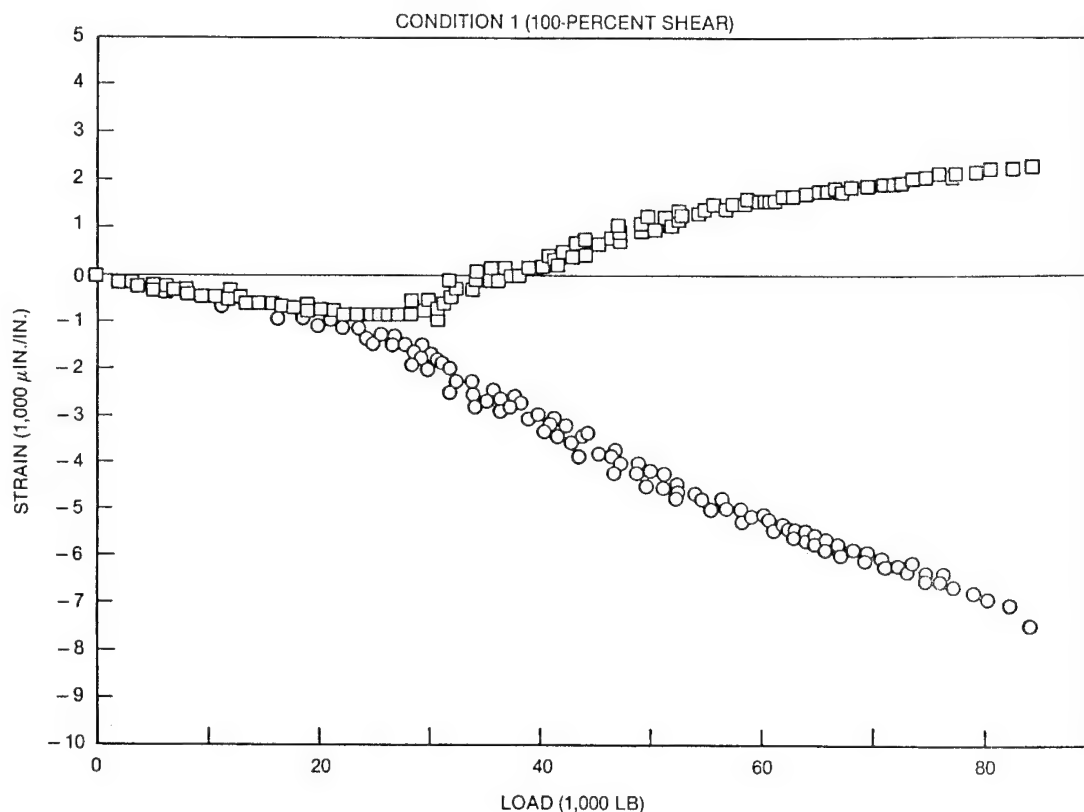


Figure 5-45. Postbuckling Response of Transverse Skin Splice Panel (Shear)

For the window belt specimen, the 30-percent (of predicted failure) envelope was applied first as a safety check prior to photoelastic measurements. Strain gage data and photoelastic measurements around the upper cutout were then taken for the 25-, 15-, and 20-percent envelopes. After examining these data, it was decided to take photoelastic readings for the 40-percent envelope also.

Just prior to reaching Condition 5 (maximum compression) for the 40-percent envelope, the first acoustic emissions were noted. While holding at the condition, (128 kips or 3,070 lb/in. compression) one further loud noise was recorded. When the panel had stabilized and emissions ceased, the panel was visually inspected as the photoelastic measurements were being taken. No damage was found.

The next envelope was the 60-percent series. While increasing the shear load to that of Condition 1 (82.5 kips or 1,380 lb/in.), additional noises were noted. After holding momentarily at Condition 1, the shear load was decreased to 60.6 kips (1,000 lb/in.) and the compression load was increased to 97.8 kips (2,400 lb/in.). (These were the test loads for Condition 2.) Posttest inspection of the videotapes revealed a sudden delamination or snap-through buckle (in one of the bays adjacent to the upper cutout), just prior to reaching this condition. Acoustic emissions (cracking sounds) were also evident at this point. The Condition 3 loads were then applied; the shear load dropped to 37.7 kips (630 lb/in.), and the compression load increased to 149.3 kips (3,600 lb/in.). Noises were noted continuously while the compression load was increasing, but for the most part subsided while holding at the condition. The panel collapsed while attempting to reach Condition 4. The failure loads were 22 kips shear (370 lb/in.) and 171 kips compression (4,100 lb/in.).

Figure 5-46 shows an overall view of the panel and points out a number of failures noted during a visual inspection. The overall failure appears to be of a general stability nature, with the middle of the panel collapsing inward. Figure 5-47 is a closeup of the upper left portion of the panel. It is apparent from the videotapes of the panel failure that this area was the first to collapse. This was also the area (referred to above) where the delamination and/or buckling was observed. The skin failure at the cutout appears to be an interlaminar tension failure induced from high compression loads. Note also how the web of the stiffener in the foreground was ripped away from the flanges, which remain attached to the skin.

Figure 5-48 is a closeup of the right-hand side of the panel. The collapse of this side of the specimen was more centered about the middle frame. The videotapes indicate that the skin failures (through the cut-outs) and the longeron failures preceded the failure of the frame. The frame failure is better seen in Figure 5-49, which is a bottom view of the same area. Local failures also occurred at the upper left and upper right corners of the panel. As these areas were not visible in the videotapes, the relative timing of these failures is unknown. Nondestructive examination of the failed panel revealed skin damage as outlined in Figure 5-50. (The light area around the cutout is the photoelastic film.)

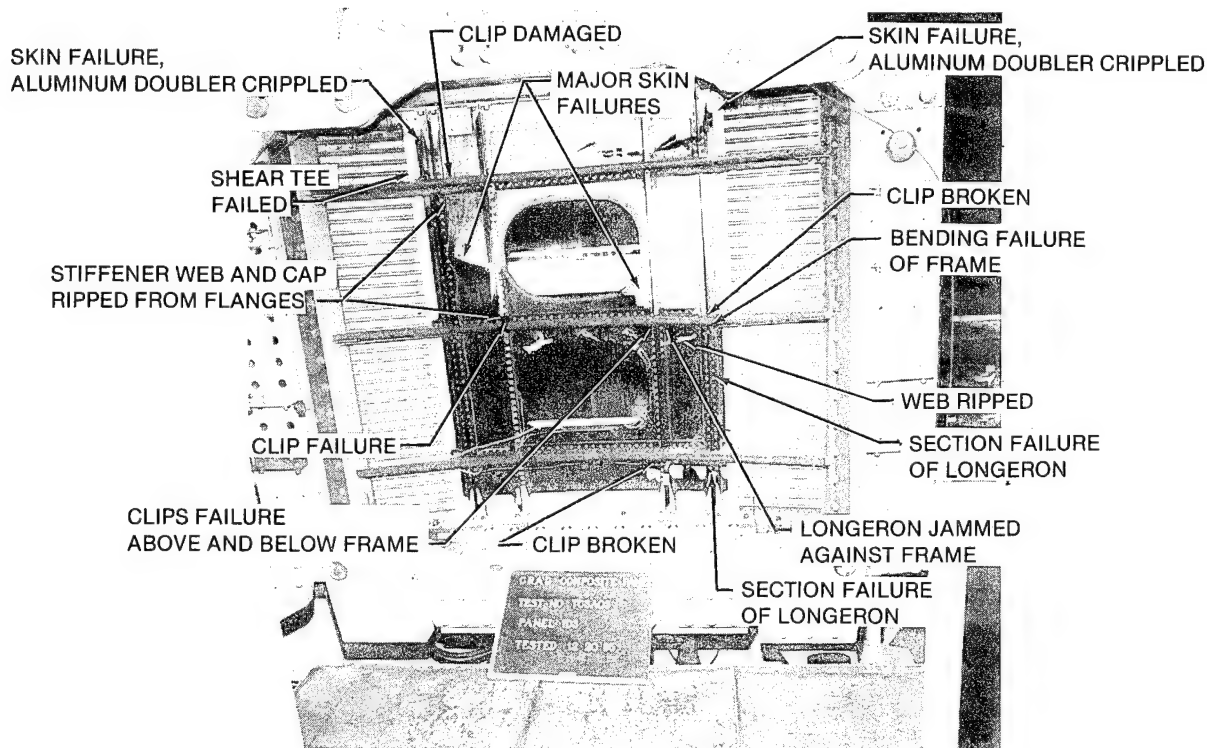


Figure 5-46. Group D Window Belt Panel Showing Failure Locations

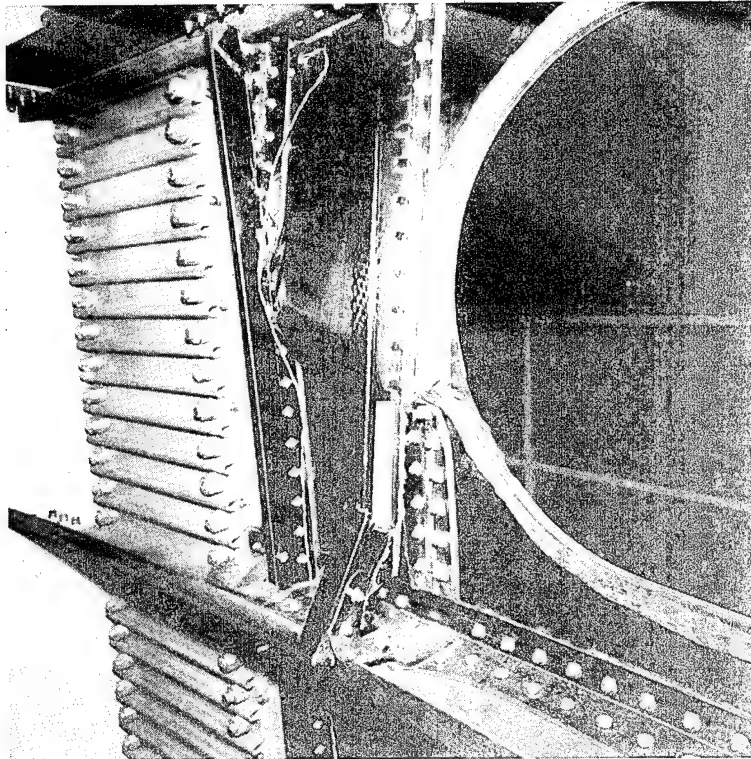


Figure 5-47. Group D Window Belt Panel — Area of Initial Failure

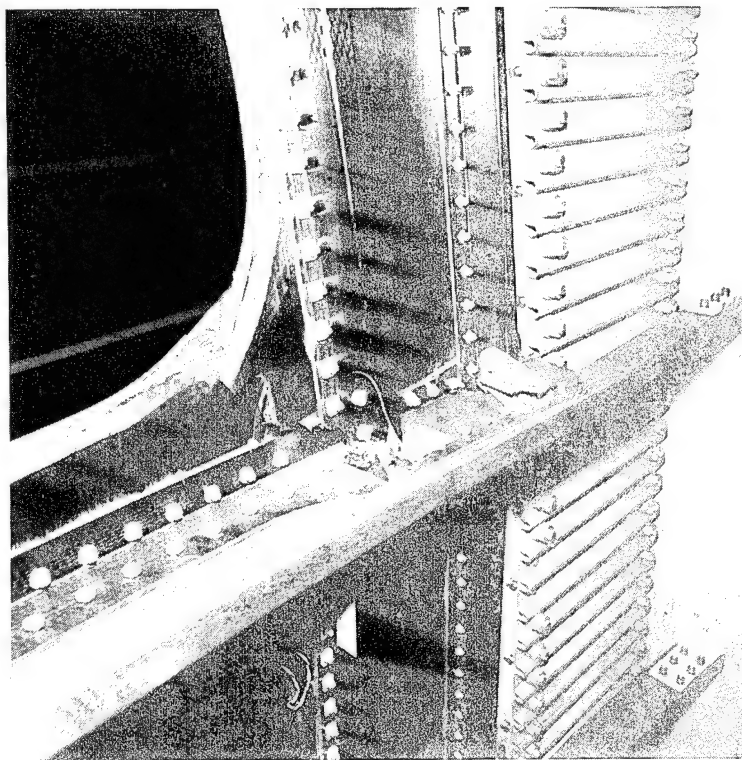


Figure 5-48. Group D Window Belt Panel — Failure of Skin, Longerons, and Frame

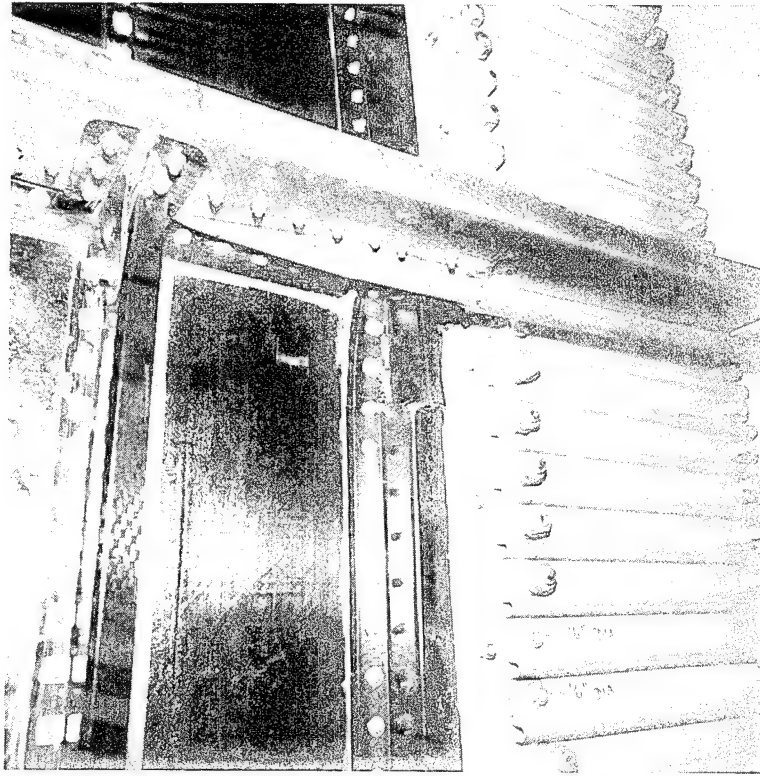


Figure 5-49. Group D Window Belt Panel — Failure of Skin, Longerons, and Frame

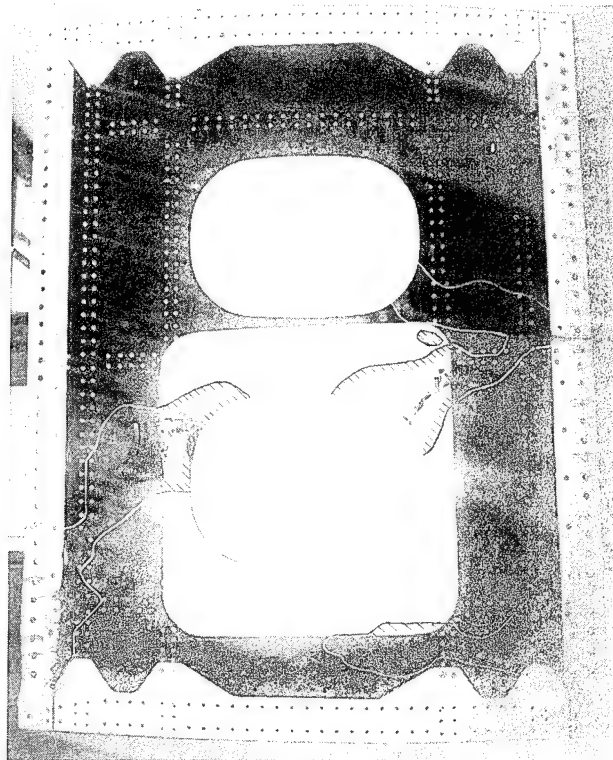


Figure 5-50. Group D Window Belt Panel — Areas of Skin Damage Detected by NDI

The strains recorded by the gages above and below the cutout remained relatively linear, and were (expectedly) higher for the shear dominated load cases. Those recorded by the gages along the left and right edges were likewise highest for the compression-dominated conditions. There was a noticeable nonlinearity in these data, indicative of either a redistribution of load in the panel, or bending along the cutout. The data from strain gages No. 12 through 15 are the most interesting. The gages located at the lower right-hand corner of the lower cutout (see Figure 5-46) showed the presence of high-compression loads for the shear-dominated conditions. Significant bending was indicated at this location by the difference in the readings from the back-to-back strain gages. These readings were also the most obviously nonlinear. The most dramatic example of this behavior is evidenced in the plot for these gages for Condition 3 (included here as Figure 5-51). It would appear from the severity of the bending indicated at this condition for the 60-percent load series, that a failure at or close to this area had already occurred. However, there was no damage to the skin in this region.

Strain gages at the upper right-hand corner of the lower cutout in Figure 5-46 also displayed a nonlinear characteristic with a moderate amount of bending. These strains were tensile for the shear-dominated conditions and compressive for the compression-dominated conditions. Although a skin failure is indicated at these gages in Figure 5-50 (the upper left corner of the lower cutout), the measured strains were quite low just prior to the collapse of the panel. This adds credence to the observation made from the videotapes that this side of the panel was not involved in the initial failure.

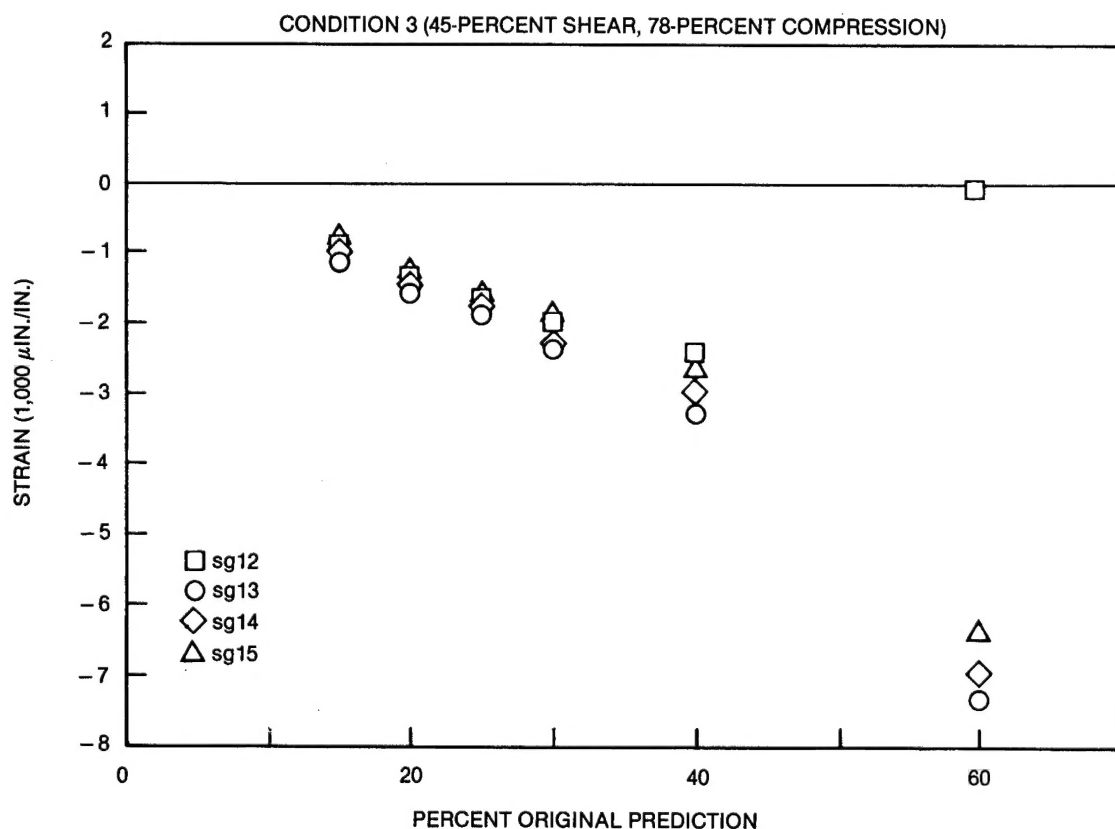


Figure 5-51. Selected Strain Gage Readings for Window Belt Panel

SECTION 6 CONCLUDING REMARKS

The significant technology issues of joints and cutouts in primary composite fuselage structure were addressed in this development contract.

Testing of the fuselage skin lay-up (33/33/33) of 12 plies indicated that the threshold of visible damage occurs at an impact energy of 4 foot-pounds when using a 0.5-inch hemispherical steel tip for the impact device. Tests have demonstrated the ability of the damaged skin to exceed 4,500 compression microstrain. This level of impact resistance is considered adequate for fuselage design.

Based on static testing, maximum shear strain should be limited to 9,000 min./in. for adequate damage tolerance requirements.

Mechanically fastened longitudinal skin splices (double-lap with two rows of 3/16-inch-diameter fasteners in each skin) proved adequate under static testing. Mechanically fastened transverse skin splices (single-lap with two rows of 3/16-inch-diameter fasteners in each skin) gave similar results.

A frame shear-tee configuration bonded to a skin panel demonstrated greater than design pull-off loads representative of cabin ultimate pressure (2P), which would apply tensile loads at the skin/shear-tee interface.

Minimum practical fuselage skin thickness at mechanically fastened splices is 0.068 inch. Significant parameters are flush 3/16-inch fasteners and near-pseudo-isotropic lay-up patterns for good joint efficiency.

Panel assemblies with secondarily bonded shear-tees and J-section longerons met design requirements.

The strategic use of S2-glass plies around cutouts has been shown by test to increase load capacity with virtually no increase in weight. Substitution of lower modulus/higher strain-to-failure fibers can be beneficial.

Large cutouts loaded in shear tend to fail first across the "compression diagonal," with the ultimate strength determined by either excessive propagation of the delamination (compressive) damage or failure across the "tension diagonals."

Double shear joints (in thicknesses representative of a fuselage) can be accurately analyzed using the methods developed under the Critical Joints Program (Reference 3).

IM6/F584 tape and broad goods demonstrated adequate processing with acceptable resin and low void contents in the cured laminate.

A weight estimate based on a composite barrel section of an advanced trijet fuselage was made. These data, extrapolated to the entire fuselage, showed an estimated fuselage weight saving of 29 percent.

REFERENCES

1. Watts, D. J., Study of Critical Joints in Large Composite Primary Aircraft Structures, NASA Report ACEE-26-TR-1671, NASA Contract NAS1-16857, November 1981.
2. Ashizawa, M. and Black, J. B., Semiempirical Approach to Failure Criterion of Laminated Composites, Douglas Paper 7556, presented to 7th DoD/NASA Conference of Fibrous Composites in Structural Design, Denver, Colorado, June 17-20, 1985.
3. Watts, D. J., et al, A Study of the Utilization of Advanced Composites in Fuselage Structures of Commercial Aircraft (Final Report), NASA Report ACEE-30-FR-3313, NASA Contract NAS1-17416, May 1984.

1. Report No. NASA CR-17246		2. Government Accession No.		3. Recipient's Catalog No.	
4. Title and Subtitle Test Results for Composite Specimens and Elements Containing Joints and Cutouts				5. Report Date March 1987	
				6. Performing Organization Code	
7. Author(s) P.T. Sumida, R. C. Madan, and A. V. Hawley				8. Performing Organization Report No. ACEE-30-FR-3610	
9. Performing Organization Name and Address McDonnell Douglas Douglas Aircraft Company 3855 Lakewood Blvd. Long Beach, CA 90846				10. Work Unit No. (TRAIS)	
				11. Contract or Grant No. NAS1-17701	
12. Sponsoring Agency Name and Address National Aeronautics and Space Administration Washington, D.C. 20546				13. Type of Report and Period Covered Contractor Report	
				14. Sponsoring Agency Code 534-06-13-35	
15. Supplementary Notes NASA Langley Technical Monitor: Dr. John G. Davis, Jr., ACST Manager Final Report					
16. Abstract Under Contract NAS1-17701, McDonnell Douglas conducted a program to develop the technology for joints and cutouts in a composite fuselage that meets all design requirements of a large transport aircraft for the 1990s. The development plan encompassed a multifaceted engineering, manufacturing, and testing effort to develop the technology for fuselage joints and cutouts. This report covers the test efforts associated with that program. An advanced trijet derivative of the DC-10 was selected as the baseline aircraft. Design and analysis of a 30-foot-long composite fuselage barrel provided a realistic basis for the test effort. The primary composite material was Hexcel F584 resin on 12K IM6 fiber, in tape and broadgoods form. Fiberglass broadgoods were used in E-glass and S-glass fiber form in the cutout region of some panels. Additionally, injection-molded chopped graphite fiber/PEEK was used for longeron-to-frame shear clips. The test effort included four groups of test specimens, beginning with coupon specimens of mono-layer and cross-ply laminates, progressing through increasingly larger and more complex specimens, and ending with two 4- by 5-foot curved fuselage side panels. One of the side panels incorporated a transverse skin splice, while the second included two cabin window cutouts.					
17. Key Words Advanced Composite Structures Technology Fuselage Joints and Cutouts Graphite-Epoxy			18. Distribution Statement FEDD Distribution Subject Category 24		
19. Security Classif. (of this report) Unclassified		20. Security Classif. (of this page) Unclassified		21. No. of Pages	
				22. Price	